KTH Electrical Engineering

Modeling and Design of Multi-hop Energy Efficient Wireless Networks for Control Applications

PIERGIUSEPPE DI MARCO

Licentiate Thesis
Stockholm, Sweden 2010

KTH School of Electrical Engineering
Automatic Control Lab
SE-100 44 Stockholm
SWEDEN

TRITA-EE 2010:055
ISSN 1653-5146
ISBN 978-91-7415-839-7

Tryck: Universitetsservice US AB

Abstract

Energy efficiency is essential for many industrial and commercial wireless network applications. In this thesis, we propose an analytical framework to model and design protocols for multi-hop wireless networks for industrial control and automation. We study the mutual interaction among medium access control (MAC), routing, and application layers. Accordingly, we provide three main contributions.

First, MAC and routing layers are considered. The carrier sense multiple access (CSMA) of the unslotted IEEE 802.15.4 standard is modeled for multi-hop communications using the specifications of the IETF routing over low power and lossy networks (ROLL). The analysis considers the effects induced by heterogeneous traffic due to the routing mechanism and the node traffic generation patterns, and the hidden terminals due to the reduced carrier sensing capabilities. The interdependence between end-to-end performance indicators (reliability, delay, and energy consumption) and routing decisions is described. It is shown that routing decisions based on reliability or delay tend to direct traffic toward nodes with high packet generation rates, with significant negative effects on the energy consumption.

Second, we propose TREnD, a cross-layer protocol solution that takes into account tunable performance requirements from the control application. An optimization problem is posed and solved to select the protocol parameters adaptively. The objective is to minimize the energy consumption while fulfilling reliability and delay constraints. TREnD is implemented on a test-bed and it is compared to existing protocols. The protocol model and analysis are validated through experiments. It is shown that TREnD ensures load balancing and dynamic adaptation for static and time-varying scenarios.

Eventually, a building automation application is presented by considering the design of a robust controller for under floor air distribution system regulation. The communication performance of an IEEE 802.15.4 network is included in the controller synthesis. We show the impact of reliability and delay on the temperature regulation for synchronous and asynchronous networks.

Acknowledgements

First, I would like to thank my supervisor Prof. Karl Henrik Johansson. Your technical ability to understand problems and give constructive feedbacks on my research is valuable as your personal ability to provide enthusiasm and passion for my work. I can definitely confirm it now, writing this page under the sun of Miami Beach. My co-supervisor Ass. Prof. Carlo Fischione deserves all my gratitude for the continuous and fundamental support and inspiration for my research.

I am grateful to all the other coauthors of papers included in this thesis: Tekn. Lic. Pangun Park, Dr. Pablo Soldati, Prof. Sinem Coleri Ergen, Prof. Emmanuel Witrant, and Dr. Corentin Briat.

Thanks to Prof. Fortunato Santucci, my advisor at the University of L'Aquila and member of my reference group, for his guidance since my undergraduate studies.

All professors, lab administrators, and colleagues in the Automatic Control lab contribute to provide a stimulating, interesting and, nevertheless, fun working environment. Pangun Park deserves a special mention as deputy supervisor for my research, committed office mate, devoted flatmate, discrete pasta chef, and sincere friend. Infinite thanks to Pablo, wise adviser and reliable friend, and to Chithrupa, kind and helpful in every moment. Thanks also to Euhanna, Burak, Zhenhua, Phoebus, José, André, Antonio, Assad, Farhad, and all other colleagues, including Ubaldo, permanent guest PhD student. It is an incredible pleasure to work, discuss and spend time with you after work.

My gratitude to the EU project FeedNetBack, the Swedish Foundation for Strategic Research, the Swedish Research Council, and the Swedish Governmental Agency for Innovation Systems for providing financial support to my research.

Many people did not participate in technical aspects of this thesis but have an important contribution in making me have a wonderful time in Stockholm. I met very good friends in three years and I would like to thank you all.

I would like to mention my friends and my family in Italy. In particular I would like to express my gratitude to my parents Rosalba and Marco for their love and support in every important moment of my life.

Finally, I would like to thank my wife Alessandra for giving me joy, happiness and making my life special every day.

Piergiuseppe Di Marco
Stockholm, December 2010.

Contents

Chapter 1

Introduction

Energy conservation is important for the sustainable development of new communication technologies. A potential infrastructure for developing energy-aware applications is represented by low power wireless networks. They include any network of devices with limited power, memory, and processing resources that are interconnected by a communication protocol such as IEEE 802.15.4, Bluetooth, or low power WiFi. Mobile ad-hoc networks (MANETs) and wireless sensor networks (WSNs) are examples of low power infrastructure interconnected by heterogeneous protocols. These networks introduce different design challenges, such as the need of energy efficient operation. In many applications, it is expected that each node of the network lasts for a long time because of the use in remote areas where recharging and replacing power supply units is difficult. In other cases, recharging is possible and not expensive but the aim of the application is to avoid users to cope with limited battery lifetime of devices. In other situations, it is important to limit the energy for communication in order not to create interference.

Currently, there is a major contrast between continuously increasing need of reliable information and energy saving. High throughput applications such as peer-to-peer file sharing are based on distributing information with high density. This means an increasing number of devices, complexity, cost, and also non negligible impact on the energy consumption of the whole system. Understanding the basic interaction between communication paradigms and application requirements is then fundamental to obtain energy efficient operation. This is more critical and complicated when multi-hop communications are involved.

In this chapter, we introduce the main challenges in modeling and designing communication protocols and applications for multi-hop energy efficient networks. We present motivating examples for the use of low power protocol design in industrial and commercial applications.

Figure 1.1: An IEEE 802.15.4-based wireless control of the froth flotation process at Boliden was tested within the SOCRADES EU project (http://www.socrades.eu/).

1.1 Motivating Examples

Multi-hop low power networks are instrumental in many applications to achieve remote connection and flexibility of the communication. In the following, we describe key examples where energy efficient operations are important, by highlighting the aspects that motivated our research. We consider both industrial and commercial applications, by focusing on industrial automation and intelligent green buildings. In addition, we illustrate the importance of analytical modeling in the design of protocols for such applications.

1.1.1 Industrial Automation

For single-hop networks, many wireless system solutions have been proposed and commercialized, e.g., the WISA (wireless interface for sensors and actuators) system [1], WirelessHART [2], and ISA SP100 [3]. Within the SOCRADES EU project, a wireless control system based on a IEEE 802.15.4 [4] network has been successfully developed for froth flotation process at Boliden (see Figure 1.1). An extension to energy efficient multi-hop networks is now a vast research area and many groups are active in the industrial community [5]. According to a research study by Frost & Sullivan [6] on industry adoption of wireless technologies in EMEA (Europe, the Middle East, and Africa), there is a 27% annual grow rate for wireless revenues for process industries. More than 80% of users look for wireless-device compatibility with automation and control solutions. For this reason, standards like WirelessHART and ISA SP100 rank very low in adoption level among the EMEA companies that participated in the Frost & Sullivan study, while Zigbee, Bluetooth, Wi-Fi, and other unlicensed technologies are widely adopted. On the other side,

Figure 1.2: Wireless control will be an important enabling technology for intelligent green buildings in the Stockholm Royal Seaport. The illustration shows the project by the construction company Folkhem and Wingårdh Architects (http://www.stockholmroyalseaport.com/).

these standards are not specifically designed for industrial control applications. In this field, we aim at investigating the current standard solutions and at proposing a design approach that takes into account typical requirements of industrial environments.

Traditional applications (e.g., monitoring) need a high probability of success in the packet delivery (high reliability). In addition to reliability, control applications ask also for timely packet delivery (low latency). If reliability and latency constraints are not met, the correct execution of control actions may be severely compromised. High reliability and low latency may demand significant energy expenditure, thus reducing the network lifetime. However, for control and automation applications a trade-off between reliability and packet delay can be exploited to minimize the energy consumption. We investigate this trade-off in Chapter 4 of this thesis, where we propose a cross-layer protocol solution for industrial automation, which guarantees energy efficient operation under tunable reliability and delay constraints.

1.1.2 Intelligent Green Buildings

Buildings currently account for about 40% of the worldwide energy demand with 33% in commercial buildings and 67% in residential buildings. Building automation systems and building energy management systems are designed to provide centralized oversight and remote control over heating, ventilation, and air conditioning (HVAC) systems, lighting and other building systems. Improved energy efficiency

as well as improved convenience are some goals of intelligent green buildings, for which currently wired systems like BACnet, LonWorks, or KNX are under development or already deployed [7]. The concept of intelligent green operation can be extended to urban districts, to form smart grids as in the Stockholm Royal Seaport [8] project that involves ABB, Fortum, and Ericsson among others (see Figure 1.2). The project is developed within the global Climate Positive Development Program, launched in May 2009 by the Clinton Climate Initiative and the US Green Building Council. Urban planners are seizing the opportunity to pioneer cutting edge solutions to minimize energy use and optimize waste management. An intelligent electricity grid will reduce annual energy consumption to a maximum of 55 KWh per square meter. The fully automated system, currently being developed, will fine-tune heating and ventilation systems to run when electricity prices are low. An integration of such systems with communication protocols is then fundamental to achieve maximum energy efficiency. With this objective, in Chapter 5 of this thesis, we illustrate the influence of performance indicators of IEEE 802.15.4 networks on the design of a robust controller for HVAC systems.

1.1.3 Why is Protocol Modeling Important?

The underlying aspect that motivates this thesis is the relevance of analytical modeling in design, protocol selection, and optimization of energy efficient communication protocols and control applications. For an automation vendor such as ABB it is often the key to profitability to have an efficient engineering process for modeling. In the design of communication systems for transmitting information through physical channels, it is convenient to use an analytical model that reproduces the most important characteristics of the transmission medium. One of the advantage is that by distinguishing the different components of the networked system, the designer can study the interaction between design parameters and the effects of these parameters on the applications running on top of the network. Same approach is applied in the design of applications on top of the communication stack. By abstracting key network features in simple models, the design can be optimized according to the specified requirements. A drawback is that the abstraction needed for the seek of simplicity in the model may be inefficient to capture the behavior and the performance of a certain application over the communication stack. In particular, the analysis of the interaction between different layers in the protocol stack can be crucial. With this aim, an analytical model that uses Markov chains to describe and study the relation between medium access control (MAC) and routing layer is developed in Chapter 3 of this thesis.

Another important aspect is protocol selection. In particular, we refer to the situation in which a set of protocols is available, and the user would like to establish which is the most appropriate protocol according to a specific objective function and given performance requirements. By using mathematical models, the process of protocol selection can be simplified and automated. In Figure 1.3, we report an example of MAC protocol selection among time division multiple access (TDMA)

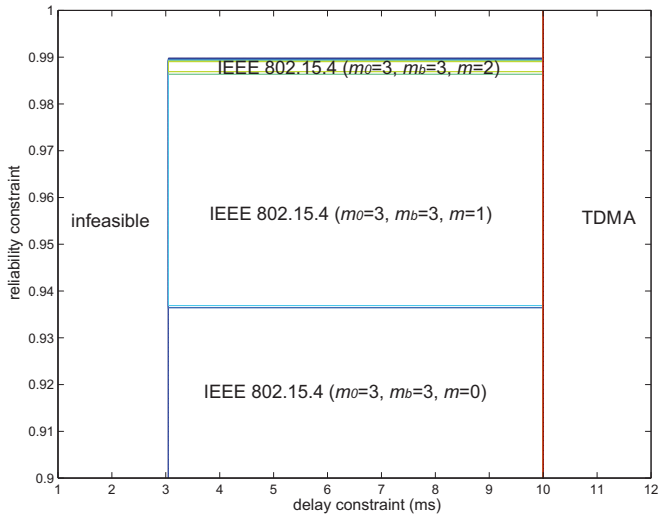

Figure 1.3: MAC protocol selection for a single-hop network with 3 nodes and packet generation period 20 ms. Depending on the reliability and delay, the optimal choice of MAC varies. Here, we consider TDMA and IEEE 802.15.4 MAC.

and contention based MAC solution of the IEEE 802.15.4 standard. The optimal MAC is defined as the one that minimizes the energy consumption for certain reliability and delay constraints. For IEEE 802.15.4, also the optimal set of MAC parameters in each region of the graph is reported. In particular, m_0 is the minimum backoff period, m_b is the maximum backoff period, and m is the number of backoffs. We describe the IEEE 802.15.4 MAC mechanism in Chapter 2.

1.2 Problem Formulation

The aim of this thesis is to provide an analytical framework to model and design MAC, routing, and application layers for energy efficient networks with specific application in industrial and building automation. The essence of our study can be represented by the block diagram in Figure 1.4, in which we synthesize the main components and the mutual interaction between the layers of interest in a wireless network protocol stack.

We abstract the complex interaction among layers by using a double feedback structure. The application sets a traffic generation rate for each node in the network which is related to the required sampling time of the sensing operation in case of WSNs, or a generic data generation rate of the application. The application layer determines performance requirements for the lower protocol layers (e.g., minimum data delivery rate and maximum packet delay that may be handled by the

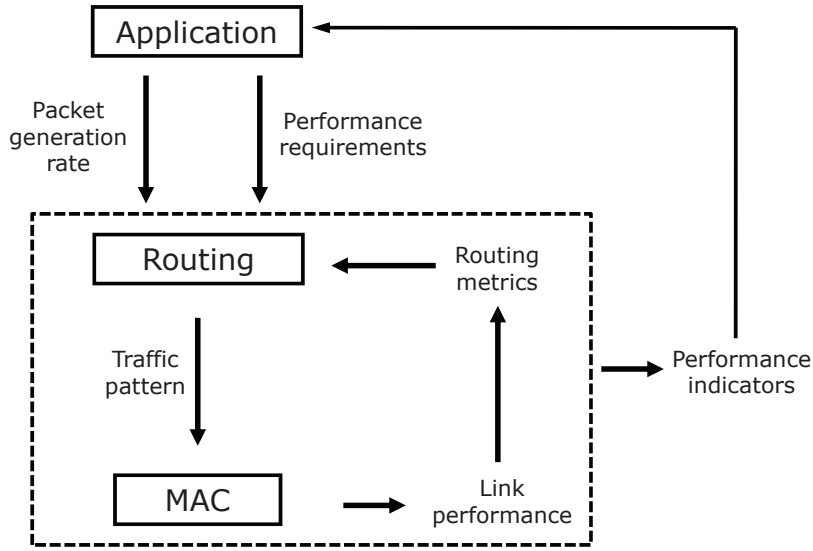

Figure 1.4: Network layers interaction for modeling and design.

controller). The routing layer combines the topological information with the application requirements in a network communication graph. Based on specific metric, the routing protocol takes appropriate decisions to distribute the end-to-end traffic flow in the network and determines a distribution of the actual traffic in each link of the network, where the communication is regulated by the MAC layer. As an output of the MAC we obtain link performance such as energy consumption, reliability, or delay. Furthermore, link performance indicators may influence directly the routing metric, so closing a first loop between MAC and routing layers. The combination of MAC and routing layers determines end-to-end performance indicators, which influences the design of the application so that a second loop is closed between communication layers and application. We remark here that for modeling purposes we do not consider the physical layer explicitly and we assume homogeneous link quality in the network. The aim is to capture the interaction between networking layers and application. For design aspects, we include the channel behavior and we validate our models through experiments on a real test-bed.

Three important features for low power networks are characterized as performance indicators:

- Energy efficiency: low energy consumption is a major objective for battery-equipped devices. This is evident for monitoring applications, in which the network lifetime is the main concern. Besides, an energy efficient operation is important also for process control application, as discussed in our motivating

examples.

- End-to-end reliability: at network layer, reliability is measured as packet delivery ratio from each transmitter to the destination. A maximization of the reliability may require a large number of packet overhead and retransmissions, thus increasing the energy consumption. Controllers may usually tolerate a certain degree of losses without an impact on the overall performance [9], therefore, a design strategy in which reliability is a tunable constraints is desirable.
- End-to-end delay: at network layer, delay is computed for successfully received packets to the destination. A minimization of the delay requires a high utilization of the transmission resources and very low duty cycling among nodes, thus requiring high energy expenditure. Similarly to the reliability, controllers may compensate for average delays with a limited variability [10], therefore a probabilistic characterization of the delay may be used as tunable constraint for design purposes.

Analytical models of performance indicators are embedded in the design methodology. In Chapter 4 an optimization problem is posed to select protocol design parameters in a cross-layer solution called TREnD. The protocol is based on a semi random routing with hybrid MAC, and duty cycling to minimize the network energy consumption, while meeting reliability and packet delay constraints. The optimization problem is

$$\begin{aligned} \min_{\mathbf{u}} \quad & E_{\text{tot}}(\mathbf{u}) \\ \text{s.t.} \quad & \mathbf{u} \in \mathcal{R} \\ & \mathbf{u} \in \mathcal{D}\,. \end{aligned}$$

In this problem, $E_{\text{tot}}(\mathbf{u})$ is the total energy consumption of the network, $\mathcal{R}$ and $\mathcal{D}$ are the feasible sets for the protocol parameters that meet the constraints in terms of reliability and delay, respectively. Decision variables in $\mathbf{u}$ are the duration of the TDMA slot, the wake up probability in transmission, and the wake up rate in reception.

1.2.1 Framework Limitations

In this section, we specify the range of validity of the framework introduced in Figure 1.4.

The protocol solution that we model and implement is based on IEEE 802.15.4 physical layer specifications [4]. A detailed modeling and performance analysis of the physical layer is not explicitly included in the communication loop. The reason is that we restrict ourselves to standardized physical layer specifications, such as the ones used by IEEE 802.15.4. For simplicity, the link between two nodes is modeled by a random variable with good channel probability γ. A Rayleigh fading channel

is introduced in Chapter 4 to test the dynamic adaptation of our proposed protocol stack solution for control application.

The communication stack model is based on Markov chains, which provide statistical modeling of the protocol behavior, and a steady state performance analysis through the stationary distribution of the chain. For this reason, our model may not be able to capture the protocol behavior under event-triggered or self-triggered approach from the control application [11, 12]. The traffic generation rate provided by the application needs to be sampling of a periodic traffic.

1.3 Thesis Outline and Contributions

In the following, we present the outline and contributions of the thesis in more detail.

Chapter 2: Background

This chapter illustrates the background on communication protocol modeling and design for energy efficient networks and surveys on the related literature.

Chapter 3: Analytical Modeling of Multi-hop IEEE 802.15.4 Networks

This chapter describes the proposed model for IEEE 802.15.4 networks. The design loop interaction between routing and MAC protocols is investigated. Link performance at MAC layer are studied by a novel Markov chain model that includes all the features of the unslotted mechanism of IEEE 802.15.4 MAC, in heterogeneous traffic condition and with limited carrier sensing range of nodes. Then, we extend this model to multi-hop networks by considering the routing specifications of the IETF routing over low power and lossy networks (ROLL) working group [13].

The material presented in this chapter is mainly based on the following publications:

- P. Di Marco, P. Park, C. Fischione, and K. H. Johansson: Analytical Modelling of Multi-hop IEEE 802.15.4 Networks. IEEE Transactions on Communications. 2010. Submitted.

- P. Di Marco, P. Park, C. Fischione, and K. H. Johansson: Analytical Modelling of IEEE 802.15.4 for Multi-hop Networks with Heterogeneous Traffic and Hidden Terminals. IEEE Global Communications Conference (GLOBECOM). Miami, Florida. December 2010.

Related studies on the IEEE 802.15.4 standard are included in the following publications:

- P. Park, P. Di Marco, C. Fischione, and K. H. Johansson: Adaptive IEEE 802.15.4 Protocol for Reliable and Timely Communications. IEEE/ACM Transactions on Networking. 2010. Submitted.
- P. Park, P. Di Marco, C. Fischione, and K. H. Johansson: Accurate Delay Analysis of Slotted IEEE 802.15.4 for Control Applications. IEEE International Conference on Communications. Kyoto, Japan. June 2011. Submitted.
- S. C. Ergen, P. Di Marco, and C. Fischione: MAC Protocol Engine for Sensor Networks. IEEE Global Communications Conference (GLOBECOM). Honolulu, Hawaii. December 2009.
- P. Park, P. Di Marco, P. Soldati, C. Fischione, and K. H. Johansson: A Generalized Markov Chain Model for Effective Analysis of Slotted IEEE 802.15.4. IEEE International Conference on Mobile Ad Hoc and Sensor Systems (MASS), (Best paper award). Macau SAR. October 2009.

Chapter 4: Protocol Design for Energy Efficient Networks

In this chapter we broaden the perspective by considering the effects of performance requirements from the application on the design of routing and MAC protocols for control and actuation. We introduce a novel cross-layer protocol solution called TREnD, which is optimized for energy efficiency and dynamically adapted to the application requirements.

The material in this chapter leverages on the following publications:

- P. Di Marco, P. Park, C. Fischione, and K. H. Johansson: TREnD: a Timely, Reliable, Energy-efficient Dynamic WSN Protocol for Control Application. IEEE International Conference on Communications. Capetown, South Africa. May 2010.
- C. Fischione, P. Park, P. Di Marco, and K. H. Johansson: Design Principles of Wireless Sensor Networks Protocols for Control Applications. Wireless Based Network Control, Springer Ed. 2010. To appear.

Chapter 5: Building Automation Application over IEEE 802.15.4 Networks

In this chapter we close the loop between application layer and communication protocol, by considering the effects of communication constraints on the design of a robust controller for building automation.

The material in this chapter covers the arguments in following publication:

- E. Witrant, P. Di Marco, P. Park, and C. Briat: Limitations and Performances of Robust Control over WSN: UFAD Control in Intelligent Buildings. IMA Journal of Mathematical Control and Information. 2010. To appear.

Chapter 6: Conclusions and Future Works

This chapter summarizes the contribution of the thesis and proposes future works and extensions of the material in this thesis.

Other Publications

The following publication is not covered in this thesis but it inspired some of the contents.

- P. Di Marco, C. Rinaldi, F. Santucci, K. H. Johansson, and N. Möller: Performance Analysis and Optimization of TCP over Adaptive Wireless Links. IEEE International Symposium on Personal, Indoor and Mobile Radio Communications. Helsinki, Finland. September 2006.

Contributions by the Author

The order of authors' names reflects the workload, where the first author had the most important contribution. In all the publications, the author participated actively both in the development of the theory and the implementation, as well as in the paper writing.

Chapter 2

Background

In this chapter, we provide an overview of the topics in the following chapters and we briefly summarize the related works. In Section 2.1, the system-level design paradigm for communication networks and control applications is presented. Section 2.2 introduces a survey of recent MAC protocols for applications in industrial and building automation. In Section 2.3, we describe the IEEE 802.15.4 standard, which is the reference MAC standard in this thesis. Section 2.4 reviews relevant routing protocol solutions for energy efficient networks. In Section 2.5, we focus on the specifications of the IETF ROLL standard proposal, which is the reference routing in this thesis. Eventually, Section 2.6 focuses on the design and synthesis of control applications by considering the communication constraints.

2.1 System-level Design

Traditional control applications are usually designed from a protocol stack point of view by a top-down approach, whereby most of the essential aspects of the network and sensing infrastructure that has to be deployed to support control applications are ignored. Here, packet losses and delays introduced by the communication network are considered as uncertainties and the controllers are tuned to cope with them without having any influence on them. The top-down approach is limited for two reasons:

- it does not consider the aspect of energy efficiency of the wireless network [5];
- it can be quite conservative and therefore inefficient, because the controllers are built by presuming worst case wireless channel conditions that may be rarely experienced in the reality.

On the other side, protocols for wireless networks are traditionally designed to maximize the reliability and minimize the delay. This is a bottom-up approach, where controller specifications are not explicitly considered even though the protocols are used for control. This approach is energy inefficient because high reliability and

low delay may demand significant energy consumption [14]. Therefore, it follows that there is the essential need of a new design approach.

Traditional sensor networks applications (e.g., monitoring) need a high probability of success in the packet delivery (reliability). In addition to reliability, control applications ask also for timely packet delivery (latency). If reliability and latency constraints are not met, the correct execution of control decisions may be severely compromised, thus creating unstable control loops [15]. High reliability and low latency may demand significant energy expenditure, thus reducing the network lifetime. Controllers can usually tolerate a certain degree of packet losses and delay [10]. For example, the stability of a closed loop control system may be ensured by high reliable communications and large delays, or by low delays when the packet loss is high. In contrast to monitoring applications, for control applications there is no need to maximize the reliability. A trade-off between latency, packet losses, and stability requirements can be exploited for the benefit of the energy consumption, as proposed by the system-level design approach [16].

Therefore, we claim that the protocol design for control needs a system-level approach whereby the need of a parsimonious use of energy and the typical requirements of the control applications are jointly taken into account and control and wireless network protocols are co-designed. In the following, we give details of the protocol layers involved in the co-design.

2.2 MAC Protocols

The MAC layer is responsible for managing access to a channel shared by several nodes. The principles of MAC layer design for low power wireless networks differ from those of traditional wireless networks mainly in two aspects: (i) energy conservation is a design concern, and (ii) distributed mechanisms are often required [17].

Idle listening is considered as one of the dominant components of energy waste in many traditional MAC protocols. Since a node does not know a priori when it can receive a message from a neighbor, its radio must be on to listen to the medium. However, the channel may be idle for most of the time. To save energy, many MAC proposals keep the radio in sleep mode (i.e., switched off) during some periods of time, trading off energy conservation for latency. Furthermore, collisions contribute to energy inefficiency, since energy is consumed for the transmission of a data unit that is not received successfully. In addition, control overhead must be kept reasonably low. Finally, because a multi-hop path requires the transmission of a data unit in several links, nodes must be appropriately organized to achieve good performance in terms of end-to-end reliability, latency, and network energy consumption.

In the following, we categorize MAC solutions in contention-based, scheduled-based and hybrid solutions.

2.2.1 Contention-based MAC

In contention-based MAC protocols, nodes compete for the medium and coordinate in a probabilistic way. Packet collisions can occur and reliability may be strongly reduced for high traffic, but packet delay is usually low and a strict synchronization is not needed.

The basic mechanism to handle channel contentions is the carrier sense multiple access (CSMA). A transmitting node tries to detect the presence of an encoded signal from another node before attempting to transmit. If a carrier is sensed, the node keeps on sensing the channel with probability p (p-persistent CSMA) or delays its transmission for a random number of time units (CSMA with collision avoidance CSMA/CA).

Contention-based MAC solutions for energy efficient operation in sensor networks are BMAC [18] and XMAC [19], which are based on preamble sampling. In these MACs, the receiver wakes up periodically to check whether there is a transmission and the sender, instead of coordinating the neighbors' wake up times, sends a preamble that is long enough to ensure the receiver wakes up during the preamble. A low power listening scheme where a node cycles between awake and sleep cycles is employed. While awake, the node listens for a long enough preamble to assess if it needs to stay awake or can return to sleep mode.

Sift [20] is a MAC protocol proposed for very low latency event-driven sensor network environments. Sift uses a non-uniform probability distribution function of picking a slot within a slotted contention window. If no node starts to transmit in the first slot of the window, then each node increases its transmission probability exponentially for the next slot assuming that the number of competing nodes is small. Energy consumption increases as overhearing and idle-listening are not negligible.

2.2.2 Scheduling-based MAC

Scheduling-based MAC protocols make use of dedicated resources for packet transmissions. The protocol selects specific time intervals for the transmission of each node in time division multiple access (TDMA) fashion. This approach assumes that nodes are synchronized, which can be performed by using time-stamps or even GPS. Since nodes do not compete for the medium and have reserved resources, scheduling-based MAC protocols are collision-free.

The traffic-adaptive medium access protocol (TRAMA) [21] is a conflict-free, scheduling-based MAC protocol designed for energy efficiency. This feature is achieved by transmission schedules and by allowing nodes to switch the radio to a low power mode when they are not involved in communications. TRAMA uses a single and time-slotted channel for data and signalling transmissions.

Time synchronized mesh protocol (TSMP) [22] is a protocol developed by Dust Networks, which provides services with the aim of contributing to end-to-end reliability particularly for industrial automation networks. TSMP, is based on a

TDMA approach and frequency hopping spread spectrum (FHSS). Hence, consecutive transmissions between two nodes take place in different frequencies as well as in different time slots. A node can participate in different frames (which comprise a number of time-slots) of different sizes to perform different tasks at once.

2.2.3 Hybrid MAC

Hybrid solutions are interesting for industrial and building applications, because of the possibility to obtain a trade-off between advantages of contention-based and collision-free mechanisms with low energy consumption.

Sensor-MAC (SMAC) [23] is based on locally managed synchronization and periodic sleep–listen schedules. Basically built in a contention-based fashion, SMAC strives to retain the flexibility of contention-based protocols while improving energy efficiency in multi-hop networks. SMAC includes approaches to reduce energy consumption from all the major sources of energy waste: idle listening, collision, overhearing, and control overhead. Neighboring nodes form virtual clusters to set up a common sleep schedule.

Timeout-MAC (TMAC) [24] is proposed to enhance the poor results of the SMAC protocol under variable traffic loads. Indeed, the static sleep–listen periods of SMAC result in high latency and lower throughput. In TMAC, the listen period ends when no activation event has occurred for a time threshold. The main drawback of this protocol is the early sleeping problem.

ZMAC [25] is a hybrid MAC scheme for sensor networks that combines the strengths of TDMA and CSMA while offsetting their weaknesses. The main feature of ZMAC is its adaptability to the level of contention in the network so that under low contention, it behaves like CSMA, and under high contention, like TDMA. By mixing CSMA and TDMA, ZMAC becomes more robust to timing failures, time-varying channel conditions, slot assignment failures and topology changes than a stand-alone TDMA. In ZMAC, a time slot assignment is performed at the time of deployment and higher overhead is incurred at the beginning.

2.3 IEEE 802.15.4 MAC

Many standard proposals and existing commercial systems for low power and low rate personal area networks are based on the IEEE 802.15.4 standard [4]. This standard plays a key role for the deployment of low power technologies in various application areas, including industrial and building automation [5, 26].

To achieve low average power consumption, IEEE 802.15.4 assumes that the amount of data transmitted is short and that it is transmitted infrequently in order to keep a low duty-cycle. IEEE 802.15.4 MAC operation is based on CSMA/CA and it allows for beacon-enabled and beacon-less functionalities.

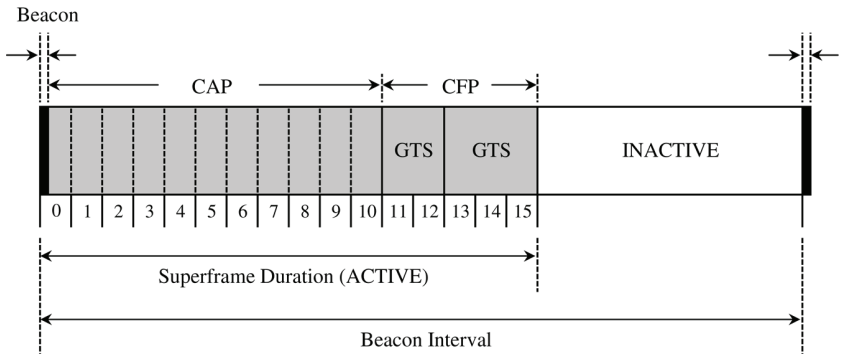

Figure 2.1: Superframe structure of slotted IEEE 802.15.4 MAC.

2.3.1 Slotted Mechanism

In slotted (beacon-enabled) mode, communication is controlled by a network coordinator, which transmits regular beacons for synchronization and association procedures. A superframe structure is imposed with active and optional inactive periods as shown in Figure 2.1. The active period of a superframe consists of a contention access period (CAP) and a contention free period (CFP). Channel access in the CAP is in the form of slotted CSMA, while the coordinator allots guaranteed time slots (GTS) in the CFP for low latency applications. The coordinator and nodes can communicate during the active period and enter a low power mode during the inactive period. The structure of the superframe is defined by two parameters, the beacon order and the superframe order, which determine the length of the superframe and its active period. In addition, the superframe is divided into 16 equally sized superframe slots of length *aBaseSlotDuration*.

The coordinator is responsible for the GTS allocation and determines the length of the CFP in a superframe. To request the allocation of a new GTS, during the CAP the node sends the GTS request command to the coordinator. The coordinator confirms its receipt by sending an ACK frame within the CAP. Upon receiving a GTS allocation request, the coordinator checks whether there are sufficient resources and, if possible, allocates the requested GTS. The maximum number of GTSs to be allocated to nodes is seven, provided there is sufficient capacity in the superframe, and the minimum lenght of the CAP is *aMinCAPLength*. Therefore, the CFP length depends on the GTS requests and the current available capacity in the superframe. If there is sufficient bandwidth in the next superframe, the coordinator determines a node list for GTS allocation based on a first-come-first-served (FCFS) policy. Then, the coordinator includes the GTS descriptor, which is the node list that obtains GTSs in the following beacon to announce the allocation information. The coordinator makes this decision within *aGTSDescPersistenceTime* superframes. Note that on receipt of the ACK to the GTS request command, the

node continues to track beacons and waits for at most *aGTSDescPersistenceTime* superframes. A node uses the dedicated bandwidth to transmit the packet within the CFP.

2.3.2 Unslotted Mechanism

In unslotted (beacon-less) mode there are no regular beacons, but the coordinator may unicast beacons to a soliciting device. Communication among devices in the beacon-less mode uses unslotted CSMA for decentralized access.

Let us consider a node trying to transmit. In the unslotted CSMA/CA of IEEE 802.15.4, first the MAC sub-layer initializes the four variables given by the number of backoffs NB, contention window CW, backoff exponent BE, and retransmission times RT. The default initialization is NB=0, CW=1, BE=*macMinBE* and RT=0.

The MAC sub-layer delays for a random number of complete backoff periods in the range $[0, 2^{\mathrm{BE}} - 1]$ units *aUnitBackoffPeriod*. When the backoff period is zero, the node performs a clear channel assessment (CCA). If the CCA is idle, then the node begins the packet transmission. If the CCA fails due to busy channel, the MAC sublayer increases the value of both NB and BE by one up to a maximum value *macMaxCSMABackoffs* and *macMaxBE*, respectively. Hence, the values of NB and BE depend on the number of CCA failures of a packet. Once BE reaches *macMaxBE*, it remains at the value of *macMaxBE* until it is reset. If NB exceeds *macMaxCSMABackoffs*, then the packet is discarded due to channel access failure. Otherwise the CSMA/CA algorithm generates a random number of complete backoff periods and repeat the process. The variable *macMaxCSMABackoffs* is the maximum number of times the CSMA/CA algorithm is required to backoff. If channel access is successful, the node starts transmitting packets and waits for an ACK. The reception of the corresponding ACK is interpreted as successful packet transmission. If the node fails to receive the ACK due to collision or ACK timeout, the variable RT is increased by one up to *macMaxFrameRetries*. If RT is less than *macMaxFrameRetries*, the MAC sublayer initializes two variables CW=1, BE=*macMinBE* and follows the CSMA/CA mechanism to re-access the channel. Otherwise the packet is discarded due to the retry limit.

In the rest of the thesis, we denote the IEEE 802.15.4 MAC parameters by $W_0 = 2^{macMinBE}$, $m_0 = macMinBE$, $m_b = macMaxBE$, $m = macMaxCSMABackoffs$, $n = macMaxFrameRetries$, and $S_b = aUnitBackoffPeriod$.

2.4 Routing Protocols

One way to classify routing protocols is based on link state and distance vector. In the first case, each node uses topological information to map routing tables, while distance vector algorithms exchange routing information among neighbors. Routers using distance vector protocol do not have knowledge of the entire path to a destination. While link state protocols typically present higher convergence speed

and less overhead, distance vector protocols are simpler, require less computational capability and have smaller storage requirements. Open shortest path first (OSPF) and optimized link state routing (OLSR) are link state protocols, while ad-hoc on-demand distance vector (AODV) and dynamic source routing (DSR) are examples of distance vector protocols for mobile ad hoc networks (MANETs), all of them proposed by the internet engineering task force (IETF) [27]. AODV is part of the ZigBee Alliance [28] protocol stack. The routing solution adopted by AODV uses an on-demand approach for finding routes, which are established only when it is required by a source node for transmitting data packets. It employs destination sequence numbers to identify the most recent path.

Low energy adaptive clustering hierarchy (LEACH) [29] is a cluster-based protocol that includes distributed cluster formation and a hierarchical clustering algorithm. LEACH randomly selects a few sensor nodes as cluster heads (CHs) and rotates this role to evenly distribute the energy load among the sensors in the network. In LEACH, the CH nodes compress data arriving from nodes that belong to the respective cluster, and send an aggregated packet to the network coordinator in order to reduce the amount of information that must be transmitted. LEACH uses TDMA MAC protocol to avoid intra-cluster collisions and code-division multiple access (CDMA) to reduce inter-cluster interference. However, data collection is centralized and performed periodically.

Other relevant studies include collection protocols. They provide best-effort, unreliable packet delivery to one of the data sinks in the network. Having a robust, highly reliable, and efficient collection protocol benefits almost every sensor network application today, as well as the many transport, routing, overlay, and application protocols that sit on top of collection trees.

Despite the proposal of numerous routing protocols for energy efficient wireless networks, there is not yet a definite solution. In the next section, we summarize the routing specifications of the IETF ROLL, which we take as a reference for our study.

2.5 Routing over Low Power and Lossy Networks

The IETF routing over low power and lossy networks (ROLL) working group [13] was created in 2007 with the aim of analyzing and eventually developing solutions for IP-based low power and lossy networks (LLNs). LLNs are made largely of constrained nodes (with limited processing power, memory, and energy when they are battery operated). These routers are interconnected by lossy links, typically time supporting only low data rates, that are usually unstable with relatively low packet delivery rates. Another characteristic of such networks is that the traffic patterns are not simply unicast, but in many cases point-to-multipoint or multipoint-to-point. Furthermore, such networks may potentially comprise up to thousands of nodes.

The working group first elaborated a list of requirements for a routing protocol

on top of LLNs in each of the following application domains: home automation, commercial building automation, industrial automation, and urban automation. Based on these requirements, the working group carried out an analysis of existing routing protocols within the IP domain with regard to their applicability to LLNs. The general requirements that can be derived from the requirements specific to each application domain are as follows:

- The routing state of a node must not increase linearly with the number of nodes in the network or in the neighborhood. A routing state that depends linearly on the number of unique destination is acceptable.
- Local events, such as the failure of a link between two nodes, must not lead to flooding broadcast messages to the whole network.
- The rate at which the routing messages are sent or received must be bounded by the rate of data packets.

According to the analysis, none of the existing IP routing protocols would fulfill all the criteria without modification. In consequence, the working group started to work on the specification of a new routing protocol suitable for LLNs. This routing protocol is called IPv6 routing protocol for low power and lossy networks (RPL).

2.5.1 RPL Specifications

The feature of RPL is the construction of destination-oriented directed acyclic graphs (DODAGs) over the network, according to optimization objectives based on metrics along the paths. In the RPL context, all edges are contained in paths oriented toward and terminating at one or more root nodes. One or more DODAGs that share the same performance criteria and constraints represent a RPL instance. A network may run multiple instances concurrently.

Each node inside a DODAG is identified by the rank, a scalar value that represents the relative position of the node with respect to other nodes and the DODAG root. The rank does not have a physical unit, it increases in a strictly monotonic fashion from the root to the leaf nodes and can be used to validate a progression from or towards the root. The exact calculation of the rank depends of an objective function (OF) but it does not represent necessarily a path cost. For rank comparisons, RPL uses only the integer part of the rank, computed by the $DAGrank()$ macro, which scales the rank by the maximum number of hops in the network (through the parameter $MinHopRankIncrease$).

The fundamental use of the rank is to avoid and detect loops. Loop avoidance is implemented by letting nodes of the network select their parents only among nodes with lower rank. However, loops may occur when nodes detaches from the DODAG and reattaches to a node in its prior sub-DOGAG. This effect is mitigated by loop detection mechanisms implemented locally.

RPL nodes build and maintain DODAGs by multicasting DODAG information object (DIO) messages to their neighbors periodically. The DIO message includes

the rank of a node, among other fields. In order to join a DODAG, a node listens to the DIO messages sent by its neighbors and selects a subset of these nodes as their parents in the DODAG. A node may also identify siblings, which are neighbors having the same rank (but does not necessarily share a common parent with this node). This allows path diversity to be increased, as a node can decide to forward a packet to a sibling. However, communications between siblings is limited to one hop to avoid loops.

A node might select one preferred parent. The rank of the node would then be computed as the rank of the preferred parent plus an increment that depends on the cost of the link between the node and the preferred parent. Although the rank is computed by using link costs, in principle, topology building and maintenance mechanisms are independent of packet forwarding procedures.

There are various metrics and constraints that can be used for path calculation and packet forwarding in RPL. The protocol supports both static and dynamic metrics. Link reliability, packet delay, and node energy consumption are measurements that can be used both as metric and constraints. Expected transmissions count (ETX) is a reliability metric that provides the number of transmissions a node expects to make to a destination in order to successfully deliver a packet. In addition, more metrics can be embedded in the same DODAG metric container.

2.6 Wireless Networked Control Systems

Control over wireless networks is an active research area [5]. In this field, we refer to wireless networked control systems (NCSs), namely, control systems in which actuators, sensors, and controllers are connected and communicate over a wireless network, which might involve multi-hop communications, as illustrated in Figure 2.2. The need of interaction between control and communication in the design of NCSs was raised in [30]. A cross-layer framework for the joint design of wireless networks and distributed controller is in [31], although undesirable interactions might be taken into account [32]. Furthermore, extensive research on the impact of communication performance on the stability of the network can be found in [10] and [33].

In the following, we summarize the important network quality measures for NCSs and related works.

- Bandwidth: when multiple devices share a common network resource, the rate at which they can transmit data over the network is limited by the resource bandwidth. This limitation imposes constraints on achievable performance. An overview of feedback control under bandwidth constraints and the derivation of the minimum bit rate needed to stabilize a linear system are given in [34] and [35]. The data rate of a network must be considered together with the packet size and overhead since data are encapsulated into packets. Notice that the size of the headers depends on the protocol design of the communication network.

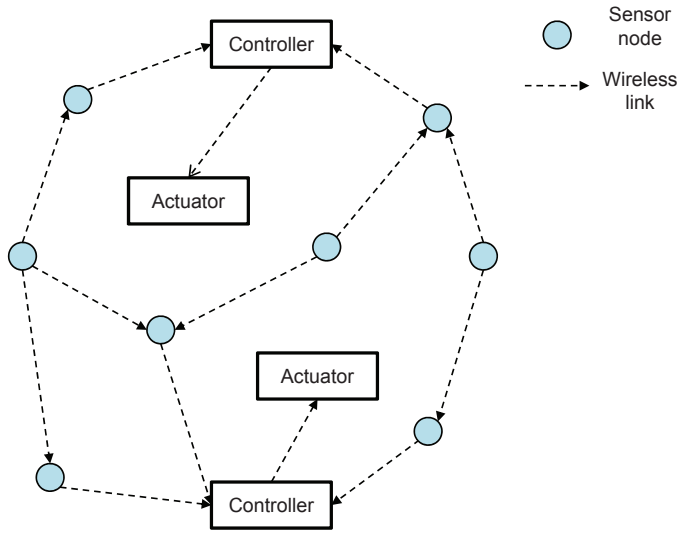

Figure 2.2: Multi-hop wireless NCS scheme.

- Delay: we refer to delay of data on the network as the total time between the data being available at the source node (e.g., sampling at the sensor) and being available at the sink node (e.g., reception at the controller). The overall delay between sampling and receiving can be highly variable. In fact, the medium access delays (i.e., the time it takes for a shared network to accept data), the network delay (i.e., the time for relay nodes in multi-hop networks to forward data), and the transmission delays (i.e., the time during which data are in transit in the medium) depend on highly variable network conditions such as routing, congestion, and link quality. In some NCSs, the data transmitted are time-stamped, which means that the receiver may have an estimate of the delay duration and can take an appropriate corrective action. Many research results have characterized maximum upper bounds on the sampling interval for which stability can be guaranteed (e.g., [36]). These results implicitly attempt to minimize the packet rate that is needed to stabilize a system through feedback. Furthermore, the jitter of the delay is critical since it can be much more difficult to compensate for, especially if the variability is large.

- Packet loss: overflows in communication buffers, transmission errors in the physical layer, and collisions cause packet losses, which affect the performance of the controller [15]. Different techniques have been developed to compensate for packet losses in wireless networks. A common approach to model losses

is to assume that packet losses are independent and identically distributed (i.i.d.) according to a Bernoulli distribution, as in [9].

In conclusion, a well designed wireless networked control system must include both communication and control aspects. Analytical modeling and system-level design approach are useful tools for an efficient co-design.

Chapter 3

Analytical Modeling of Multi-hop IEEE 802.15.4 Networks

In this chapter, we present our analytical modeling of multi-hop low power networks. This analytical study considers jointly routing and IEEE 802.15.4 MAC, and highlights the interdependence between routing decisions and the end-to-end performance indicators. In particular, we focus on the CSMA/CA MAC with Binary Exponential Backoff (BEB) of unslotted IEEE 802.15.4 standard, extended to multi-hop topologies, according to the routing specifications of ROLL. We show how the IEEE 802.15.4 MAC may influence substantially the routing decisions. Specifically, a different distribution of traffic load in the network determines different performance in terms of reliability, delay, and energy consumption of the links. This effect strongly depends on the carrier sensing range of nodes in different routing paths in the network. We derive conditions in which a routing metric based only on reliability and delay performance may become critical for the load distribution and stability of the network.

The chapter starts with an outline of related works. Then we describe the system model and the main assumptions. The analytical model is first described for single-hop networks and then extended to multi-hop networks. After this, simulation results are presented and a short summary concludes the chapter.

3.1 Related Works

While the performance of single-hop IEEE 802.15.4 star networks is well investigated, there is not yet a clear understanding of the performance over multi-hop networks. For single-hop networks, many papers in the literature have proposed models for capturing the behavior of the IEEE 802.15.4 MAC, with saturated or unsaturated traffic, acknowledgements, and retransmissions [37]–[41]. The model proposed in [39] is also validated through real test-bed experiments in [42]. These studies are based on extensions of the Markov chain model originally proposed by Bianchi for the IEEE 802.11 MAC protocol [43]. In fact, IEEE 802.15.4 MAC is

related to IEEE 802.11 MAC. Other interesting approaches include [44]. However, in all these contributions, traffic is assumed to be homogeneous, both in saturated and in unsaturated scenarios. This assumption is a major limitation in at least three important situations:

1. In single-hop networks, nodes may have different traffic generation rates as a result of different services they provide.

2. In multi-hop networks, the traffic load varies according to the routing along the paths. Some nodes may experience a heavier cross traffic, thus transmitting more packets, than nodes that are traversed by less routing paths. It follows that the traffic is not homogeneous, regardless that nodes generate their own packets at the same rate.

3. In networks with hidden terminals, the traffic perceived by the nodes is different, even in the case when every node generates the same traffic. This is due to that some nodes may not perceive the ongoing transmissions of other nodes.

In the situations mentioned above, which we believe are the most interesting and common, existing analytical studies of the IEEE 802.15.4 MAC are not adequate. Studies for IEEE 802.11 and for IEEE 802.15.4 with heterogenous traffic conditions can be found in [45]–[47], where two traffic classes have been considered. For the case of single-hop IEEE 802.11 star network topologies and saturated traffic, the effects of hidden terminals have been studied in [48] and [49]. In [50], multi-hop communication is modeled for IEEE 802.11 networks but, again, with single traffic flow. In [51], the work of [50] has been extended to multiple non-saturated flows. However, we note that these models can not be directly applied to IEEE 802.15.4 networks due to the different access mechanism of IEEE 802.11 MAC. In [52], a Markov chain model is presented for multi-hop networks, but the model is limited to nodes that communicate to the coordinator through an intermediate relay node, which is assumed as not generating traffic and competing for channel access. To the best of our knowledge, there is no analytical study in literature that models the effect of routing over multi-hop networks using unslotted IEEE 802.15.4 MAC.

3.2 System Model and Assumptions

Consider a network of N nodes that use the unslotted IEEE 802.15.4 MAC. We focus on this MAC modality because it is common and relevant for the ROLL standardization [13]. In the following, we illustrate the system model by considering two topologies, as reported in Figure 3.1. However, the analytical results that we derive in this chapter are general and are not limited to a specific topology.

The topology in Figure 3.1a refers to a single-hop (star) network where nodes forward their packets[1] with single-hop communication to the root node V_0. In star

[1]Throughout this chapter, we refer to packets as MAC protocol data units.

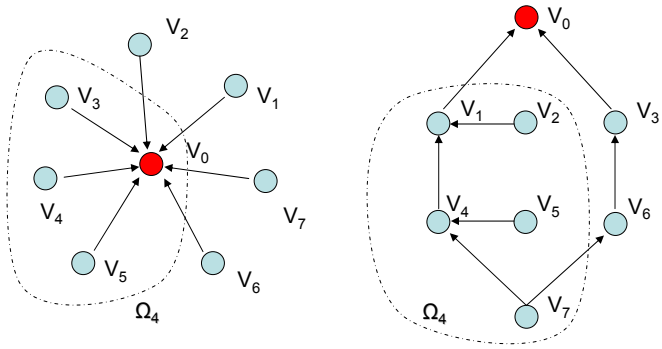

a) Single-hop topology b) Multi-hop topology

Figure 3.1: Example of a single-hop topology (left) and a multi-hop topology (right) for an IEEE 802.15.4 network. The dash-dotted area Ω_4 delimits the carrier sensing range of node V_4, namely the largest set of nodes that can be heard by V_4 while doing the CCA.

networks, we denote by l the link between node V_l and V_0, $l = 1, \ldots, N$. The topology in Figure 3.1b is an example of multi-hop network in which nodes forward traffic according to the uplink routing policy to V_0. In multi-hop networks, we label by l, $l = 1, \ldots, G$ the link between a pair of communicating nodes V_i and V_j, where G is the number of such pairs.

For every node V_i, we define a *neighborhood* set Ω_i, which contains all the nodes in the carrier sensing range of V_i (delimited by dash-dotted lines in Figure 3.1). The carrier sensing range is the set of nodes that can be heard by a node while performing the IEEE 802.15.4 clear channel assessment (CCA). We denote by $|\Omega_i|$ the cardinality of Ω_i. We assume that the channel is symmetric, so that if $V_k \in \Omega_i$, then $V_i \in \Omega_k$, which is natural when transmitting and receiving over similar frequencies. We let the communication range be equal to the carrier sensing range of a node. Such assumptions are widely adopted, e.g., [37]–[50].

We define a *parent* set $\Gamma_i \subset \Omega_i$, which contains all nodes that may be next-hop nodes of V_i, and *children* set $\Delta_i \subset \Omega_i$, which contains all nodes that have V_i as next-hop node. For each link (V_i, V_j), we define a set $\Omega_{j\setminus i} = \Omega_j - \Omega_i \bigcap \Omega_j$, that is the hidden node set of V_i with respect to V_j, namely all nodes that are in the carrier sensing range of the receiver V_j, but that do not belong to the carrier sensing range of the transmitter V_i. As a reference routing protocol, we consider the specifications of ROLL. The knowledge of the topological sets Ω_i and Γ_i is then specified by the standard.

Coherently with the ROLL specifications, the root node generates a destination-oriented directed acyclic graph (DODAG). In a DODAG all edges are oriented such that no cycles exist. Directional routes in the network are indicated by arrows in

Figure 3.1b. We consider a simple routing example to illustrate our analysis. We test the situation in which there are two main paths to the destination. Node V_7 may decide to route its packets either through nodes V_4 and V_1, which forwards traffic also from other nodes (V_2 and V_5), or through V_6–V_3, which is less loaded in terms of traffic forwarding. We assume homogeneous link quality between a node and each one of its parents. The decision is based on routing metrics such as maximum end-to-end reliability or minimum end-to-end delay, which depend on the single link performance at MAC layer. As we show in Section 3.5, the interaction between MAC layer and routing decisions varies substantially between the routing paths, according to the coupling effect of the carrier sensing range.

We describe the interaction between ROLL and unslotted IEEE 802.15.4 MAC layers through the block diagram in Figure 3.2. The input from the application layer is given by information on the network topology (number of nodes N and connectivity graph) and the node traffic generation rate λ_l, $l = 1, \ldots, N$. We abstract the interdependence between the two layers by a feedback mechanism. Routing decisions determine the distribution of the traffic along the different nodes of the network by considering the routing metrics and the inputs from the application. Routing metrics are directly influenced by the performance indicators at MAC level (i.e., reliability and delay). We remark here that we do not consider the physical layer and the link quality. In particular, our model scenario refers to a situation is which the routing layer utilizes the link quality information to build the DODAG, and then, within the parent set, the packet forwarding decision mainly depends on the performance indicators at MAC level.

A list of all symbols used in our model description is reported in Table 3.15, at the end of the chapter.

In the following section, we introduce the model for multi-hop unslotted IEEE 802.15.4 MAC and we derive the basic relations with the routing policy, as illustrated in Figure 3.2.

3.3 Unslotted IEEE 802.15.4 MAC

In this section, a generalized model of a heterogeneous unslotted IEEE 802.15.4 network is proposed. The analysis aims at deriving the network performance indicators, namely the reliability as probability of successful packet reception, the delay for successfully received packets, and the average node energy consumption. We first analyze a single-hop case, and then we generalize the model equations to the multi-hop case. Main original contributions of such a model, with respect to the Markov chain model in [39] or [53] is the presence of heterogeneous traffic with different node packet generation rates, the hidden terminal problem, and the multi-hop routing.

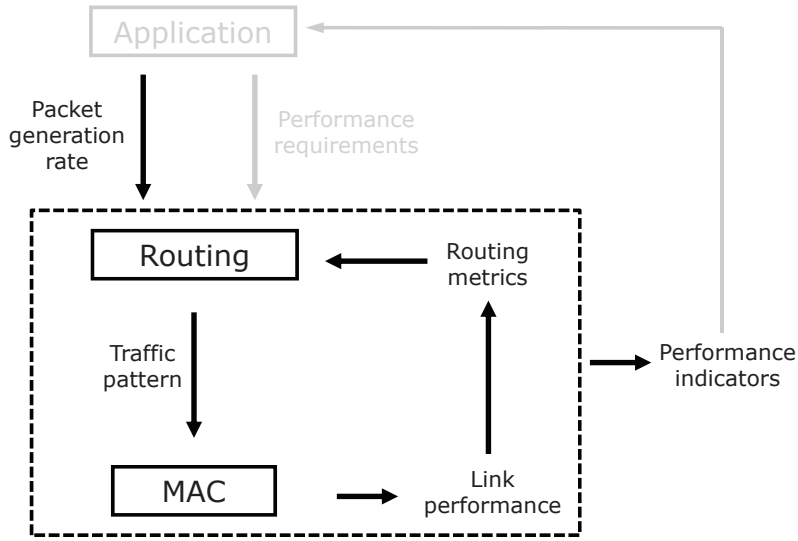

Figure 3.2: Layers interaction for modeling and design: IEEE 802.15.4 MAC and IETF ROLL. The analysis does not assume any specific application.

3.3.1 Markov Chain Model

We develop some results for a single-hop network implementing unslotted IEEE 802.15.4 MAC, which we then extend to multi-hop networks. Details on the operation in the unslotted IEEE 802.15.4 MAC are presented in Section 2.3.2.

In particular, here we derive the probability that node V_l attempts a CCA in a randomly chosen time unit, τ_l, the probability that CCA is busy at link l, α_l, and the probability that a transmitted packet encounters a collision at link l, $P_{\text{coll},l}$.

The generation of unsaturated traffic at node V_l is modeled by a packet generation probability q_l, namely the probability of generating a new packet in each time unit when the node is in idle state.

Let $s_l(t), c_l(t)$, and $r_l(t)$ be the stochastic processes representing the backoff stage, the state of the backoff counter, and the state of retransmission counter at time t experienced by node V_l to transmit a packet. By assuming independent probability that nodes start sensing, the stationary probability τ_l that V_l attempts a carrier sensing in a randomly chosen slot time is constant. The triple $(s_l(t), c_l(t), r_l(t))$ is the three-dimensional per-link Markov chain in Figure 3.3, where we use (i, k, j) to denote a particular state. We recall the IEEE 802.15.4 MAC parameters $W_0 = 2^{macMinBE}$, $m_0 = macMinBE$, $m_b = macMaxBE$, $m = macMaxCSMABackoffs$, $n = macMaxFrameRetries$, and $S_b = aUnitBackoffPeriod$.

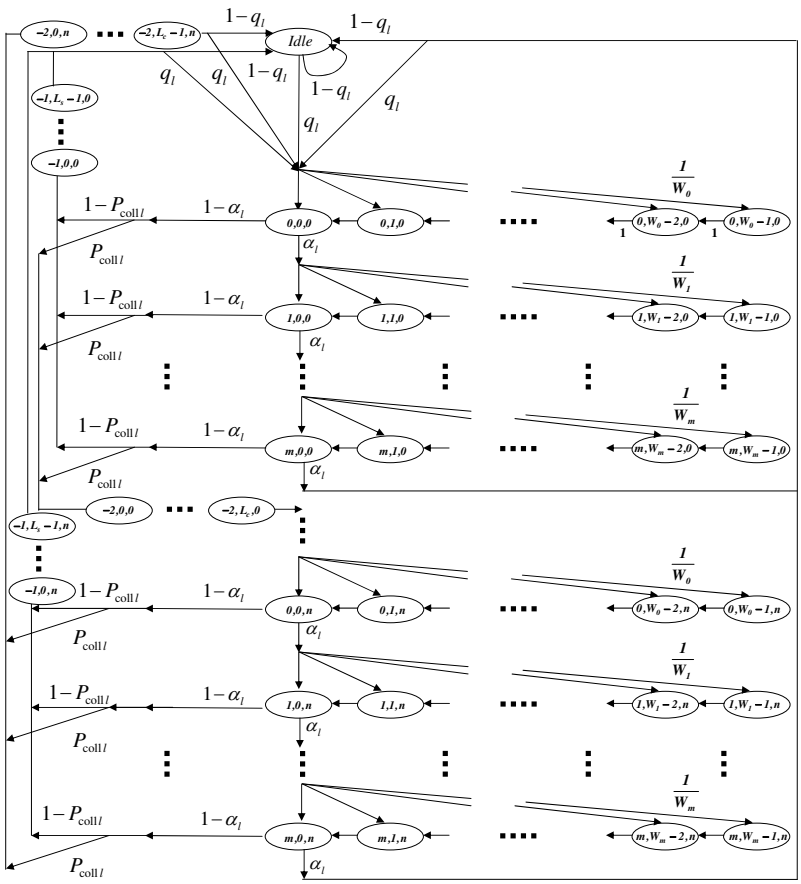

Figure 3.3: Markov chain model of the CSMA/CA algorithm of a transmitting node of the link l for unslotted IEEE 802.15.4 MAC. We remark that compared to existing work from the literature, the chain considers the hidden terminal problem and heterogeneous traffic with different packet generation rates per node.

The Markov chain consists of four main parts corresponding to the idle states, backoff states, CCA states, and packet transmission states. The state $Idle$ corresponds to the idle-queue state when the packet queue is empty and the node is waiting for the next packet generation time. The states from $(i, W_m - 1, j)$ to $(i, W_0 - 1, j)$ represent the backoff states. The states $(i, 0, j)$ represent the CCA. The states $(-1, k, j)$ and $(-2, k, j)$ correspond to the successful transmission and packet collision, respectively. The generation of unsaturated traffic at node V_l is modeled by a packet generation probability q_l, namely the probability of generating

a new packet in each time unit when the node is in idle state. We define the packet successful transmission time L_s and the packet collision time L_c as

$$\begin{aligned} L_s &= L + t_{\text{ack}} + L_{\text{ack}} + IFS\,, \\ L_c &= L + t_{\text{m,ack}}, \end{aligned} \tag{3.1}$$

where L is the total length of a packet including overhead and payload, t_{ack} is ACK waiting time, L_{ack} is the length of ACK frame, IFS is the inter-frame spacing, and $t_{\text{m,ack}}$ is the timeout of the ACK, see details in [4].

By finding the stationary probabilities for each chain, we can derive the probability τ_l that node V_l attempts CCA. Then, we couple all the per-link Markov chains to obtain a set of equations that give the network operating point, namely the busy channel probabilities α_l, and the collision probabilities $P_{\text{coll},l}$, for $l = 1, \ldots, N$.

We define $b^{(l)}_{i,k,j} = \lim_{t\to\infty} \Pr[s_l(t) = i, c_l(t) = k, r_l(t) = j], i \in (-2, m), k \in (0, \max(W_i - 1, L_s - 1, L_c - 1)), j \in (0, n)$ the stationary distribution of the Markov chain of Figure 3.3. We remark that these probabilities are associated to link l. Then, we have the following result:

Proposition 3.3.1. *Suppose that the probability to start sensing for each node is independent of the number of retransmissions suffered. Let α_l be the probability that CCA is busy and let $P_{\text{coll},l}$ the probability that a transmitted packet encounters a collision for $l = 1, \ldots, N$. Then, the probability τ_l that a node V_l attempts CCA in a randomly chosen time unit is*

$$\tau_l = \left(\frac{1-\alpha_l^{m+1}}{1-\alpha_l}\right)\left(\frac{1-y_l^{n+1}}{1-y_l}\right) b^{(l)}_{0,0,0}\,, \tag{3.2}$$

where

$$b^{(l)}_{0,0,0} = \begin{cases} \Big[\frac{1}{2}\left(\frac{1-(2\alpha_l)^{m+1}}{1-2\alpha_l}W_0 + \frac{1-\alpha_l^{m+1}}{1-\alpha_l}\right)\frac{1-y_l^{n+1}}{1-y_l} + (L_s(1-P_{\text{coll},l}) \\ +L_c P_{\text{coll},l})\,(1-\alpha^{m+1})\frac{1-y_l^{n+1}}{1-y_l} + \frac{1-q_l}{q_l}\left(\frac{\alpha_l^{m+1}(1-y_l^{n+1})}{1-y_l}\right. \\ \left. +P_{\text{coll},l}(1-\alpha_l^{m+1})y_l^n + (1-P_{\text{coll},l})\frac{(1-\alpha_l^{m+1})(1-y_l^{n+1})}{1-y_l}\right)\Big]^{-1}, \\ \quad \text{if } m \le \bar{m} = m_b - m_0 \\ \Big[\frac{1}{2}\left(\frac{1-(2\alpha_l)^{\bar{m}+1}}{1-2\alpha_l}W_0 + \frac{1-\alpha_l^{\bar{m}+1}}{1-\alpha_l} + \ (2^{m_b}+1)\alpha_l^{\bar{m}+1}\frac{1-\alpha_l^{m-\bar{m}}}{1-\alpha_l}\right)\frac{1-y_l^{n+1}}{1-y_l} \\ +(L_s(1-P_{\text{coll},l}) + L_c P_{\text{coll},l})(1-\alpha^{m+1})\frac{1-y_l^{n+1}}{1-y_l} + \frac{1-q_l}{q_l}\left(\frac{\alpha_l^{m+1}(1-y_l^{n+1})}{1-y_l}\right. \\ \left. + P_{\text{coll},l}(1-\alpha_l^{m+1})y_l^n \ + (1-P_{\text{coll},l})\frac{(1-\alpha_l^{m+1})(1-y_l^{n+1})}{1-y_l}\right)\Big]^{-1}, \\ \quad \text{otherwise,} \end{cases} \tag{3.3}$$

and $y_l = P_{\text{coll},l}(1-\alpha_l^{m+1})$.

Proof. A proof is provided in Appendix A. □

This probability τ_l depends on the probability α_l that CCA is busy and the probability $P_{\text{coll},l}$ that a transmitted packet encounters a collision. We study these two probabilities next.

We derive the busy channel probability as follows:

$$\alpha_l = \alpha_{\text{pkt},l} + \alpha_{\text{ack},l}\,, \tag{3.4}$$

where $\alpha_{\text{pkt},l}$ is the probability that node V_l senses the channel and finds it occupied by a packet transmission in the neighborhood Ω_l, whereas $\alpha_{\text{ack},l}$ is the probability of finding the channel busy due to ACK transmission from V_0.

The probability that node V_l finds the channel busy due to a packet transmission is the combination of two events: (i) at least one node accesses the channel in one of the previous L time units; (ii) at least one of the nodes that accessed the channel found it clear. We would like to remark here a major difference with the Markov chain model proposed in [39]. In homogeneous networks with full sensing range, the busy channel probability is network information; it is same for all the nodes. In our case, it depends on the access and busy channel probabilities of each node in the neighborhood. This introduces substantial analytical challenges.

Denote by $\mathscr{S}_l$ the event that node V_l is sensing, and by $\mathscr{T}_l$ the event that node V_l is transmitting. Denote also by $\mathscr{F}_l$ the event that there is at least one transmission in Ω_l. Then,

$$\alpha_{\text{pkt},l} = \Pr[\mathscr{F}_l|\mathscr{S}_l] = \sum_{i=0}^{|\Omega_l|-2} \sum_{j=1}^{C_{l,i}} \Pr\left[\bigcup_{k=1}^{i+1} \mathscr{T}_{k_j}|\mathscr{S}_l\right], \tag{3.5}$$

where $C_{l,i} = \begin{pmatrix} |\Omega_l|-1 \\ i+1 \end{pmatrix}$. The index k accounts for the events of simultaneous transmissions in the channel and the index j enumerates the combinations of events in which a number of i channel accesses are performed in the network simultaneously. Therefore, the index k_j refers to the node in the k-th position in the j-th combination of i elements out of Ω_l, so that

$$\Pr\left[\bigcup_{k=1}^{i+1} \mathscr{T}_{k_j}|\mathscr{S}_l\right] = \prod_{k=1}^{i+1} \tau_{k_j} \left(1 - \prod_{k=1}^{i+1} \alpha_{k_j}\right) \prod_{h=i+2}^{|\Omega_l|} (1-\tau_{h_j})\,.$$

To illustrate this formula, we give an example (see Figure 3.1a). Assume that there are two contending nodes in the neighborhood of V_4, $\Omega_4 = \{V_0, V_3, V_5\}$. Note that V_0 does not generate packets. Then, the event of busy channel for node V_4, is given by the sum of three contributions:

1. Only node V_3 accessed the channel and found it clear. The probability of this event is $L\tau_3(1-\tau_5)(1-\alpha_3)$.

2. Only node V_5 accessed the channel and found it clear. Similarly to the previous case, the probability is $L\tau_5(1-\tau_3)(1-\alpha_5)$.

3. Both nodes accessed the channel and at least one node found it clear. Note that V_5 may not belong to Ω_3. This probability is upper bounded by $L\tau_3\tau_5(1-\alpha_3\alpha_5)$.

Equation (3.5) follows as a generalization of this example.

Let R_h be the reliability for the link h. A busy channel assessment due to ACKs depends on the probability of successful packet reception in Ω_0. It follows that

$$\alpha_{\mathrm{ack},l} = L_{\mathrm{ack}} \sum_{h\in\Omega_0 h\neq l} q_h R_h \,, \tag{3.6}$$

where L_{ack} is the length of the ACK and q_h is the packet generation rate of node V_h. By summing up Equations (3.5) and (3.6), we can compute α_l in Equation (3.4).

$P_{\mathrm{coll},l}$ is the probability that the packet transmission from node V_l to the root node V_0 encounters a simultaneous packet transmission. There are three situations that give a packet collision:

1. at least one node in Ω_0 senses the channel in the same time slot as node V_l;

2. at least one node in $\Omega_{0\setminus l}$ (hidden node) has started a packet transmission in one of the previous L backoff units;

3. at least one node in $\Omega_{0\setminus l}$ starts a packet transmission before node V_l ends its transmission.

We define by $\mathscr{A}_l$, the event of simultaneous sensing with node V_l in Ω_0, and by $\mathscr{B}_l$, the event of carrier sense failure, due to hidden terminals in $\Omega_{0\setminus l}$. Therefore, the collision probability $P_{\mathrm{coll},l}$ is given by

$$P_{\mathrm{coll},l} = \Pr[\mathscr{A}_l] + (1-\Pr(\mathscr{A}_l))\Pr[\mathscr{B}_l] \,.$$

If a generic node V_k senses the channel with probability τ_k, the event $\mathscr{A}_l$ occurs with probability

$$\Pr[\mathscr{A}_l] = 1 - \prod_{\substack{k\in\Omega_0\\ k\neq l}} (1-\tau_k) \,.$$

The probability of event $\mathscr{B}_l$ is given by the busy channel probability in the set $\Omega_{0\setminus l}$, hence,

$$\begin{aligned}\Pr[\mathscr{B}_l] &= \sum_{i=0}^{|\Omega_{0\setminus l}|-2} \sum_{j=1}^{C_{l,i}} \Pr\left[\bigcup_{k=1}^{i+1} \mathscr{T}_{k_j} | \mathscr{S}_l\right] \\ &= 2L \sum_{i=0}^{|\Omega_{0\setminus l}|-2} \sum_{j=1}^{C_{l,i}} \prod_{k=1}^{i+1} \tau_{k_j} \left(1 - \prod_{k=1}^{i+1} \alpha_{k_j}\right) \prod_{h=i+2}^{|\Omega_l|} (1-\tau_{h_j}) \,.\end{aligned}$$

In the next subsections, we use this results to derive the expressions of the reliability, the delay for successful received packets, and the energy consumption.

3.3.2 Reliability

In this subsection, we derive an expression of the reliability for each link of the network. In slotted CSMA/CA, packets are discarded due to either of the following reasons: (i) channel access failure or (ii) retry limits. Channel access failure happens when a packet fails to obtain clear channel within $m+1$ backoffs. Furthermore, a packet is discarded if the transmission fails due to repeated collisions after $n+1$ attempts. Following the Markov model presented in Figure 3.3, the probability that the packet is discarded due to channel access failure is

$$P_{\mathrm{cf},l} = \frac{\alpha_l^{m+1}(1-(P_{\mathrm{coll},l}(1-\alpha_l^{m+1}))^{n+1})}{1-P_{\mathrm{coll},l}(1-\alpha_l^{m+1})}\,. \tag{3.7}$$

The probability of a packet discarded due to retry limits is

$$P_{\mathrm{cr},l} = (P_{\mathrm{coll},l}(1-\alpha_l^{m+1}))^{n+1}\,. \tag{3.8}$$

Therefore, by using Equations (3.7) and (3.8), the reliability is

$$R_l = 1 - P_{\mathrm{cf},l} - P_{\mathrm{cr},l}\,. \tag{3.9}$$

The expressions of the carrier sensing probability τ_l, the busy channel probability α_l, and the reliability R_l, for $l = 1,\ldots,N$, form a system of non-linear equations that can be solved through numerical methods. The solution of these equations provides us with the link reliability for a single-hop networks.

3.3.3 Delay

We define the delay D_l for a successfully received packet as the time interval from the instant the packet is ready to be transmitted at the head of the MAC queue of node V_l, until an ACK for such a packet is received. If a packet is dropped due to either the limited number of backoffs m or the finite retry limit n, its delay is not included into the average delay.

Let $D_{l,j}$ be the delay for a node that sends a packet successfully at the j-th attempt. The expected value of the delay D_l is

$$\mathbb{E}[D_l] = \sum_{j=0}^{n} \Pr(\mathscr{C}_j|\mathscr{C})\,\mathbb{E}[D_{l,j}]\,. \tag{3.10}$$

where

$$\mathbb{E}[D_{l,j}] = L_s + j\,L_c + \sum_{h=0}^{j} \mathbb{E}[T_h]\,, \tag{3.11}$$

T_h is the backoff stage delay, L_s and L_c are the time periods in number of time units for successful packet transmission and collided packet transmission in Equation (3.1). The event $\mathscr{C}_j$ denotes the occurrence of a successful packet transmission at time $j+1$ given j previous unsuccessful transmissions, whereas the event $\mathscr{C}$ denotes the occurrence of a successful packet transmission within n attempts. We then have

$$\begin{aligned}\Pr(\mathscr{C}_j|\mathscr{C}) &= \frac{P_{\text{coll},l}^j(1-\alpha_l^{m+1})^j}{\sum_{k=0}^{n}\left(P_{\text{coll},l}(1-\alpha_l^{m+1})\right)^k} \\ &= \frac{\left(1-P_{\text{coll},l}(1-\alpha_l^{m+1})\right)P_{\text{coll},l}^j(1-\alpha_l^{m+1})^j}{1-\left(P_{\text{coll},l}(1-\alpha_l^{m+1})\right)^{n+1}}\,, \end{aligned} \tag{3.12}$$

where we recall that $P_{\text{coll},l}$ is the collision probability and $1-\alpha_l^{m+1}$ is the probability of successful channel accessing within the maximum number of m backoff stages. Note that the probability of the event $\mathscr{C}_j$ is normalized by considering all the possible events of successful attempts $\mathscr{C}$.

Let $T_{h,i}$ be the random time to obtain a successful CCA from the selected backoff counter value in backoff level i. By following a similar approach as the one for the characterization of D_l, we see that the expected total backoff delay is modeled by

$$\mathbb{E}[T_h] = \sum_{i=0}^{m}\Pr(\mathscr{D}_i|\mathscr{D})\,\mathbb{E}[T_{h,i}]\,,$$

where

$$T_{h,i} = (1+i)T_{sc} + \sum_{k=0}^{i} T_{h,k}^b\,, \tag{3.13}$$

and where T_{sc} is the sensing time in the unslotted mechanism, and $\sum_{k=0}^{i} T_{h,k}^b$ is the total backoff time at backoff stage i. Since the backoff time $T_{h,k}^b$ is uniformly distributed in $[0, W_k-1]$, we can rewrite the expected backoff delay $\mathbb{E}[T_h]$ as

$$\mathbb{E}[T_h] = T_{sc} + \sum_{i=0}^{m}\Pr(\mathscr{D}_i|\mathscr{D})\left(i\,T_{sc} + \sum_{k=0}^{i}\frac{W_k-1}{2}\,S_b\right). \tag{3.14}$$

The event $\mathscr{D}_i$ denotes the occurrence of a busy channel for i consecutive times, and then of idle channel at the $i+1$th time. By considering all the possibilities of busy channel during two CCAs, the probability of $\mathscr{D}_i$ is conditioned on the successful sensing event within m attempts $\mathscr{D}$, given that the node senses an idle channel in CCA. It follows that

$$\Pr(\mathscr{D}_i|\mathscr{D}) = \frac{\alpha_l^i}{\sum_{k=0}^{m}\alpha_l^k} = \frac{\alpha_l^i(1-\alpha_l)}{1-\alpha_l^{m+1}}\,. \tag{3.15}$$

By replacing Equations (3.11)–(3.15) in Equation (3.10), the average delay for successful received packets is computed.

3.3.4 Energy Consumption

Here we develop the expression of the total energy consumption. By considering the Markov chain model given in Figure 3.3, the average energy consumption of node V_l is given as follow

$$\begin{aligned} E_{\text{tot},l} =& P_i \sum_{i=0}^{m} \sum_{k=1}^{W_i-1} \sum_{j=0}^{n} b_{i,k,j}^{(l)} + P_{sc} \sum_{i=0}^{m} \sum_{j=0}^{n} b_{i,0,j}^{(l)} \\ &+ P_t \sum_{j=0}^{n} \sum_{k=0}^{L-1} (b_{-1,k,j}^{(l)} + b_{-2,k,j}^{(l)}) + P_i \sum_{j=0}^{n} (b_{-1,L,j}^{(l)} + b_{-2,L,j}^{(l)}) \\ &+ \sum_{j=0}^{n} \sum_{k=L+1}^{L+L_{\text{ack}}+1} (P_r\, b_{-1,k,j}^{(l)} + P_i\, b_{-2,k,j}^{(l)}) + P_{sp}\, b_{\text{idle}}^{(l)}\,, \end{aligned} \tag{3.16}$$

where P_i, P_{sc}, P_t, P_r, and P_{sp} are the average energy consumption in idle-listen, channel sensing, transmit, receiving, and idle-queue states, respectively. We assume that the radio is set in idle-listen state during the backoff stages and the timeout of ACK, $t_{\text{m,ack}} = L_{\text{ack}} + 1$, in time units S_b. In Equation (3.16), the first and second terms take into account the energy consumption during idle backoff state and channel sensing state, respectively. The third, fourth, and fifth terms consider the energy consumption of packet transmission stage. The last term is the energy consumption of idle stage without packet generation. By substituting Equations (A.12)–(A.14) into Equation (3.16), we obtain the average energy consumption in closed form. In the next section, we generalize the analysis to the multi-hop case.

3.4 Extension to Multi-hop Networks

In a multi-hop topology, the number of links G is not equal to the number of nodes N. Recall that we associate to each link l a pair transmitter–receiver (V_i, V_j). The proposed Markov chain model is extended to a generic network in which information is routed through multi-hop communications to a root node. The Markov chain model should be solved for each link of the network, by considering now that the generic destination node V_j in each link has a different neighborhood Ω_j, and forwards a traffic Q_j.

Let $\lambda = [0, \lambda_1, ..., \lambda_N]$ be a vector of node traffic generation rates, where each component is associated to a node. In addition to λ_i, a node V_i has to forward traffic generated by nodes in its children set Δ_i. We measure the forwarded traffic in link l as

$$Q_l = \frac{q_l}{aUnitBackoffPeriod} \quad \text{pkt/s}\,,$$

where q_l is the probability of having a new packet to transmit in each time unit when the transmitting node is in idle state (see Figure 3.3) and where *aUnitBackoffPeriod*

is the duration of the basic time unit in IEEE 802.15.4. We remark that Q_l is an upper bound for the actual traffic rate, because it does not consider the generation of packets during the random backoff and during the packet transmission time. We adopt it because of analytical simplicity. As we show later, this approximation is accurate, particularly for low traffic.

The aim of the following analysis is to provide an expression of the total traffic load Q_l, which we associate to the probability q_l in the per-link Markov chain in Figure 3.3. To do so, we must characterize the traffic distribution in the network according to a routing policy.

Define $\pi_{i,j}$ the metric associated to link (V_i, V_j) to build the routing graph, as specified by ROLL. In a practical example, $\pi_{i,j}$ may be the end-to-end reliability or delay from node V_i to V_0, by choosing node V_j as next-hop node. At the routing layer, metrics are chosen to be static if the network is stationary. Anyhow, due to the dynamic nature of wireless connectivity, link attributes including reliability and delay may change over time and the routing metrics are updated accordingly. We can represent this dynamical behavior using a statistical analysis. The effect of routing can be described by a matrix $\mathbf{M} \in \mathbb{R}^{(N+1)\times(N+1)}$, in which element $M_{i,j}$ corresponds to the probability that the metric in link $l = (V_i, V_j)$ is the highest among the set of candidate receivers Γ_i, i.e.,

$$M_{i,j} = \Pr\left[\pi_{i,j} = \max_{V_h \in \Gamma_i} \pi_{i,h}\right] .$$

The distribution of the traffic flows along the network can be modeled by the matrix $\mathbf{M}$, and by scaling it by the probability of successful reception in each link (only successfully received packets are forwarded). Therefore, we define a matrix $\mathbf{T}$ such that $T_{i,j} = M_{i,j} R_l$ where R_l is the reliability in the link $l = (V_i, V_j)$, as derived in Section 3.3.2. It follows that the vector of node traffic generation probabilities $Q = [0, Q_1, \ldots, Q_N]$ is the solution of a system of flow balance equations $Q = Q\,\mathbf{T} + \lambda$. In steady state, we have

$$Q = \lambda \left[\mathbf{I} - \mathbf{T}\right]^{-1} , \tag{3.17}$$

where $\mathbf{I} \in \mathbb{R}^{(N+1)\times(N+1)}$ is the identity matrix. We remark the the inverse matrix $[\mathbf{I} - \mathbf{T}]^{-1}$ always exists, because it is easy to show that $\mathbf{T}$ has spectral radius $\rho(\mathbf{T}) < 1$.

Equation (3.17) gives the relation between the idle packet generation probability q_l, the effect of routing (through the matrix $\mathbf{M}$), and the performance at MAC layer (through the link reliability R_l). To obtain the multi-hop network model, we couple Equation (3.17) with the expressions for τ_l, α_l, and R_l, as obtained by Equations (3.2), (3.4), and (4.2). Furthermore, in the derivation of the busy channel probability in multi-hop networks due to ACK transmission $\alpha^{\mathrm{mh}}_{\mathrm{ack},l}$, we replace Equation (3.6) by

$$\alpha^{\mathrm{mh}}_{\mathrm{ack},l} = L_{\mathrm{ack}} \sum_{j \in \Omega_i} \sum_{h \in \Delta_j} q_h T_{i,j} , \tag{3.18}$$

which includes the effect of limited carrier sensing range at the destination and the routing matrix $\mathbf{M}$. Recall that Δ_j is the set of children nodes of V_j and the index i refers to the transmitting node in link l.

We derive the end-to-end reliability of V_i by the product of each link reliability in the path to V_0. Similarly, the end-to-end delay is the sum of the delays in the path from the transmitter V_i to the root node V_0. The energy consumption for each node considers that nodes are in idle-listen state during the idle-queue stage in the Markov chain and include the cost for receiving packets and transmitting ACKs. Consequently, Equation (3.16) is extended in the multi-hop case to

$$\begin{aligned} E^{\mathrm{mh}}_{\mathrm{tot},l} =& P_i \sum_{i=0}^{m} \sum_{k=1}^{W_i-1} \sum_{j=0}^{n} b^{(l)}_{i,k,j} + P_{sc} \sum_{i=0}^{m} \sum_{j=0}^{n} b^{(l)}_{i,0,j} \\ &+ P_t \sum_{j=0}^{n} \sum_{k=0}^{L-1} (b^{(l)}_{-1,k,j} + b^{(l)}_{-2,k,j}) + P_i \sum_{j=0}^{n} (b^{(l)}_{-1,L,j} + b^{(l)}_{-2,L,j}) \\ &+ \sum_{j=0}^{n} \sum_{k=L+1}^{L+L_{\mathrm{ack}}+1} (P_r\, b^{(l)}_{-1,k,j} + P_i\, b^{(l)}_{-2,k,j}) + (P_r L + P_i + P_t L_{\mathrm{ack}}) \\ &\cdot \sum_{h \in \Delta_i} q_h T_{h,j}\, b^{(l)}_{\mathrm{idle}} + P_i \left(1 - (L + L_{\mathrm{ack}} + 1) \sum_{h \in \Delta_i} q_h T_{h,j} \right) b^{(l)}_{\mathrm{idle}} . \end{aligned} \tag{3.19}$$

3.5 Simulation Results

In this section, we present extensive Monte Carlo simulations to validate our analysis. The simulations are based on the specifications of the IEEE 802.15.4 [4] with several values of the traffic pattern and node sensing range. We set the MAC parameters to $m_0 = 3$, $m = 4$, $m_b = 7$, $n = [0\,,\, 1]$, $L = 7$, $L_{\mathrm{ack}} = 2$. Other settings give results similar to those discussed next. First, we consider single-hop and then multi-hop networks.

3.5.1 Single-hop Network

In this first set of simulation results, we validate the model proposed in Section 3.3 for a single-hop topology, see Figure 3.1a.

We consider two basic scenarios to study the impact of hidden terminals, namely $|\Omega_l| = N$, which is denoted by *full sensing* capability, and $|\Omega_l| = 3$ which represents *reduced sensing* capability (the neighborhood is composed by the root node V_0 and two adjacent nodes).

Figure 3.4 shows the average reliability computed over all the links for a single-hop network with homogeneous traffic. On the x-axis the node packet generation rate is reported. Results are shown for different sizes of the network ($N = 7$, $N = 14$), and by considering both full and reduced sensing capabilities. As a reference, we report the reliability obtained from the single-hop homogeneous model with

full sensing capabilities, which was presented in [39] and experimentally validated in [42], and here is readapted to the unslotted mechanism of IEEE 802.15.4. A good agreement between simulations and analytical results is observed. By reducing the carrier sensing capabilities, the model proposed in this thesis allows us to observe a negative impact on the reliability, which cannot be predicted by the earlier model proposed in [39] and [42]. However, in the case of full sensing capabilities, our proposed model coincides with the unslotted version proposed in [39] and [42]. There is a small gap between the two models for high traffic and number of nodes, due to the different assumption in the derivation of the busy channel probability, as we motivated in Section 3.3.1.

In Figure 3.5 we present the average delay over all the links for a single-hop network with homogeneous traffic by varying the node packet generation rate. As for the reliability, results are shown for different sizes of the network ($N = 7$, $N = 14$), and by considering both full and reduced sensing capabilities. There is a good matching between the simulations and the analytical model. The small gap when the traffic rate increases is due to the assumption of independent busy channel probabilities. This effect depends on the size of packets. As we discuss later in Section 3.5.3, our model compensates for this effect and it is a better approximation than the one in [39] and [42]. We notice here that nodes with reduced sensing capability have a positive effect on the delay performance. This is in contrast with the effect on the reliability in Figure 3.4. The reason is that the average delay is evaluated only for successfully received packets: reduced sensing capabilities decrease the number of competitor nodes for the free channel assessment, thus decreasing the busy channel probability, which in turn decreases the average delay.

In Figure 3.6, the analysis is reported for the node energy consumption. We show the results for default MAC parameters with $n = 1$. The energy consumption is dominated by the actual traffic for each node, because the cost for transmitting and receiving packets is much higher than the other cost components. For this reason, reduced sensing capabilities, which influence the number of collisions, have a stronger impact on the energy consumption with respect to an increasing of the size of the network from $N = 7$ to $N = 14$ nodes. Furthermore, with $N = 14$, the number of transmissions reduces with respect to $N = 7$ due to the higher probability that a packet is discarded due to channel access failures.

Let us consider now the interaction between a heterogeneous traffic and the reduced sensing capability of the single-hop topology of Figure 3.1a. In Figure 3.7, we report the link reliability associated to each node. We plot analytical results and simulation of the reliability for a single-hop network with $N = 7$ nodes. In the *homogeneous* case, each node generates the same traffic $\lambda_l = 5$ pkt/s, $l = 1, \ldots, N$. In the *heterogeneous* case, node V_4 generates a traffic $\lambda_4 = 20$ pkt/s, while the rest of the network has nodes with $\lambda_l = 5$ pkt/s. The effect of an increased traffic of V_4 leads to a decreasing of the reliability in the rest of the network, whereas the reliability of V_4 is only marginally affected. This effect is more significant when there are reduced sensing capabilities.

In Figure 3.8, we report the delay associated to each node. With full sensing

capabilities, the effect of an increased traffic in V_4 is an increasing of the delay in the rest of the network, whereas the delay of V_4 is not affected. With reduced sensing capabilities, it is interesting to notice that the delay increases only for nodes that are in the sensing range of V_4 (i.e., V_3 and V_5).

In Figure 3.9, we show the energy consumption for each node. The increasing traffic on V_4 in the heterogeneous condition affects significantly its own energy consumption in both full and reduced sensing capabilities, and in a lower quantity, it increases the energy consumption of nodes outside its sensing range. Nodes V_3 and V_5, which are in the sensing range, are not noticeably influenced.

We conclude that heterogeneous traffic conditions and hidden terminals have remarkable and complex effects on each one of the performance indicators (reliability, delay, and energy consumption), and the effects are well predicted by our model. In particular, dominant nodes, namely nodes with heavy forwarded traffic load, affect negatively the performance of the other nodes of the network. In the next section, we show how routing decisions are influenced by traffic, carrier sensing range and performance indicators in multi-hop networks.

3.5.2 Multi-hop Network

In this section, we validate the analysis for multi-hop networks proposed in Section 3.4. We consider the topology of Figure 3.1b. However, the results we present are general and can be applied to any topology. Without loss of generality, we also assume that each node generates the same traffic, but the forwarded traffic from each node varies as a consequence of the multi-hop routing. We focus on two cases, which we denote by *Path 1* and *Path 2*. In Path 1, we analyze the end-to-end reliability from node V_7, which routes its packets along the path V_4–V_1 to the root node V_0. In Path 2, V_7 forwards its packets along the path V_6–V_3. We also distinguish between *isolated* and *coupled* paths. Coupling happens when the carrier sensing range of nodes in a path includes nodes in the other path, up to two hops away. In the isolated case, nodes along the two paths (Path 1 and Path 2) do not sense each other, with exception of V_0.

In Figure 3.10, we report the end-to-end reliability from node V_7 to the root node V_0, by varying the node packet generation rate, when the two paths are isolated. From both analytical results and simulations, Path 2 outperforms Path 1 in terms of reliability and the difference increases as the traffic increases, since Path 2 has lower traffic load than Path 1.

Figure 3.11 shows the end-to-end reliability for analytical model and simulations of the multi-hop network where Path 1 and Path 2 are coupled. Compared to Figure 3.10, the result is different and the best performance in terms of reliability is now on Path 1. Nodes in Path 1 result to be dominant in terms of traffic load and affect negatively the performance of nodes in Path 2. The reason is that the reliability of a contention access scheme increases as the average number of contenders in each time unit reduces. Consider a routing metric based only on on the maximization of the end-to-end reliability. If there is a strong coupling in

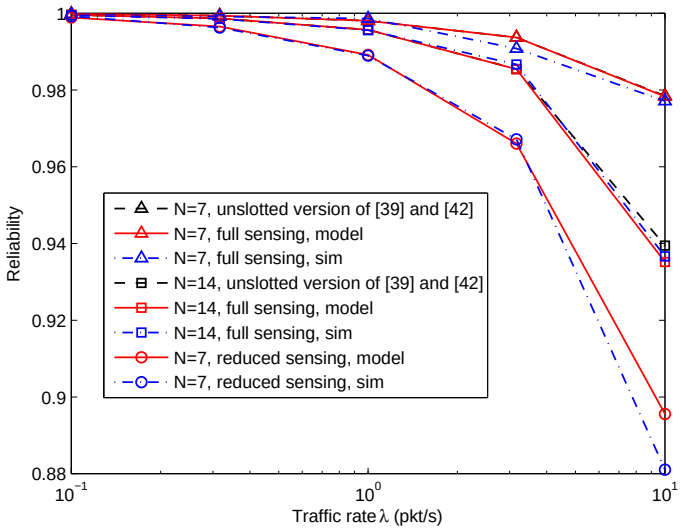

Figure 3.4: Reliability vs traffic rate λ for the single-hop topology of Figure 3.1a. Full sensing and reduced sensing corresponds to $|\Omega_l| = N$ and $|\Omega_l| = 3$, respectively. Unslotted version of [39] and [42] refers to the single-hop model presented in [39], and experimentally validated in [42], which is limited only to the homogeneous case. Note that for $N = 7$ and full sensing the curve of the proposed model coincides with the unslotted version of [39] and [42].

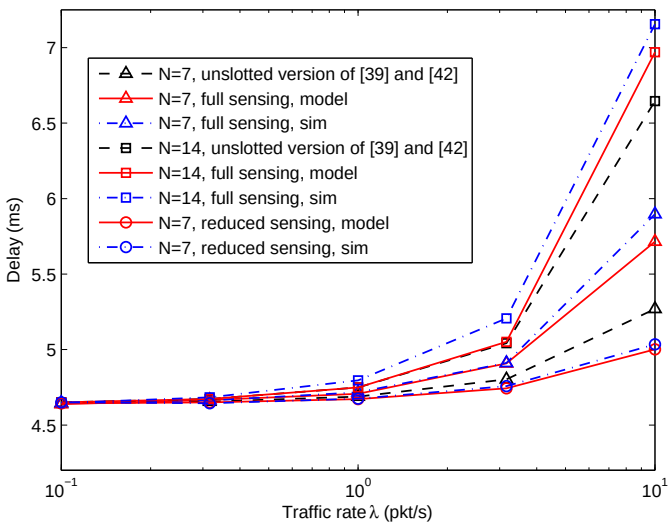

Figure 3.5: Delay vs traffic rate λ for the single-hop topology of Figure 3.1a: Full sensing and reduced sensing corresponds to $|\Omega_l| = N$ and $|\Omega_l| = 3$, respectively.

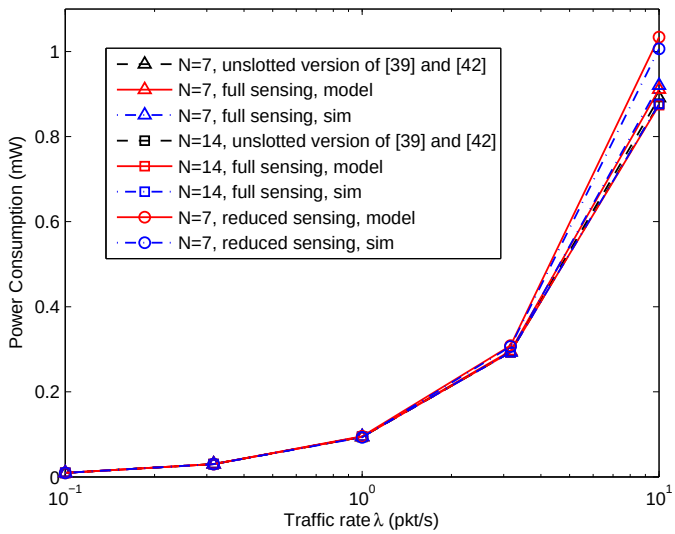

Figure 3.6: Energy consumption vs traffic rate λ for a single-hop topology of Figure 3.1a: Full sensing and reduced sensing corresponds to $|\Omega_l| = N$ and $|\Omega_l| = 3$, respectively.

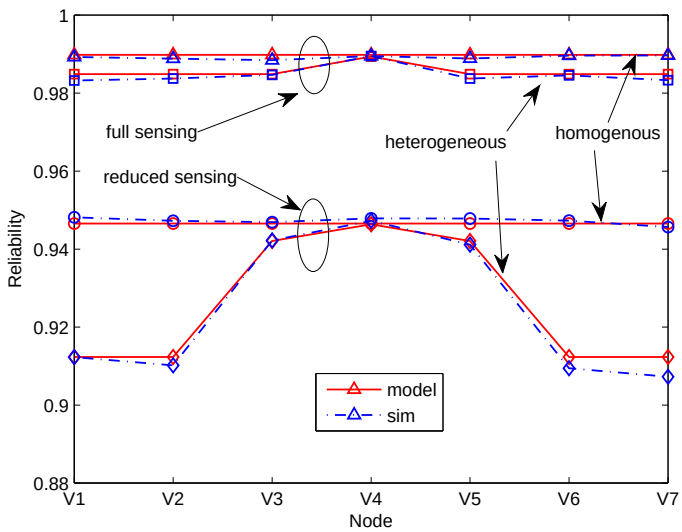

Figure 3.7: Reliability of each node for a single-hop topology in Figure 3.1a: Full sensing and reduced sensing corresponds to $|\Omega_l| = N$ and $|\Omega_l| = 3$, respectively. In homogeneous case, $\lambda_l = 5$ pkt/s, for $l = 1, \ldots, N$. In heterogeneous case, $\lambda_4 = 20$ pkt/s, $\lambda_l = 5$ pkt/s, for $l \neq 4$.

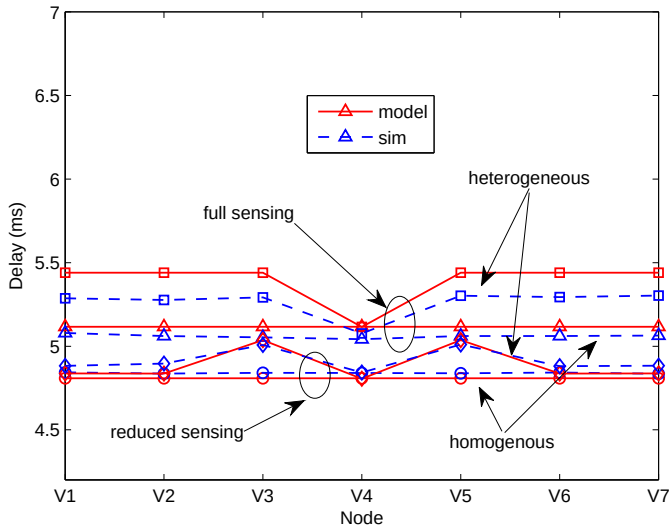

Figure 3.8: Average node delay for a single-hop topology of Figure 3.1a. Full sensing and reduced sensing corresponds to $|\Omega_l| = N$ and $|\Omega_l| = 3$, respectively. In homogeneous case, $\lambda_l = 5$ pkt/s, for $l = 1, \ldots, N$. In heterogeneous case, $\lambda_4 = 20$ pkt/s, $\lambda_l = 5$ pkt/s, for $l \neq 4$.

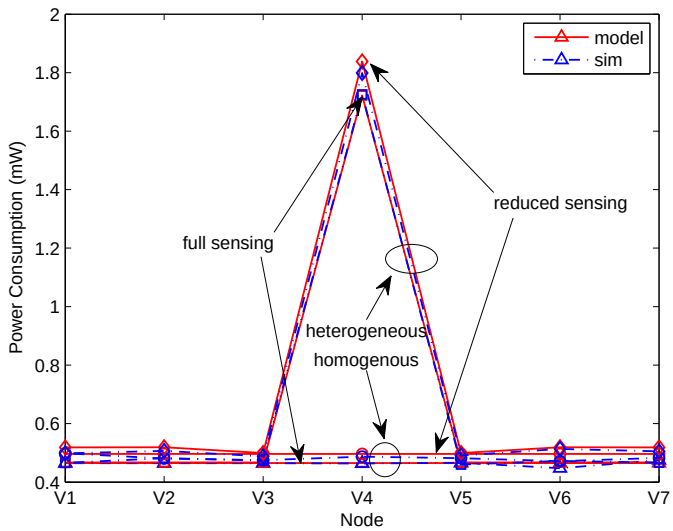

Figure 3.9: Node energy consumption for the single-hop topology of Figure 3.1a: Full sensing and reduced sensing corresponds to $|\Omega_l| = N$ and $|\Omega_l| = 3$, respectively. In homogeneous case, $\lambda_l = 5$ pkt/s, for $l = 1, \ldots, N$. In heterogeneous case, $\lambda_4 = 20$ pkt/s, $\lambda_l = 5$ pkt/s, for $l \neq 4$.

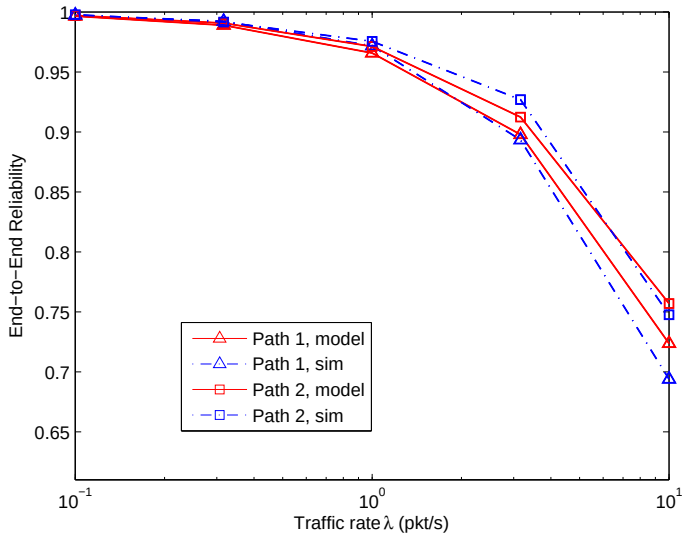

Figure 3.10: End-to-end reliability for isolated paths of the multi-hop topology of Figure 3.1b. Path 1 is V_7-V_4-V_1-V_0, when the link V_7-V_6 is disabled. Path 2 is V_7-V_6-V_3-V_0, when the link V_7-V_4 is disabled. Notice the different scale on the y axis compared to the link reliability in Figures 3.4 and 3.7.

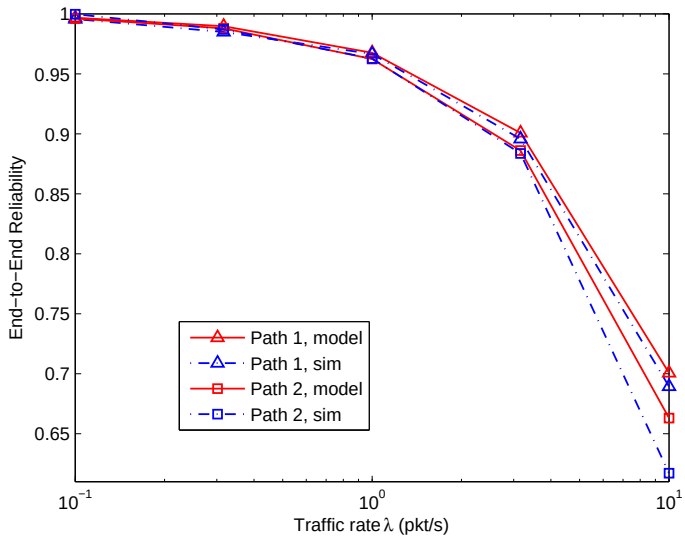

Figure 3.11: End-to-end reliability for coupled paths for a multi-hop topology of Figure 3.1b. Path 1 is V_7-V_4-V_1-V_0, when the link V_7-V_6 is disabled. Path 2 is V_7-V_6-V_3-V_0, when the link V_7-V_4 is disabled.

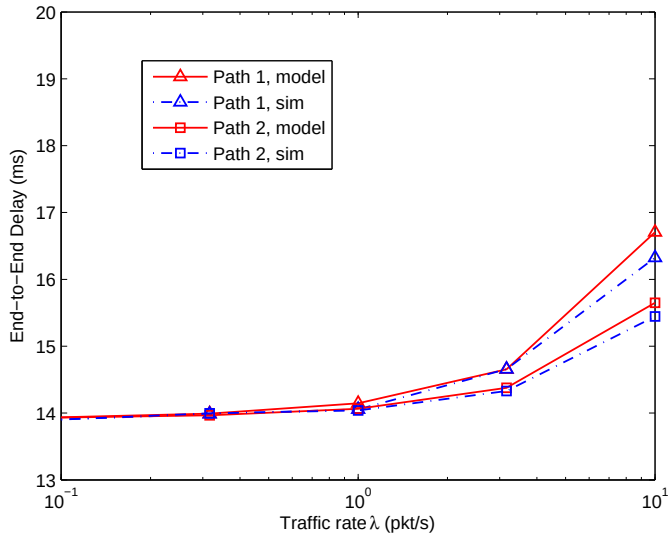

Figure 3.12: End-to-end delay for isolated paths for the multi-hop topology of Figure 3.1b. Path 1 is V_7-V_4-V_1-V_0, when the link V_7-V_6 is disabled. Path 2 is V_7-V_6-V_3-V_0, when the link V_7-V_4 is disabled.

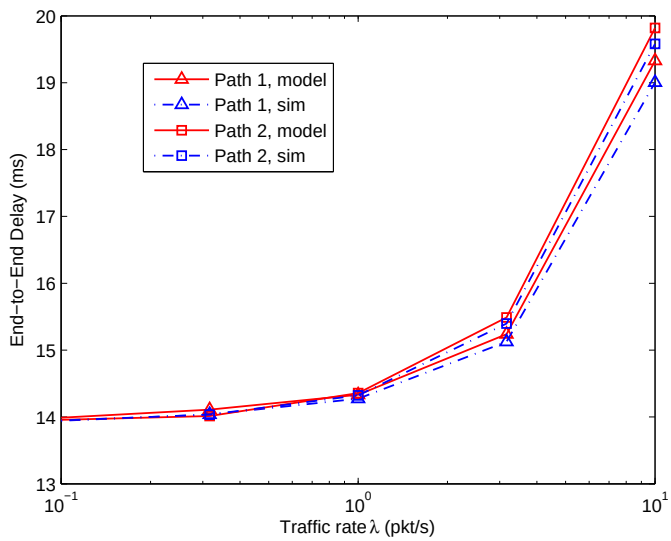

Figure 3.13: End-to-end delay for coupled paths for the multi-hop topology of Figure 3.1b. Path 1 is V_7-V_4-V_1-V_0, when the link V_7-V_6 is disabled. Path 2 is V_7-V_6-V_3-V_0, when the link V_7-V_4 is disabled.

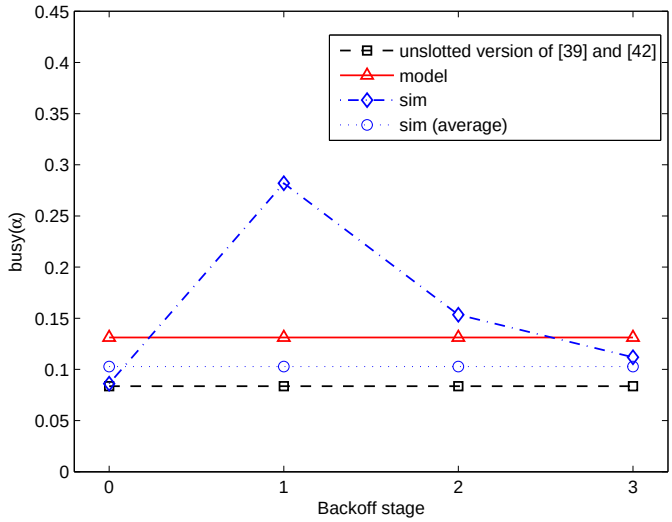

Figure 3.14: Busy channel probability vs. backoff stage for the single-hop topology in Figure 3.1a, with $N = 7$, $\lambda_l = 5$ pkt/s, for $l = 1, \ldots, N$, with full sensing capabilities. Unslotted version of [39] and [42] refers to the single-hop model presented in [39], and experimentally validated in [42], which is limited only to the homogeneous case.

the network, the routing decision leads to unbalanced distribution of traffic load, because the routing layer forces the forwarded traffic to more dominant nodes, so that the average number of contenders in each time unit is lower. If not taken into account, this phenomenon may be catastrophic for the network and cause stability issues when considering limited node buffer size and energy constraints.

In Figures 3.12 and 3.13, the end-to-end delay from node V_7 to the root node V_0 is shown for isolated paths and coupled paths, respectively. Path 2 outperforms Path 1 when the paths are isolated, but Path 1 has a lower delay when the two paths are coupled. Similarly to the reliability analysis, if the routing metric is based only on the minimization of the end-to-end delay, and there is coupling in the network, the result is an unbalanced traffic distribution to dominant nodes. Once again, this could lead to a catastrophic effect.

3.5.3 Model Limitations

In this section, we investigate the limitations of the model for IEEE 802.15.4 multi-hop networks. The basic model assumption is the independent busy channel probability α_l along the backoff stages of the Markov chain. In practice, this is realistic for many situations, but not for all. In Figure 3.14, we report the average busy

channel probability in different backoff stages of the chain (i.e., $i = 0$ $i = 1$, $i = 2$). We consider $N = 7$ nodes with no hidden terminals, MAC parameters $m_0 = 3$, $m = 4$, $m_b = 7$, $n = 0$, traffic rate $\lambda_l = 5$ pkt/s for $l = 1, ..., N$, packet size $L = 7$, ACK size $L_{\text{ack}} = 2$, and we compare results from the analytical model with Monte Carlo simulations. As a reference, we report the busy channel probability obtained from the single-hop homogeneous model with full sensing capabilities, presented in [39] and [42]. The simulation results show a significant increasing of the busy channel probability between the initial backoff stage ($i = 0$), and the second backoff stage ($i = 1$), then the probability decreases in the following backoff stages to agree with the analysis. The reason of this increasing is due to the transmission time (of packets plus ACKs), which is not negligible with respect to the backoff time. If the channel is busy after the initial backoff, there is a certain probability that the same transmission is still ongoing after the second backoff. This probability reduces as the backoff increases in the following stages. In [39] and [42], as in the previous literature, the busy channel probability is constant for the entire network. As we see in Figure 3.14, the value predicted by the theoretical model well approximates the busy channel probability of the simulation in the initial backoff ($i = 0$), but it underestimates the average busy channel probability. Our multi-hop model assumes that for each node V_l, α_l is computed independently of the busy channel probability of other nodes. This analytical approach tends to overestimate the busy channel probability in the initial backoff stage but it compensates for the increasing of α_l in the following backoff stages.

The analytical derivation of the impact of packet size on the busy channel probability in the different backoff stages is a formidable task. However, as shown in the previous sections, an approximation by a busy channel probability that is independent of the packet size is accurate enough to derive the network reliability, delay, and energy consumption.

3.6 Summary

In this chapter we proposed a new framework for the analysis of multi-hop networks using the unslotted IEEE 802.15.4 MAC protocol. We proposed an analytical model that includes the important features of multi-hop networks, such as heterogeneous distribution of the traffic and hidden terminal nodes. We showed the mutual influence between routing decisions and MAC performance in terms of reliability, delay, and load balancing.

Table 3.15: Main symbols used in Chapter 3.

α_i	busy channel probability of node V_i
λ_i	packet generation rate of node V_i
$\pi_{i,j}$	routing metric in link (i, j)
τ_i	probability of node V_i attempting CCA
Γ_i	parent set of node V_i
Δ_i	children set of node V_i
Ω_i	neighborhood set of node V_i
$\Omega_{j/i}$	hidden node set of V_i with respect to V_j
m_0	initial backoff exponent
m	maximum number of backoffs
m_b	maximum backoff exponent
n	maximum number of retransmission
q_i	packet generation probability of node V_i in idle state
t_{ack}	ACK waiting time
$t_{m,\text{ack}}$	timeout of ACK
D_l	delay for link l
G	number of links in the network
L	packet length
L_{ack}	ACK length
L_c	packet collision time
L_s	successful packet transmission time
$\mathbf{M}$	traffic distribution matrix
N	number of nodes in the network
$P_{\text{coll},l}$	probability of collision of IEEE 802.15.4
P_i	energy (per unit time) spent during idle-listening
P_t	energy (per unit time) spent during packet transmission
P_r	energy (per unit time) spent during packet reception
P_{sp}	energy (per unit time) spent in sleeping state
Q_l	forwarded traffic rate in link l
R_l	reliability for link l
S_b	backoff unit duration
$\mathbf{T}$	routing matrix
T_{sc}	channel sensing time
V_i	i-th node
W_i	backoff window size at backoff i

Chapter 4

Protocol Design for Energy Efficient Wireless Networks

In this chapter we study the design of energy efficient protocols for control and actuation applications. We consider a multi-hop low power network that is deployed to measure state information in specific regions needed to a remote controller for real-time actions. Recalling the general flow diagram in Figure 4.1, we extend the analysis of the communication loop (MAC and routing) by including the influence of tunable performance requirements from the control application. In agreement with the fundamental approach followed in this thesis, we consider the following performance requirements:

- Reliability: data must be sent to the controller with a guaranteed probability of success.
- Delay: data must reach the controller within a certain deadline.

The objective is to minimize the total energy consumption of the network, while guaranteeing the performance requirements. The efficient design and operations of a multi-hop network for these applications require extra challenges with respect to the modeling study in Chapter 3. In particular, we are interested in implementation-oriented solutions, in which energy efficient, reliable, and low delay operations are designed for a specific control application to offer:

- A simple algorithm: protocol operations must be simple and computationally light to be embedded in resource constrained network nodes.
- Dynamic adaptation: the protocol should consider and adapt to the time-varying traffic and channel conditions.

We consider all the aforementioned features and offer a holistic design approach to develop TREnD[1], a cross-layer protocol for energy efficient wireless networks for

[1]The acronym aims to remark the four significant characteristics of the protocol, namely, timeliness, reliability, energy efficiency, and dynamic adaptivity.

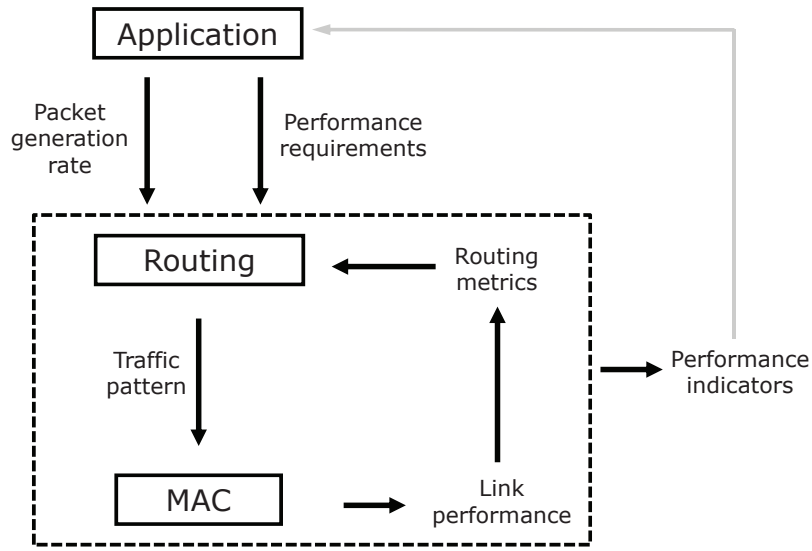

Figure 4.1: Layers interaction for modeling and design: TREnD protocol for control applications. The effects of performance indicators on the controller synthesis are not considered.

industrial control and automation applications. TREnD is designed by addressing the routing specifications of ROLL [13], and in compliance with IEEE 802.15.4 [4] standard.

This chapter starts by introducing related works on communication protocols for industrial control. The system model is then introduced followed by a description of the protocol stack. The optimization problem is then described and the protocol operation is illustrated. After this, we describe the fundamental limitations of the protocol. Finally, experimental results are presented and discussed. The chapter concludes with a brief summary.

4.1 Related Works

In Chapter 2, a survey of existing MAC and routing protocols for energy efficient wireless networks is presented. System level design approach and related literature are introduced and described in Section 2.1. In this section, we focus on relevant protocol design solutions for industrial applications to highlight the original characteristics of TREnD.

In Table 4.2, we report relevant protocols for industrial applications by evidencing different performance indicators (energy consumption, reliability, delay) and

Table 4.2: Protocol Comparison - The letters **E**, **R**, and **D** denote energy, reliability, and delay. The circle denotes that a protocol is designed by considering the indication of the column, but it has not been validated experimentally. The circle with plus denotes that the protocol is designed by considering the indication and experimentally validated. The dot denotes that the protocol design does not include indication and hence cannot control it, but simulation or experiment results include it. Physical, medium access, routing, and transport layers are denoted by PHY, MAC, ROU, and TRA, respectively.

Protocol	E	R	D	Layer
GAF [54]	◯	·	·	MAC, ROU
SPAN [55]	◯	·	·	MAC, ROU
GERAF [56]	◯		◯	MAC, ROU
Dozer [57]	⊕	⊕		MAC, ROU
ESRT [58]		◯		MAC
RMST [59]		◯		MAC, TRA
Flush [60]		⊕		MAC
MMSPEED [61]		◯	◯	ROU
SERAN [16]	◯		◯	MAC, ROU
Breath [62]	⊕	⊕	⊕	PHY, MAC, ROU
TREnD	⊕	⊕	⊕	PHY, MAC, ROU

communication layer.

The GAF [54] and SPAN [55] protocols mainly consider the energy efficiency as performance indicator. GAF and SPAN propose algorithms to achieve the energy efficiency under the routing layer and above the MAC layer. The simulation results of reliability and delay reported in [54] and [55] do not consider an accurate analysis. One of the first protocol for wireless networks designed to offer a high reliability is RMST [59], but no delay and energy consumption of the network have been accounted for. The same lack of energy efficiency and delay constraints can be found in the reliable solutions presented in [58] and [60]. Energy efficiency with a delay requirement for a MAC and randomized routing is considered in GERAF [56], without simulation or experimental validation. Dozer [57] comprises MAC and routing layers to minimize the energy consumption while guaranteeing a reliability constraint, without considering an analytical study. Experimental results of Dozer show good performance in terms of energy efficiency and reliability under very low traffic intensity, but the delay is not explicitly considered. The purposes of these protocols are the maximization of energy efficiency or reliability or minimization of the delay without considering any specific application requirement. In other words, none of these protocol supports the dynamic adaptation to changes of the

application requirements.

MMSPEED [61], SERAN [16], and Breath [62] are protocols that explicitly support application requirements. The MMSPEED routing protocol proposes simultaneous optimization of reliability and delay, but no energy consumption is considered. The protocol satisfies the high reliability constraint by using the duplicated packets of multi-path. However, these duplicated packets will increase the traffic load with negative effect on the stability and energy efficiency. In SERAN [16] and Breath [62] a relevant system-level design methodology has been presented for control application over WSNs. However, SERAN does not support average-high traffic regimes and tunable reliability requirements, which limits the applicability. Furthermore, load balancing and fair duty cycling are not taken into account in SERAN. On the other hand, Breath is limited to scenarios with line topologies and source nodes at the edge of the network. We conclude that, to the best of our knowledge, there is no protocol from the literature suitable for control applications over WSNs, that is able to embrace all the techniques that concur to the energy efficiency (radio power control, MAC, routing, duty-cycling, and load balancing) and, at the same time, able to guarantee reliability and delay constraints over multi-hop communication.

The original contribution of TREnD is a novel protocol stack for the class of industrial control applications in clustered multi-hop wireless networks. TREnD is based on a simple algorithm that allows the network to adapt dynamically to requirements variations typical of controllers. In contrast to SERAN and Breath, we adopt a novel MAC solution based on sleeping discipline and a beacon mechanism, that offers high reliability and energy efficiency, and we assume a uniform distribution of sensing nodes throughout the network. An original analysis of the performance of TREnD is provided. Finally, TREnD is completely implemented on Tmote Sky sensors [63] by using TinyOS [64]. The experimental results allow us to assess the theoretical analysis and the protocol performance.

4.2 System Model

TREnD considers a general scenario for an industrial control application: the state of a plant must be monitored at locations where cabling is not available or cannot be extended, so that wireless sensor nodes are an appealing technology.

Information taken by nodes, which are uniformly distributed in clusters, are sent to the sink node by multi-hop communication. The clustered topology is motivated by the energy efficiency, since transmitting data directly to the sink may consume more than routing through relays. The cluster formation is conducted according to the DODAG formation of ROLL (see Section 2.5). Specifically, nodes with same rank at routing layer are grouped into clusters.

In Figure 4.3, the system model is reported. Nodes are deployed in an indoor environment with rooms. Each dotted curve defines a cluster of nodes. To simplify the analysis, we assume that nodes of a cluster are allowed to send packets only to

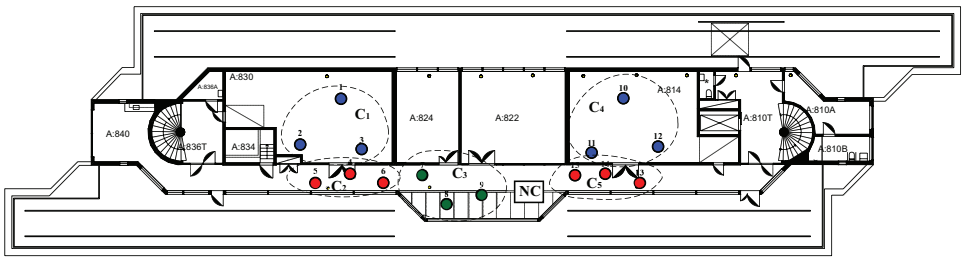

Figure 4.3: System model scenario: a test-bed of 15 nodes is deployed in the Automatic Control laboratory at KTH.

the nodes of next cluster toward the root node. The root node is directly connected to the controller, which takes appropriate actions upon the timely and reliable reception of source information.

We assume that the controller knows cluster locations and the average number of nodes in each cluster, and nodes know to which cluster they belong (through the rank computation). We assume that the neighborhood set of each node includes all nodes in the same cluster and nodes in the parent and children cluster, so that the hidden terminal problem is avoided. The controller estimates the amount of data generated by each cluster, which is used to adapt the protocol to the traffic regime. These assumptions are reasonable in industrial environments [5].

A list of all symbols used in this chapter is reported in Table 4.14, at the end of the chapter.

4.3 TREnD Protocol Stack

In this section, we introduce the protocol stack of TREnD.

Similarly to SERAN [16], the routing algorithm of TREnD is hierarchically subdivided into two parts: a static route at inter clusters level and a dynamical routing algorithm at node level. This is supported at the MAC layer by an hybrid TDMA/CSMA solution.

The static schedule establishes which one is the next cluster to which nodes of a given cluster must send packets, by calculating the shortest path from every cluster to the controller. The network controller runs a simple combinatorial optimization problem of delay-constrained minimum spanning tree generation [65]. Alternatively, if the number of clusters is large, the static routing schedule is pre-computed off-line for a set of cluster topologies and stored in the sink node in a look-up array. No intra cluster packet transmission is allowed, which is reasonable for routing loop prevention.

The static routing algorithm is supported at MAC level by a weighted TDMA scheme that regulates channel access among clusters. Nodes are awake to transmit and receive only during the TDMA-slot associated to the cluster for transmission

and reception, respectively, thus achieving consistent energy savings. The organization of the TDMA-cycle must consider the different traffic regimes depending on the cluster location. Since clusters closer to the sink may experience higher traffic intensity, more than one transmitting TDMA-slot is assigned to them. It is natural to first forward packets of clusters close to the controller, since this minimizes the storage requirement in the network. To minimize the global forwarding time, the evacuation of packets of a cluster is scheduled path-by-path. By following these rules, the controller is able to generate an appropriate TDMA scheduling table.

The dynamic routing is implemented by forwarding the packets to a node within the next-hop cluster in the path chosen at random, as proposed in [29] and [56]. In such an operation, no cluster-head node is needed within clusters, and nodes need to be aware only of the next-hop cluster connectivity. The procedure for random selection of next-hop node is performed by considering a duty cycling in the receiving cluster combined with beacon transmissions.

The communication stage between nodes during a TDMA-slot is managed at MAC layer by a receiver-initiated p-persistent CSMA/CA scheme, to offer flexibility for the introduction of new nodes, robustness to node failures, and support for the random selection of next-hop node. As we will see in Section 4.7, in hybrid TDMA/CSMA solutions our receiver-initiated p-persistent MAC gives better performance than the standard BEB mechanism used by IEEE 802.15.4, which we illustrated in Section 2.3.2. However, TREnD is implemented to support the BEB mechanism in the dynamic MAC, in order to be compliant with the standard.

MAC operations of nodes are illustrated in Figure 4.4 and described in the following. Each node in the transmitter cluster having a packet to be sent wakes up in CSMA-slots with probability τ and enters in listening state. At the receiver cluster, each node wakes up with probability ω and multicasts a small length of beacon message to the nodes in the transmitter cluster. An awake node that correctly receives the beacon at the transmitter side, senses the channel and, if clean, tries to unicast its packet to the beacon sender. An acknowledgement (ACK) may conclude the communication if a retransmission mechanism is implemented. If no beacon is sent or there is a collision, the awake nodes in the transmitter cluster keep on listening in the following CSMA-slot with probability τ or go to sleep with probability $1 - \tau$.

To compare TREnD and SERAN [16], we recall that SERAN communication is initiated by the transmitter. The drawback of SERAN is that nodes in the receiver cluster have to be listening for the overall TDMA-slot duration, due to a contention-based transmission of the ACKs. In TREnD, the selection of the forwarding nodes follows a random policy regulated by ω. The main advantage of this novel solution is the absence of delays between packets exchange during a CSMA-slot. This allows TREnD to work with a much higher traffic regime when compared to SERAN.

TREnD offers the option of data aggregation to fairly distribute the traffic load and energy consumption among clusters. The aggregation has the advantage of reducing the number of TDMA-slots per cluster and of the traffic for clusters closer to the sink. However, packet aggregation gives significant advantages only when the

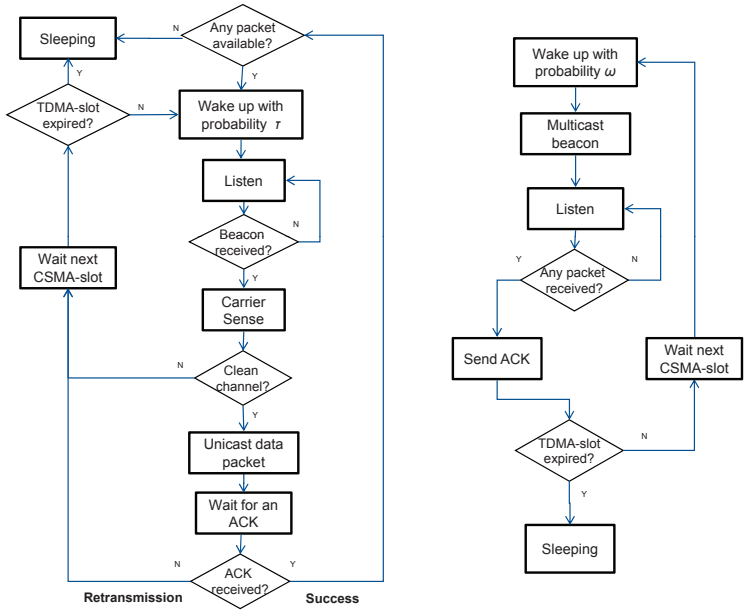

Figure 4.4: MAC operations of TREnD in transmission and reception.

traffic is sufficiently high, as we will see in Section 4.7, because nodes have to idle-listen longer to catch more than one packet per time and perform the aggregation, and idle-listening is energy inefficient.

4.4 Protocol Optimization

In this section, we pose and solve an optimization problem to select the TREnD protocol parameters by minimizing the overall energy consumption of the network under reliability and delay constraints:

$$\min_{S,\tau,\omega} \quad E_{\text{tot}}(S,\tau,\omega) \tag{4.1}$$

$$\text{s.t} \quad R(S,\tau,\omega) \geq R_{\min} \tag{4.2}$$

$$\Pr[D(S,\tau,\omega) \leq D_{\max}] \geq \delta\,. \tag{4.3}$$

In this problem, $E_{\text{tot}}(S,\tau,\omega)$ is the total energy consumption of the network, $R(S,\tau,\omega)$ is the reliability constraint, and $R_{\min}$ is the minimum desired reliability imposed by the control application. We denote by $D(S,\tau,\omega)$ the random variable describing the distribution of the delay, by $D_{\max}$ the maximum delay desired by the control application, and by δ the minimum probability with which such a maximum delay should be achieved. The parameters $R_{\min}$, $D_{\max}$, and δ are the requirements

of the control application. The decision variables of the optimization problem are the TREnD parameters, namely the TDMA-slot duration S, the wake up probability in transmission τ, and the wake up probability in reception ω. In the following, we develop the expressions needed in the optimization problem, and derive the solution. Since such a solution must be implemented by a computationally affordable algorithm solved at the sink node of the network, thus the expressions are derived by doing simplifications and approximation without giving up to the accuracy, as we show later.

4.4.1 Reliability Constraint

In this section, we study the reliability constraint in Equation (4.2). Considering a single CSMA-slot, in which p-persistent CSMA and duty cycling in reception are used, we have the following result:

Claim 4.4.1. *Let k be the number of packets awaiting to be forwarded in the cluster. Then, the probability of successful transmission is*

$$p_k = \gamma\, p_{\mathrm{bc}} \left(1 - (1-\tau)^k\right) (1 - p_{\mathrm{cl}})^{\tau(k-1)}, \tag{4.4}$$

where $p_{\mathrm{bc}} = \gamma N \omega (1-\omega)^{N-1}$ is the successful beacon probability and p_{cl} is the probability of an erroneous sensing of a node, when it competes with another node.

Proof. A proof is provided in Appendix B. □

In TREnD, a radio power control is implemented, so that the attenuation of the wireless channel is compensated by the radio power, which ensures a desired packet loss probability, as proposed in [62] and [66]. As a consequence of the power control, the channel is abstracted by a random variable with good channel probability γ. Such a modeling has been adopted also in other related works (e.g., [16], [59]). Considering the collision probability p_{cl}, we observe that for optimization purposes an upper bound suffices. Experimental results, presented later, show that a good upper bound is $p_{\mathrm{cl}} = 0.2$.

By using Claim 4.4.1, we derive the following result:

Claim 4.4.2. *Let $V(n) = \{1 - p_n, 1 - p_{n+1}, ..., 1 - p_k\}$, where p_n is given in Equation (4.4) and let $A(n) = [a_{i,j}]_{M_c}^{S-k+n}$ be a matrix containing all the M_c combinations with repetition of the elements in $V(n)$, taken in groups of $S - k + n$ elements. Let $h_{\max}$ be the maximum number of hops in the network. Then, the reliability of TREnD is*

$$R(S, \tau, \omega) = \left[\sum_{n=0}^{k} \frac{k-n}{k} \prod_{l=n+1}^{k} p_l \left(\sum_{i=1}^{M_c} \prod_{j=1}^{S-k+n} a_{i,j} \right) \right]^{h_{\max}}. \tag{4.5}$$

Proof. A proof is provided in Appendix B. □

When packet aggregation is enabled, the following result holds:

Claim 4.4.3. *Let h_i be the number of hops in the path i. Let R_z be the reliability in a single hop when z packets are aggregated. The reliability of a packet that experiences j hops to the controller is*

$$R_j^{\text{ag}}(S,\tau,\omega) = R_{j-1}^{\text{ag}}\, r_{h_i-j+1}\,, \tag{4.6}$$

where $r_j = \sum_{i=1}^{j}(1-r_{i-1})\prod_{z=1}^{j-i+1} R_z$ *, with* $r_0 = 0$ *.*

Proof. A proof is provided in Appendix B. □

If the data aggregation is disabled or the size of aggregated packets does not change significantly, then we simplify Equation (4.6) and obtain the relation in Equation (4.5). The previous claims are verified by experiments in Section 4.7.1.

4.4.2 Delay Constraint

Here we develop the expression of the constraint in Equation (4.3). The furthest cluster from the controller is the one experiencing the highest delay. Therefore, the delay of packets coming from such a cluster must be less than or equal to a given value $D_{\max}$ with a probability δ.

Recalling that the maximum number of hops in the network is $h_{\max}$, an upper bound on the TDMA-slot duration S is

$$S_{\max} = \frac{D_{\max}}{h_{\max}}\,. \tag{4.7}$$

The random variable describing the delay is modeled by

$$D(S,\tau,\omega) = (h_{\max}-1)S + T_e\,,$$

where T_e is a random variable describing the time to evacuate k packets. Then, we provide the following result:

Claim 4.4.4. *The delay constraint in Equation* (4.3) *is well approximated by*

$$\Pr[D(S,\tau,\omega) \le D_{\max}] \approx 1 - \frac{1}{2}\text{erfc}\left(\frac{A-\mu}{\sigma}\right)\,, \tag{4.8}$$

$$\text{where}\quad A = \begin{cases} S & \text{if} \quad S \le \frac{D_{\max}}{h_{\max}} \\ D_{\max} - (h_{\max}-1)S & \text{if} \quad S > \frac{D_{\max}}{h_{\max}} \end{cases}$$

$\mu = \sum_{j=1}^{k} 1/p_j$*, and* $\sigma^2 = \sum_{j=1}^{k}(1-p_j)/p_j^2$*.*

Explanation. Details of the approximation are provided in Appendix B. □

The previous claim is verified by experiments in Section 4.7.1.

4.4.3 Energy Consumption

The total energy consumed by the network over a period of time is given by the combination of two components: listening and transmitting cost[2].

Listening for a time t gives an energy consumption that is the sum of a fixed wake up cost E_w and a time dependent cost $E_{\text{list}}t$. The energy consumption in transmission is given by four components: beacon sending E_{bc}, clear channel assessment E_{cca}, packet sending E_{pkt}, and ACK sending E_{ack}.

Consider a general topology with N nodes and maximum number of hops $h_{\max}$. Let us define W the number of listening TDMA-slots in a TDMA-cycle and the TDMA-cycle duration $T_{\text{cyc}} = SM_s$ where M_s is the number of TDMA-slots in a TDMA-cycle. We have the following result:

Claim 4.4.5. *For a given packet generation rate λ, the total energy consumed in the network in a period T_{tot} is*

$$E_{\text{tot}}(S,\tau,\omega) = \frac{T_{\text{tot}}}{\gamma\, S} \sum_{j=1}^{\lambda T_{\text{cyc}}} j\tau\omega\, E_{\text{cca}} + T_{\text{tot}} M_s \lambda \left(E_{\text{pkt}} + E_{\text{ack}}\right) + \omega\, \frac{N\, W\, T_{\text{tot}}}{M_s} \left(\frac{E_{\text{bc}}}{d} + \frac{E_w}{S} + E_{\text{list}}\right). \tag{4.9}$$

Proof. A proof is provided in Appendix B. □

4.4.4 Protocol Optimization

In the previous sections, we have established the expressions of the energy consumption in Equation (4.9), the reliability in Equation (4.6), and the delay constraint in Equation (4.8). We observe that all these expressions are highly non-linear in the decision variables. Sensor nodes are not equipped with a high processing capacity to use these equations, therefore, we provide a computationally affordable sub-optimal solution to the optimization problem. In the following, we show that such a strategy still gives satisfactorily results.

First, we determine the wake up probability in transmission τ and wake up probability in reception ω, for a given TDMA-slot duration S. Since the main component of the energy consumption in a TDMA-slot is given by the number of channel accesses, the parameters are selected such that the channel utilization is optimized or, equivalently, the reliability is maximized. The following claim provides empirical results on τ and ω.

Claim 4.4.6. *The wake up probability in transmission τ^* and in reception ω^* that maximize the reliability in Equation* (4.5) *depend on S according to the following*

[2]Note that the costs for the initialization of the network are negligible in the energy balance

relations:

$$\tau^* = \frac{c_1}{\lambda\, S\, M_s + c_2}\,, \tag{4.10}$$

$$\omega^* = \frac{1}{N}\,, \tag{4.11}$$

with coefficients $c_1 = 2.17$, $c_2 = 1.81$. *We recall that* λ *is the cluster traffic rate,* M_s *is the number of TDMA-slots in a TDMA-cycle, and* N *is the number of nodes.*

Proof. A proof is provided in Appendix B. □

We note here that such choices are sub-optimal because are limited to strategies with constant wake up probabilities per each node.

By using Equation (4.10) for the wake up probability in transmission and wake up probability in reception, and by assuming S as a real-valued variable, we notice that E_{tot}, given in Equation (4.9), and the reliability R in Equation (4.6) are monotonically decreasing functions of S, while the delay D in Equation (4.8) is a monotonically increasing function of S. It follows that a simple solution for the TDMA-slot duration, S^*, is given by the maximum integer value of S that satisfies the two constraints in problem (4.1). The search of the optimal S is done by a simple additive increasing multiplicative decreasing algorithm, which we initialize at $S^* = S_{\max}$. Indeed, as shown in Section 4.4.2, the delay requirement $D_{\max}$ provides an upper bound for S, given by $S_{\max} = D_{\max}/h_{\max}$.

4.5 Protocol Operation

Suppose that the network user deploys a WSN of nodes implementing the TREnD protocol, and sets the desired control application requirements $R_{\min}, D_{\max}$, and δ. During an initial phase of operation the sink node retrieves the traffic and the cluster topology by the received packets. After computing or reading from a look-up array the static routing schedule and TDMA-cycle, the sink computes the optimal parameters as described in Section 4.4.4. Then, the sink communicates these values to the nodes of the network by DIO messages. Such a message passing procedure ensures synchronization among nodes and allows for initializing and self configuring of the nodes to the optimal working point of the protocol. The DIO messages are then forwarded by the nodes closer to the sink to other nodes of the clusters far away by using the ACK mechanism described in [16]. Such messages need also to be updated so that our protocol adapts dynamically to new nodes added in the clusters, variations in the source traffic, control application requirements, and time drift of the clocks. We experienced that a 20 TDMA-cycles period for the refreshing procedure gives satisfactory performance to maintain an optimal network operation with negligible extra energy consumption.

4.6 Fundamental Limits

The analysis of the fundamental limits of TREnD is critical for the appropriate application of the protocol. In this section, we investigate the minimum reliability and delay requirement, and the minimum number of nodes needed to support the protocol operation.

First, we characterize the minimum CSMA-slot duration d, that the application can set. It holds that

$$d \geq t_b + t_m + t_p + t_a \,,$$

where we consider the packet transmission time t_m, the processing time t_p, the ACK transmission time t_a, and the beacon transmission time t_b. Numerically, we derive that the minimum affordable CSMA-slot size of TREnD is 10 ms, which is compliant with the slotted solution adopted by WirelessHART [2]. This is a strong improvement with respect to SERAN MAC solution where the minimum sustainable CSMA-slot size is 100 ms [16]. Given the limit on d, the range of feasibility for the reliability and delay constraints depends on the traffic rate λ.

From Equation (4.6), the feasible zone of reliability requirement is

$$R_{\min} \leq R(\lambda, d) \,.$$

In addition, from Equation (4.7) we derive a lower bound for the delay constraint,

$$D_{\max} \geq \frac{h_{\max} d}{\lambda T_s} \,.$$

Given a maximum storage capacity C_{st} in number of packets for each node, a lower bound to the number of nodes in a cluster is

$$N \geq \left\lceil \frac{\lambda S M_s}{C_{\text{st}}} \right\rceil \,,$$

where $\lceil x \rceil$ is the ceiling value of x.

4.7 Experimental Implementation and Validation

In this section, we present an implementation of TREnD by using TinyOS 2.x [64] and Tmote Sky nodes [63]. To benchmark our protocol, we implemented also SERAN [16] and the BEB mechanism of the IEEE 802.15.4 [4] standard. We used the default MAC parameters of IEEE 802.15.4 so that the protocol fits in the higher level TDMA structure and routing algorithm of SERAN and TREnD.

We reproduced the reference test-bed topology reported in Figure 4.3, where clusters are placed in an indoor environment. Each cluster is composed by 3 sensors, deployed at random within a circle with one meter radius. We analyze different scenarios with different sets of traffic rate λ and control application requirements

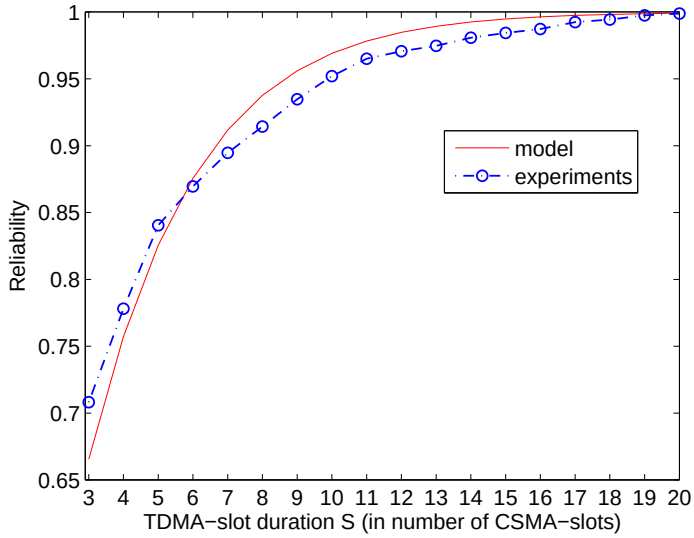

Figure 4.5: Reliability vs. TDMA-slot duration S, for $k = 3$ packets in the cluster and $S \geq k + 1$.

($R_{\min}$, $D_{\max}$, and δ), which we report in Table 4.13. For each scenario, Table 4.13 shows also the optimal TDMA-slot duration and wake up probabilities as obtained by the optimization in Section 4.4.4. We measured the duty cycle of nodes as indicator of the energy efficiency.

4.7.1 Protocol Validation

To validate our analysis, we conducted an experimental measurement campaign to capture the sensitivity of the reliability and delay requirements to variations of the decision variables. Figure 4.5 shows the reliability of TREnD by varying TDMA-slot duration S for $k = 3$ packets in the cluster. The results achieved by experiments follows well the theoretical analysis.

In Figure 4.6, we report the delay analysis by comparing experimental and analytical results. In this case we fixed a large S, and determine average and variance of the evacuation time of a cluster, by varying the number of packets k (i.e, by tuning the wake up probability in transmission τ, according to Equation (4.10)), for a fixed wake up probability in reception in Equation (4.11). The analytical model matches well with the experimental results. In Figure 4.7, we report the delay distribution for cluster C_1 and C_2 (located at 3 and 2 hops), respectively. The furthest cluster presents a larger variance, due to the multi-hop. From the figures, we observe that the Gaussian distribution we have adopted is a fair approximation.

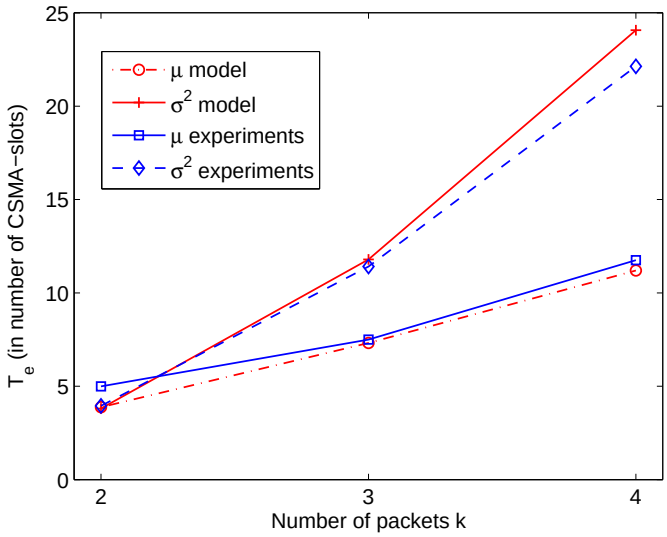

Figure 4.6: Average and variance of the cluster evacuation time T_e vs. the number of packets k in the cluster.

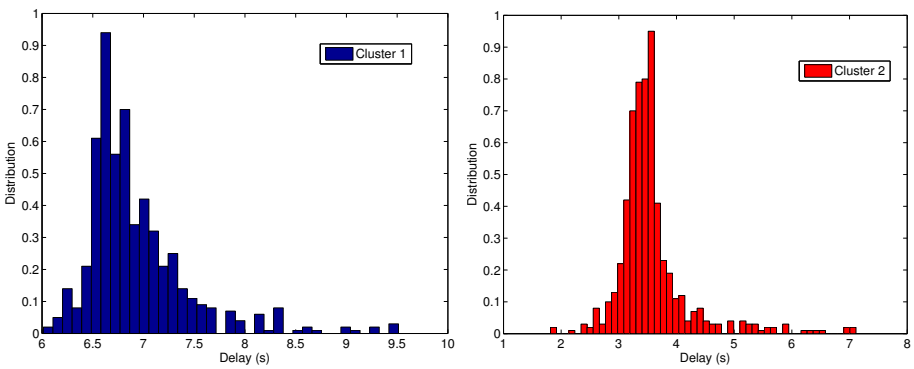

Figure 4.7: Delay distribution for clusters C_1 and C_2.

4.7.2 Performance Comparison

In the first set of experiments, we show the performance improvements in TREnD, when compared to SERAN. In Figure 4.8, the reliability is reported as function of the traffic rate λ, by fixing $R_{\min} = \delta = 95\%$, and $D_{\max} = [3\,,9]$ s. TREnD has high reliability for all traffic rate conditions and SERAN is significantly outperformed. In particular with $D_{\max} = 3$ s, as traffic rate increases over $\lambda = 0.3$ pkt/s, the reliability of SERAN significantly decreases.

In Figure 4.9 we compare the energy consumption of the two protocols, showing the average duty cycle of each node, for fixed $R_{\min} = \delta = 95\%$, $D_{\max} = 3$ s and $\lambda = 0.3$ pkt/s. As discussed above, in this operative condition both SERAN and TREnD meet the reliability and delay constraints. By implementing TREnD with data aggregation, we observe a more balanced duty cycle among clusters, particularly for the last hop clusters. However, the price to pay for having a better load balancing is a slight increasing of the average duty cycle. In fact, TREnD presents a slightly higher duty cycle for most of the nodes, but it reduces of about 30% the energy consumption for nodes 7, 8, and 9 (cluster C_3), which are critical for the network operation since they also forward information from clusters C_1 and C_2. This suggests that packet aggregation is a viable choice only for the clusters supporting high traffic, as those next to the sink. In conclusion, TREnD ensures higher reliability, load balancing, and a longer network lifetime than SERAN, without any significant difference in the complexity of the scheme.

Given these results, in the following performance evaluation of TREnD we disregard SERAN and consider IEEE 802.15.4. We present two sets of experimental results, evaluated for scenarios $\mathcal{L}$ and $\mathcal{H}$ as specified in Table 4.13. Figure 4.10 reports the average values of reliability, delay, and duty cycle as achieved by the experiments for TREnD and IEEE 802.15.4. Data of clusters belonging to the same paths are joined by lines. We see that TREnD always ensures the satisfaction of the reliability and delay constraints specified in Table 4.13. TREnD guarantees much better reliability, in particular for cluster C_1 (3 hops). In fact in C_1, IEEE 802.15.4 does not fulfill the requirement. The average delay of IEEE 802.15.4 is slightly lower than TREnD, but observe that the delay of IEEE 802.15.4 is computed only for packets arriving successfully at the sink. We observe similar behavior also for other scenarios. Finally, we present some results about the duty cycle. According to the traffic load supported by the clusters and their allotted TDMA-slots, we observe that the duty cycle depends on the number of times a cluster wakes up for the forwarding procedure. The duty cycle is the same for the clusters far away from the sink (C_1 and C_4, see Figure 4.3), but for all other clusters TREnD gives a consistent reduction of the duty cycle with respect to IEEE 802.15.4.

We remark here that the duty cycle strongly depends on the traffic load in the network. In Dozer [57], an average duty cycle 0.2% is achieved for a network of 40 nodes with a packet generation period of 120 s each (total traffic load $\simeq 0.3$ pkt/s). TREnD gives an average duty cycle 2.5%, but the total traffic load is much higher ($\simeq 5$ pkt/s) than Dozer.

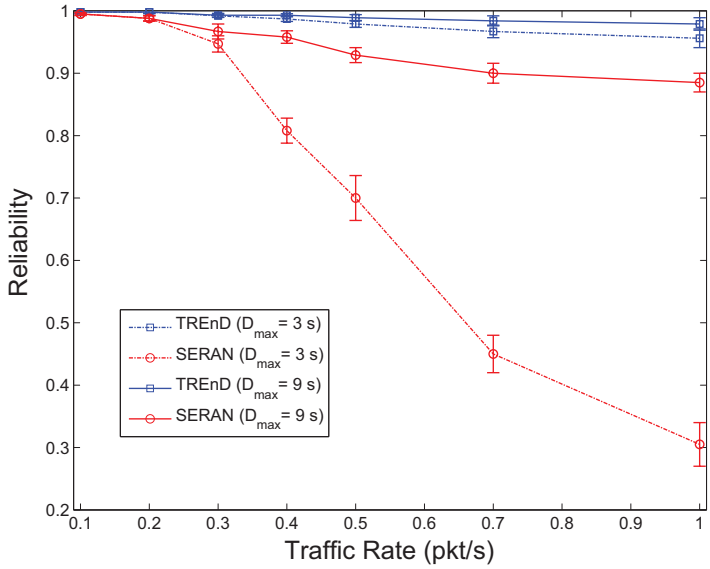

Figure 4.8: TREnD and SERAN: reliability vs. traffic rate λ, for $R_{\min} = \delta = 95\%$.

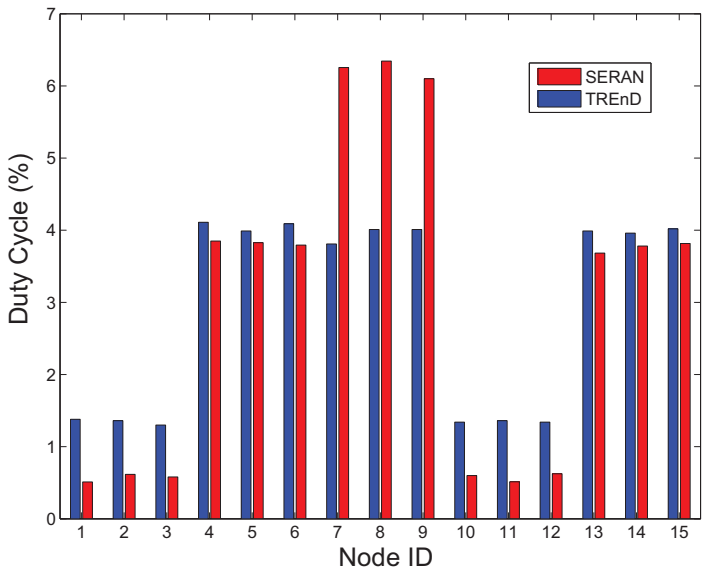

Figure 4.9: TREnD and SERAN: duty cycle distribution among nodes for $\lambda = 0.3$pkt/s, $R_{\min} = \delta = 95\%$.

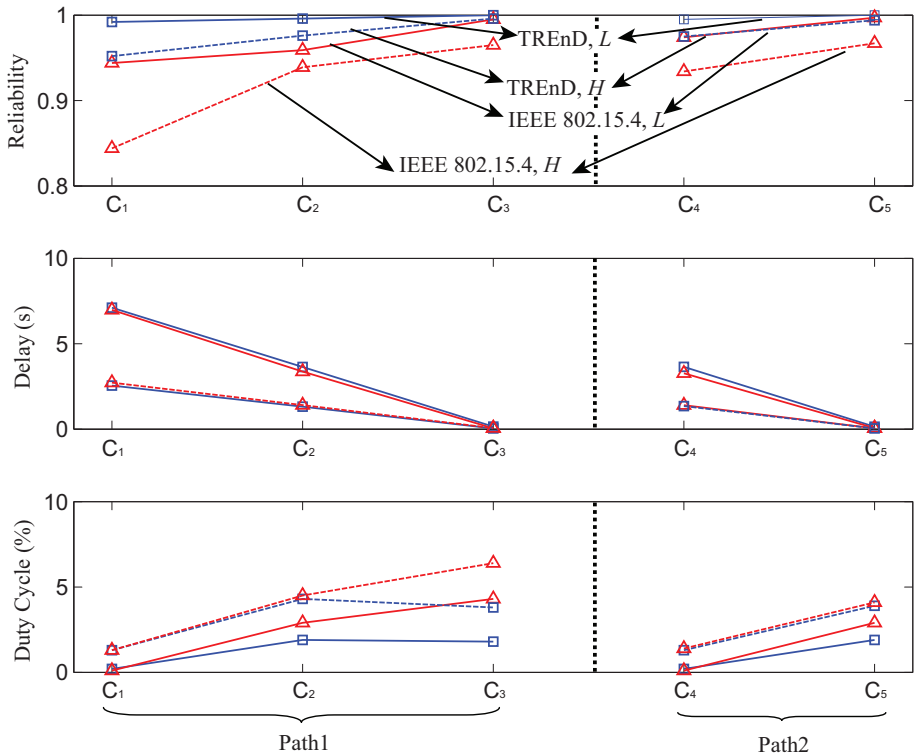

Figure 4.10: TREnD and IEEE 802.15.4: reliability, delay, and duty cycle for scenarios $\mathcal{L}$ and $\mathcal{H}$.

4.7.3 Dynamic Adaptation

In the previous section, we used a static network topology where each node is placed at fixed position and the application requirements do not change with time. In this section, we show the dynamical behavior of the protocol. As we discussed before, no protocol in literature allows for a dynamical adaptation of the parameters to the application requirements.

We present the experimental results of dynamic changes between two scenarios ($\mathcal{L}$ and $\mathcal{H}$ in Table 4.13) in static and time-varying channel conditions. A Rayleigh fading channel is obtained by moving the nodes around their initial position and also by placing metal obstacles in front of the source nodes so that the line-of-sight with the sink is lost. The network starts with scenario $\mathcal{L}$ and static channel, then after 20 TDMA-cycles we introduce a Rayleigh fading channel which persists until the TDMA-cycle 60. At TDMA-cycle 40, the application requirements change to scenario $\mathcal{H}$.

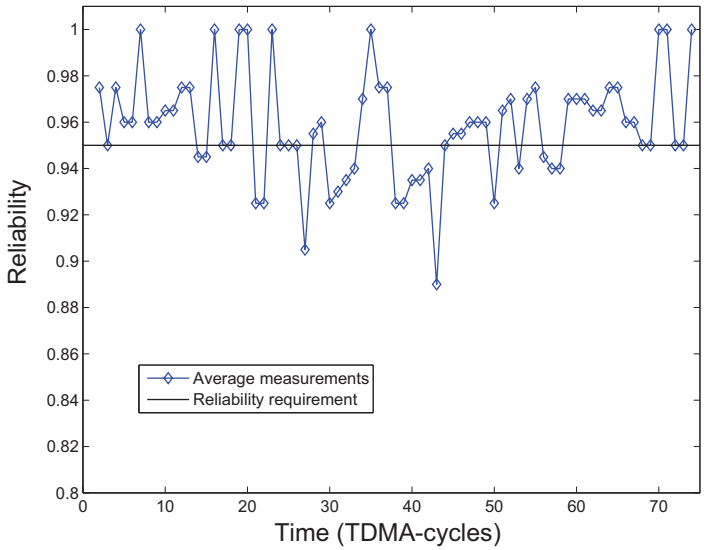

Figure 4.11: TREnD: reliability trace given by the experiments.

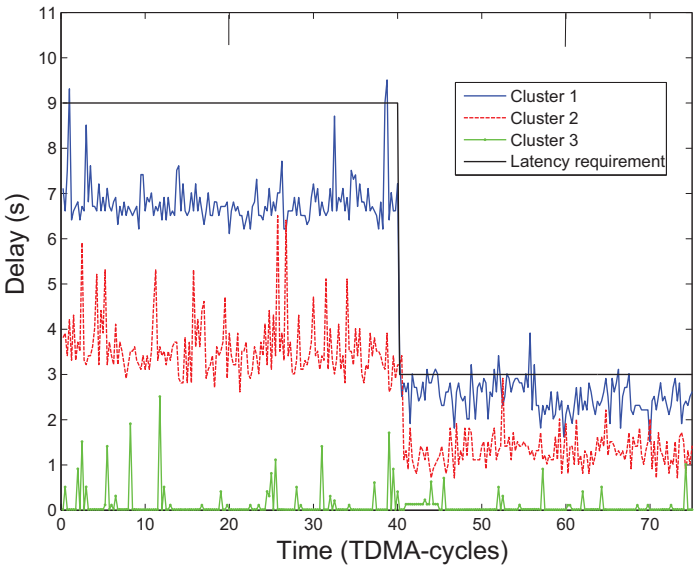

Figure 4.12: TREnD: delay trace given by the experiments.

Table 4.13: Application requirements and experimental results.

Scenario	λ	$D_{\max}$	δ	$R_{\min}$	S^*	τ^*	ω^*
$\mathcal{L}$	0.1 pkt/s	9 s	95%	95%	3.3 s	0.41	0.33
$\mathcal{H}$	0.3 pkt/s	3 s	95%	95%	1.2 s	0.43	0.33

Figures 4.11 and 4.12 report the resulting snapshot of the experiment in terms of reliability and delay. The reliability is measured at the sink node as average on each TDMA-cycle, while the delay is measured for each successfully received packet. In Figure 4.11, we observe that TREnD guarantees the reliability requirement for both static and Rayleigh fading conditions, continuously adapting to the severe fading. The protocol is also robust to the change of scenario at TDMA-cycle 40. In Figure 4.12 a snapshot of the delay is reported for clusters at different hops to the controller. We observe that the peaks of delay are limited due to the TDMA structure, the average and dynamics of the delay are slightly increasing in the time-varying stage but the delay constraint is fulfilled. Moreover, the protocol adapts well to the change of scenario at TDMA-cycle 40.

4.8 Summary

We proposed a novel approach to the design of protocols for control applications over energy efficient multi-hop wireless networks. The approach guarantees the respect of control requirements on reliability and delay while minimizing energy consumption. Duty-cycle, routing, data link, and physical layers were considered all together to maximize the network lifetime by taking into account the tradeoff between energy consumption and application requirements for control applications in compliance with the ROLL specifications for routing and IEEE 802.15.4 standard. The design approach was based on optimization problems to select the protocol parameters by simple algorithms that can run on resource constrained nodes.

The design methodology was illustrated by the proposal of the protocol TREnD, a novel cross-layer solution for control applications over wireless networks, which satisfies application requirements on reliability and delay while minimizing energy consumption. We posed and solved an optimization problem to select the protocol parameters by approximations and a simple algorithm.

We provided a complete test-bed implementation of the protocols that we designed on the base of the method proposed in this chapter. We built a WSN with TinyOS and Tmote sensors. An experimental campaign was conducted to test the validity of TREnD in an indoor environment. Experimental results showed that the protocol achieves the reliability and delay requirements, while minimizing the energy consumption. TREnD outperformed a standard IEEE 802.15.4 implementation in terms of both energy efficiency and reliability. In addition, the protocols showed good load balancing performance, and is scalable with the number of nodes.

Table 4.14: Main symbols used in Chapter 4.

γ	good channel probability
δ	outage probability constraint
λ	cluster packet generation rate
τ	wake up probability in transmission
ω	wake up probability in reception
d	CSMA-slot duration
h_i	number of hops in the path i
$h_{\max}$	maximum number of hops
p_k	successful transmission probability in a CSMA-slot with k packets
p_{bc}	successful beacon transmission probability in a CSMA-slot
p_{cl}	CCA failure probability in a CSMA-slot
t_a	ACK transmission time
t_b	beacon transmission time
t_m	packet transmission time
t_p	processing time
C_i	ith cluster
C_{st}	maximum storage capacity
D	end-to-end delay
$D_{\max}$	delay constraint
E_{ack}	energy spent for a single ACK transmission
E_{cca}	energy spent for a single CCA
E_{pkt}	energy spent for a single packet transmission
E_w	energy spent for a single wake up
M_s	number of CSMA-slots in a TDMA-slot
N	number of nodes in the network
P_i	energy (per unit time) spent during idle-listening
$R_{\min}$	reliability constraint
R	end-to-end reliability
S	TDMA-slot duration
T_{cyc}	TDMA-cycle duration
T_e	cluster evacuation time
T_{sc}	channel sensing time
W	number of listening TDMA-slots in a TDMA-cycle

Chapter 5

Building Automation Application over IEEE 802.15.4 Networks

In this chapter, the synthesis of a robust controller for intelligent building automation over energy efficient wireless networks is characterized. In Figure 5.1, we highlight what is studied in this chapter, with respect to the general problem formulation in Section 1.2. A loop is closed between application and underlying layers, so that the performance indicators from the communication level are considered explicitly in the controller.

The communication stack follows the IEEE 802.15.4 MAC over a WSN with star topology. We focus on intelligent buildings ventilation control, which is a challenging automation problem with objectives that comprise several research areas of immediate actuality, such as the wireless automation and the control of complex interconnected subsystems. The complexity arises from the different physical properties and associated dynamics of the subsystems.

Recent results have illustrated the interest for under floor air distribution (UFAD) solutions in comparison with traditional ceiling-based ventilation, as mentioned in [67]. Well-designed UFAD systems can reduce life-cycle building costs, improve thermal comfort, ventilation efficiency, and indoor air quality, conserve energy, and reduce floor-to-floor height.

The purpose of this chapter is to illustrate the effects of an IEEE 802.15.4 network on the control performance of a UFAD regulation system. Here we aim at studying control strategies that are robust enough to cope with variations and disturbances due to Markovian processes and nonlinearities in the system model and delays and losses in the wireless network. The H_∞ control approach has been selected due to its intrinsic emphasis on robustness, the existence of a well established systematic design procedure, and its efficiency in a wide range of applications, in particular with time delays as illustrated in [68]. Given that the delay induced by the network has a saw-tooth shape, it can be attacked with methods described in [69]–[71]. A mixed sensitivity H_∞ synthesis is compared with two approaches that explicitly take into account the communication network performance.

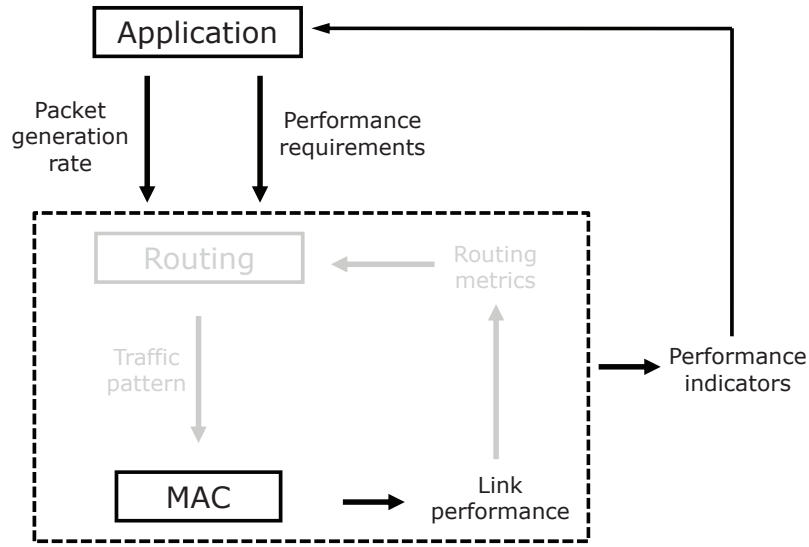

Figure 5.1: Layers interaction for modeling and design: UFAD controller over IEEE 802.15.4 MAC. The effects of the routing layer are not included.

This chapter is outlined as follows. First, we introduce the system architecture and describe the physical model of the UFAD system. By using a hybrid state-space model, we describe different approaches for the controller synthesis. Eventually, simulation results are presented. The chapter is concluded by a short summary.

A list of all symbols used in this chapter is reported in Table 5.11, at the end of the chapter.

5.1 System Architecture

In this section, we describe the system architecture given by the UFAD regulation system and the communication network architecture.

5.1.1 UFAD System

An UFAD indoor climate regulation process is set with the injection of a fresh airflow from the floor and an exhaust located at the ceiling level, as depicted in Figure 5.2. The considered system is composed of ventilated rooms, fans, and plenums. Note that we consider the specific case where a common plenum is used at both the underfloor and ceiling levels.

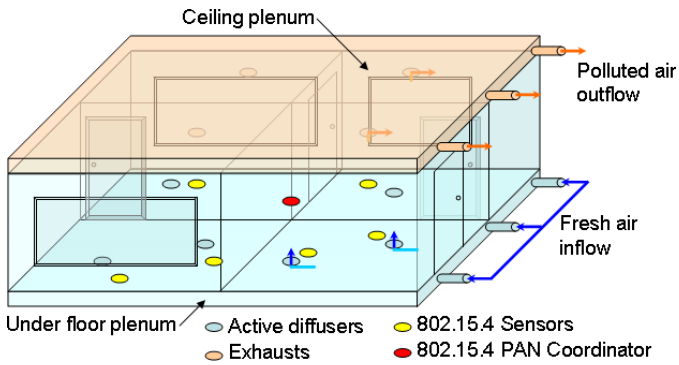

Figure 5.2: UFAD system overview.

Feedback regulation is a key element for an optimized system operation and it can be achieved thanks to actuated diffusers and distributed measurements provided by an energy efficient WSN deployed in the ventilated area.

In order to use a model-based control approach, we derive the thermodynamics properties of the ventilation process with a control volume approach. We show that it allows for a reduced-order, easily reconfigurable system description, but includes nonlinearities and discrete events (doors, internal power sources, etc.). Such events are handled specifically with a Markovian approach and the resulting system is described as a hybrid state-space model. The distributed sensing capabilities are described in the next section.

5.1.2 Wireless Sensor Network

The communication network consists of a WSN where N nodes contend to send data to a root node, which operates as personal area network (PAN) coordinator, attached to a controller. Each node uses a IEEE 802.15.4 MAC. We assume that the network generates unsaturated traffic, which is a natural scenario for many control applications.

In Chapter 3, a generalized analysis of the IEEE 802.15.4 MAC protocol in terms of reliability, delay, and energy consumption has been presented. In particular, the time-varying packet delay due to the random access scheme is modeled. It is possible to look at the source of packet delay for different frequency domains [72]:

- high frequency delays, due to the packet transmission time;
- middle frequency delays, which depend on the random backoff time (m_0, m_b) and the number of backoffs m;
- low frequency delays, related to the number of retransmissions due to packet collisions n.

From an application perspective, performance in terms of reliability and delay are translated into a single indicator, which is the delay in receiving a new packet at the controller, denoted hereafter as saw-tooth packet delay, which depends on the traffic generation mode.

In our system setup we refer to two models for traffic generation. Let *sync* mode and *async* mode be the situations where each node synchronously or asynchronously generate packets with the sampling interval $T_s(t)$, respectively. In sync mode, all nodes of the network are synchronized and generate data packets at the same time with a fixed sampling interval $T_s = 1/\lambda$. In async mode, each node asynchronously generates packets. When a node sends a packet successfully, or discards a packet, or when the sampling interval is expired, it stays for T_s seconds without generating further packets. Figure 5.3 shows the saw-tooth packet delay of each node for two traffic generation models. The saw-tooth packet delay increases with the unit time T_u until the root node receives a data packet. If a data packet is received, the saw-tooth packet delay is reset to the received packet delay. Therefore, the saw-tooth packet delay includes also packet losses (i.e., packet loss will increase the saw-tooth packet delay to a higher level than T_s). Figures 5.3(a) and 5.3(b) show the saw-tooth packet delay of sync mode and async mode, respectively. We remark here that although both sync mode and async mode have almost the same time interval T_s, the reliability of async mode is higher than the one of sync mode. The reason is that async mode effectively distributes the sensing time of each sensor node based on the history of contention. It can be observed that the sampling time instant of async mode is spread for the different nodes of the network. The data packet transmission is successful if an ACK packet is received. The command on control action is piggybacked on ACK packet and does not require any additional message from the root node to sensor nodes.

5.2 UFAD Model

To provide a model that is suited for real-time feedback control, we consider a 0-D model based on the mass and energy conservation. Each room is interconnected with the other building elements, as depicted in Figure 5.4. The interconnections are defined by the mass flow rate and heat transport. A model of an UFAD system is derived next.

5.2.1 Physical Model

The room dynamics is illustrated using the fundamental laws of thermodynamics [73]. The internal state of room i, represented by its density ρ_i and temperature T_i, is determined based on the following hypotheses:

H1. the flow is incompressible: $\rho_i = \rho_{\text{air}}$;

H2. the control volume (CV) remains constant relative to the coordinate frame;

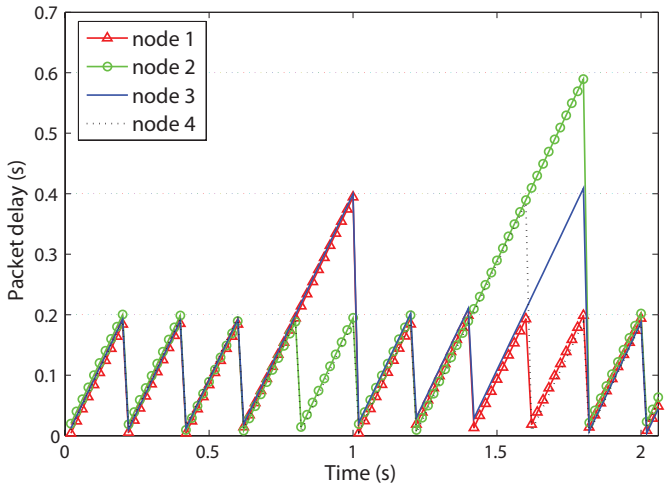

(a) Saw-tooth packet delay of sync mode.

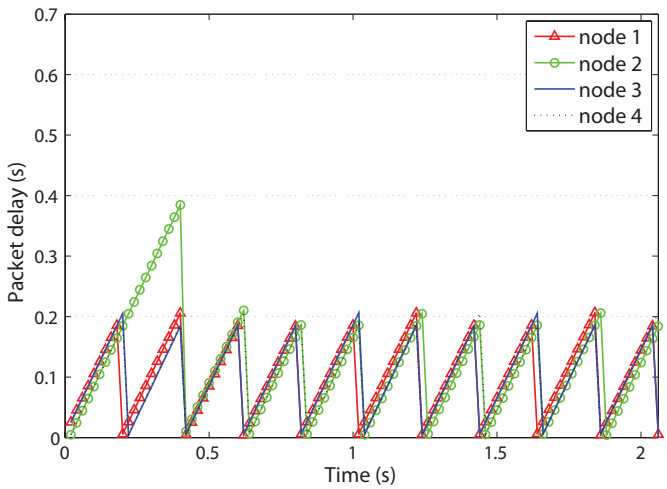

(b) Saw-tooth packet delay of async mode.

Figure 5.3: Saw-tooth packet delay with packets of 70 bytes, $N = 4$, $T_s = 0.2$ sec, and two traffic generation models.

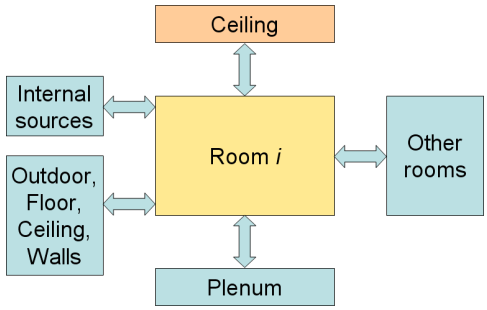

Figure 5.4: UFAD block diagram model.

H3. the state of mass within the CV is uniform at any time;

H4. the state of the mass crossing the CV is constant with time but the mass flow rates may vary;

H5. the kinetic and potential energy of the gas within the room are neglected.

Hypothesis (*H1*) is straightforward considering the low speed of the airflow within the rooms. (*H2*)-(*H4*) are classical for uniform-state, uniform-flow processes, i.e., when there is no change in the state of mass (we consider only gas in our case). (*H5*) is associated with the fact that the gas moves slowly in the room and that the mass of the gas in the CV does not generate significant potential energy. The CV considered is strictly limited to the inside room volume: it does not include the underfloor and ceiling plenums.

The continuity equation, along with incompressibility (*H1*), implies mass conservation $\sum \dot{m}_{\mathrm{in}_i} = \sum \dot{m}_{\mathrm{out}_i}$, where $\dot{m}_{\mathrm{in}}$ and $\dot{m}_{\mathrm{out}}$ are the input and output mass flow rates, respectively. The first law of thermodynamics with (*H2*)-(*H4*) gives the energy exchange in the room CV as:

$$\frac{dE_i}{dt} = \dot{Q}_i + \sum \dot{m}_{\mathrm{in}_i} h_{\mathrm{tot,in}_i} - \sum \dot{m}_{\mathrm{out}_i} h_{\mathrm{tot,out}_i} ,$$

where E_i is the room energy, $\dot{Q}_i$ the heat exchange, and h_{tot} the total enthalpy, approximated as $h_{\mathrm{tot}} = C_p T$, at temperature T, with C_p the constant pressure specific heat. Considering (*H5*), the room energy is the internal energy

$$E_i = \rho_{\mathrm{air}} V_i C_v T_i ,$$

where V_i is the room volume and C_v is the constant volume specific heat. For air at 25° C and 1 atm, $C_v = 717$ J/(kg· K), $C_p = 1004$ J/(kg· K) and $\rho_{\mathrm{air}} = 1.169\,\mathrm{kg/m^3}$.

The heat exchange Q_i can be decomposed, depending on the nature of the heat transfers, as:

- conduction (Fourier's law):

$$\dot{Q}_{\text{cond}} = k\,A\,\frac{\Delta T}{\Delta x}\,,$$

where k [W/(m·K)] is the conductivity ($\approx$ 10 for glass, 0.1 for insulation materials) and A the surface area where exchange occurs;

- convection (Newton's law):

$$\dot{Q}_{\text{conv}} = A\,h\,\Delta T\,,$$

where h [W/m^2] is the heat transfer coefficient (typically $5-25$ for natural convection and $25-250$ for forced convection;

- radiation (electromagnetic waves):

$$\dot{Q}_{\text{rad}} = \epsilon\,\sigma\,A\,T_s^4\,,$$

where ϵ is the emissivity (0.92 for nonmetallic surfaces), $\sigma = 5.67 \times 10^{-8}$ W/(m$^2 \cdot$ K^4) is the Stephan-Boltzmann constant and T_s is the surface temperature.

Under the previous hypotheses, the mass flow rate $\dot{m}$ going from a high temperature volume T_h to a low temperature volume T_l through a section A is obtained by combining Bernoulli's and the ideal gas equations as:

$$\dot{m} = \rho A\sqrt{2(C_p - C_v)(T_h - T_l)}\,. \tag{5.1}$$

5.2.2 Room Dynamics

Based on the previous description, we obtain the room temperature dynamics:

$$\begin{aligned}\frac{dT_i}{dt} =& \frac{1}{\rho_{\text{air}} V_i C_v}\left[\dot{Q}_{\text{conv}} + \dot{Q}_{\text{cond}} + \dot{Q}_{\text{rad}} + \dot{Q}_{\text{sources}}\right.\\ &\left. + C_p \sum \dot{m}_{\text{in}_i} T_{\text{in}_i} - C_p \sum \dot{m}_{\text{out}_i} T_i\right]\,,\end{aligned}$$

where we introduced the additional source $\dot{Q}_{\text{sources}}$ to model the internal heat sources (computers, printers, etc.) and considered the outflow temperature as the room temperature (which is a direct consequence of the 0-D approximation). A simplified classification of the heat sources for room i is proposed in Table 5.5, where T_j indicates the temperature in an adjacent room, A_x the exchange surface areas, and Δx_x the thicknesses. Note that the last three components correspond to discrete events while the previous ones have continuous variations. This description is easily refined by introducing additional terms (walls radiation, windows airflow, etc.), depending on the desired level of model accuracy.

Table 5.5: Energy sources in room i.

Component	Associated energy
Inside walls	$\dot{Q}_{iw} = -k_{iw}\, A_{iw}\, \frac{(T_i - T_j)}{\Delta x_{iw}}$
Outside walls	$\dot{Q}_{ow} = -\left(k_{ow}\, \frac{A_{ow}}{\Delta x_{ow}} + k_{\text{glass}}\, \frac{A_{\text{glass}}}{\Delta x_{\text{glass}}}\right)(T_i - T_{\text{out}})$
Plenum	$\dot{Q}_{pl} = C_p\, \dot{m}_{pl}\, T_{pl}$
Floor	$\dot{Q}_f = -k_{pl}\, A_{pl}\, \frac{(T_i - T_{pl})}{\Delta x_{pl}}$
Ceiling	$\dot{Q}_c = -C_p\, \dot{m}_c\, T_i$
People	$\dot{Q}_b = \epsilon\, \sigma\, A_b\, (T_b^4 - T_i^4)$
Inside sources	$\dot{Q}_{\text{sources}}$
Doors	$\dot{Q}_d = C_p\, \rho\, A_d \sqrt{2(C_p - C_v)(T_j - T_i)}\, T_j$, if $T_j > T_i$
	$\dot{Q}_d = C_p\, \rho\, A_d \sqrt{2(C_p - C_v)(T_i - T_j)}\, T_i$, if $T_i > T_j$

The ceiling, plenum, and door mass flow rates are constrained by the conservation of mass (continuity) with (setting $\dot{m} > 0$ when the flow is entering the room):

$$\dot{m}_{c_i} + \sum_{l=1}^{N_{pl}} \dot{m}_{pl_i,l} + \sum_{l=1}^{N_d} \dot{m}_{d_{ij},l} = 0\,,$$

where N_{pl} is the number of diffusers in the room and N_d denotes the number of doors. The door mass flow rate can be computed thanks to Bernoulli's equation (5.1) as

$$\dot{m}_d = \text{sgn}(T_j - T_i)\, \rho\, A_d \sqrt{2(C_p - C_v)|T_j - T_i|}\,,$$

where the sign function is introduced to indicate the flow direction.

The temperature regulation is achieved by controlling the mass flow rate from the plenum $\dot{m}_{pl_i,l}(t)$, considering a given underfloor temperature $T_{pl}(t)$ (regulated globally for the whole building). We suppose in the following that there is only one diffuser per room ($N_{pl} = 1$) and that the WSN provides the temperature measurements.

Finer models, including the height-dependency of the temperature variations, can be derived using the stratified flow theory [74, 75] or buoyancy driven flow dynamics [76]. The WSN measurements can also be set to determine the temperatures distribution shape, along the lines suggested in [77]. The use of a coarse global model based on the proposed 0-D approach is motivated by the fact that the WSN directly provides the necessary measurements for feedback control. The aim of the model is then to give the proper directions of the regulated states according to the actuation and disturbances.

5.3 Hybrid State-space Model

In this section, we describe the hybrid state-space model by distinguishing between continuous dynamics and discrete events.

5.3.1 Continuous Dynamics

The continuous dynamics of the model is set by the walls, ceiling, and plenum. According to the physical laws described in Section 5.2.2 and supposing that all the doors are closed and that there is no power source within the room, the temperature dynamics for room i is given as:

$$\begin{aligned}\frac{dT_i}{dt} = F_i(t) =& \frac{1}{\rho_{\text{air}} V_i C_v}\left[\dot{Q}_{\text{conv}} + \dot{Q}_{\text{cond}} + \dot{Q}_{\text{rad}} + C_p \dot{m}_{pl_i}(T_{pl} - T_i)\right] \\ =& \frac{1}{\rho_{\text{air}} V_i C_v}\left[-\sum_{l=1}^{N_{iw}} \alpha_{iw_l}(T_i - T_l) - \sum_{l=1}^{N_{ow}} \left(\alpha_{ow_l} + \alpha_{\text{glass}_l}\right)(T_i - T_{\text{out}})\right. \\ & \left. + C_p \dot{m}_{pl_i} T_{pl} - \alpha_{pl_i}(T_i - T_{pl}) - C_p \dot{m}_c T_i\right] \\ =& \frac{1}{\rho_{\text{air}} V_i C_v}[-(\Theta_i + C_p \dot{m}_{pl_i})T_i + \sum_{l=1}^{N_{iw}} \alpha_{iw_l} T_l + \sum_{l=1}^{N_{ow}} \left(\alpha_{ow_l} + \alpha_{\text{glass}_l}\right) T_{\text{out}} \\ & + (C_p \dot{m}_{pl_i} + \alpha_{pl_i}) T_{pl}]\,, \end{aligned} \tag{5.2}$$

where

$$\Theta_i = \sum_{l=1}^{N_{iw}} \alpha_{iw_l} + \sum_{l=1}^{N_{ow}} \left(\alpha_{ow_l} + \alpha_{\text{glass}_l}\right) + \alpha_{pl_i}\,,$$

$\alpha_x = k_x A_x / \Delta x_x$ for component x, N_{iw} is the number of connected inside walls, N_{ow} is the number of outside walls, and $F_i(t)$ denotes the continuous part of the dynamics for room i.

By defining the state as the vector of room temperatures $x = [T_1 \dots T_n]^T$, the controlled input as $u = [\dot{m}_{pl_1} \dots \dot{m}_{pl_n}]^T$ and the exogenous input as $w = [T_{pl}\ T_{\text{out}}]^T$, where n is the number of rooms, the system dynamics is

$$\dot{x} \quad = \quad (A_1 + A_2(u))x + B_u u + B_w w\,, \tag{5.3}$$

where the state matrices A_1 and A_2, and the input matrices B_u and B_w are computed according to Equation (5.2). Note that this model is fully determined by the building architecture and constant physical variables. Let us illustrate through a simple example.

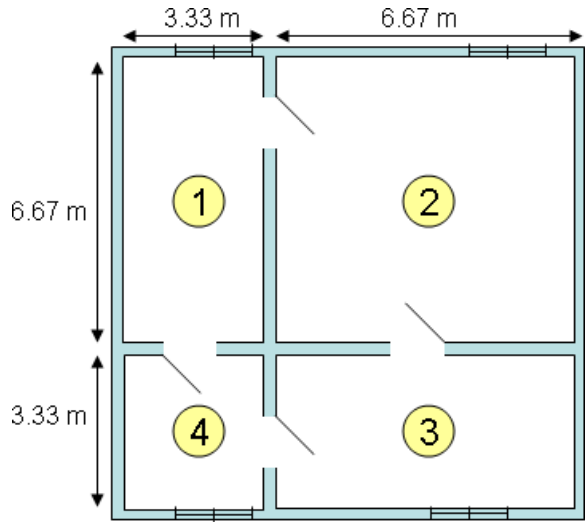

Figure 5.6: Flat architecture for the test case.

Example 5.1

We consider the rooms flat presented in Figure 5.6: each room has two doors and one window. The plenum temperature T_{pl} is given, the state is $x = [T_1 \dots T_4]^T$, the controlled input is $u = [\dot{m}_{pl_1} \dots \dot{m}_{pl_4}]^T$ and the exogenous input is $w = [T_{pl}\ T_{\text{out}}]^T$. The state and input matrices are

$$A_1 = \begin{bmatrix} a_{11}^1 & a_{12}^1 & 0 & a_{14}^1 \\ a_{21}^1 & a_{22}^1 & a_{23}^1 & 0 \\ 0 & a_{32}^1 & a_{33}^1 & a_{34}^1 \\ a_{41}^1 & 0 & a_{43}^1 & a_{44}^1 \end{bmatrix}, \quad B_w = \begin{bmatrix} b_1^{w1} & b_1^{w2} \\ b_2^{w1} & b_2^{w2} \\ b_3^{w1} & b_3^{w2} \\ b_4^{w1} & b_4^{w2} \end{bmatrix},$$

$$A_2(u) = \text{diag}(a_i^2) \cdot \text{diag}(u_i), \qquad B_u = -\text{diag}(a_i^2) \cdot T_{pl},$$

$$a_{ii}^1 = -\frac{\Theta_i}{\rho_{\text{air}} V_i C_v}, \quad a_{ij}^1 = \frac{\alpha_{iw,ij}}{\rho_{\text{air}} V_i C_v} \quad i \neq j, \quad a_i^2 = -\frac{C_p}{\rho_{\text{air}} V_i C_v},$$

$$b_i^{w1} = \frac{\alpha_{pl_i}}{\rho_{\text{air}} V_i C_v}, \quad b_i^{w2} = \frac{1}{\rho_{\text{air}} V_i C_v} \sum_{l=1}^{4} \left(\alpha_{ow_l} + \alpha_{\text{glass}_l} \right),$$

with $i, j = 1, ..., 4$.

5.3.2 Discrete Dynamics

The discrete events are induced by the power sources and the doors. Concerning the doors influence, the proposed energy-based model implies that for a given room i and adjacent room j (supposing that there is no return from the upper plenum):

- if $T_i > T_j$ then the flow going out of room i equals the inflow $\dot{m}_{pl_i}$ and the fact that it is leaving through the ceiling or the open door does not change the energy balance;
- if $T_i < T_j$ then an extra term $C_p \dot{m}_d (T_j - T_i)$ has to be introduced, with $\dot{m}_d = \rho A_d \sqrt{2(C_p - C_v)(T_j - T_i)}$.

The room temperature is then obtained as (supposing that only one door is open in room i at a given time, to simplify the notations):

$$\frac{dT_i}{dt} = F_i(t) + \frac{\sum_{k=0}^{N_q} \delta_{q,ik} \dot{Q}_{s,ik}}{\rho_{\text{air}} V_i C_v} + \begin{cases} 0, & \text{if } T_i > T_j \\ \delta_{d,ij} \frac{C_p \sqrt{2(C_p - C_v)}}{\rho_{\text{air}} V_i C_v} (T_j - T_i)^{3/2}, & \text{if } T_i < T_j \end{cases}$$

where $F_i(t)$ is the continuous dynamics from Equation (5.2), N_q is the number of power sources, and $\delta_{q,ik}$ and $\delta_{d,ij}$ are introduced to denote the on/off operation of power sources and doors opening in room i. The discrete transitions are set by Markovian independent processes, constrained by the maximum and minimum periods during which a given event can occur. Further details are available in [78].

5.4 Robust Control Synthesis

The aim of this section is to present the MIMO control design procedure for the problem presented above. Considering the discrete perturbations induced by the doors and power sources along with the communication constraints, the robustness issue appears as critical. The control setup refers to multi-objectives H_∞ design approach [79, 80].

5.4.1 Steady-state and Variation

The first step is to rewrite the system dynamics (5.3) with a change of variables that allows for removing the known exogenous inputs, in order to set the feedback on the tracking error. Defining the steady-state variables x_{ss}, u_{ss} as constrained by the algebraic relationship

$$(A_1 + A_2 \operatorname{diag}(u_{ss}))x_{ss} + B_u u_{ss} + B_w w = 0\,,$$

the input that provides for a given reference state x_{ss} is given by:

$$u_{ss} \quad = \quad -(A_2 \operatorname{diag}(x_{ss}) + B_u)^{-1}(A_1 x_{ss} + B_w w).$$

Introducing the variations $\tilde{x}(t) \doteq x(t) - x_{ss}$ and $\tilde{u}(t) \doteq u(t) - u_{ss}$, the regulated dynamics are obtained from Equation (5.3) as

$$\begin{aligned} \frac{d\tilde{x}}{dt} &= (A_1 + A_2\,\mathrm{diag}(u_{ss} + \tilde{u}))(x_{ss} + \tilde{x}) + B_u(u_{ss} + \tilde{u}) + B_w w \\ &\approx (A_1 + A_2\,\mathrm{diag}(u_{ss}))\tilde{x} + (A_2\,\mathrm{diag}(x_{ss}) + B_u)\tilde{u}\,. \end{aligned} \tag{5.4}$$

The aim of the control design is then to ensure that $\tilde{x}$ converges exponentially to the origin while satisfying given closed-loop specifications.

5.4.2 Mixed-sensitivity H_∞ Synthesis

A mixed-sensitivity approach is chosen to tackle a multi-objective control design that can achieve performance, robustness, and input boundary specifications. The main idea (see [79] for more details) is to introduce the closed-loop specifications as weights on the sensitivity functions prior to the H_∞ norm minimization. Denoting the system sensitivity function as $S(s)$ and the complementary sensitivity as $T(s)$, the MIMO controller $K(s)$ is then designed to minimize

$$\left\| \begin{bmatrix} W_p S W_d \\ W_u K S \\ W_t T \end{bmatrix} \right\|_\infty ,$$

where the specific choice of the weight is achieved as follows (considering n rooms):

- the performance weight $W_p(s)$ is set as

$$W_p(s) = \mathrm{diag}\left\{ \frac{s/M + \omega^*_{Bi}}{s + \omega^*_{Bi} A} \right\}, \quad i = 1 \ldots n\,,$$

  where $A = 10^{-4}$ ensures an approximate integral action with $S(0) \approx 0$, $M = 2$, and ω^*_{Bi} is different for each output (a large value yields a faster response for the corresponding output);

- the input weight

$$W_u(s) = \mathrm{diag}\left\{ \frac{s}{s + \omega_u} \right\},$$

  gives tight control at low frequency, with ω_u being approximately the closed-loop bandwidth;

- the disturbance weight

$$W_t(s) = \mathrm{diag}\left\{ \frac{s + \omega^*_{Ti}/M}{As + \omega^*_{Ti}} \right\}, \quad i = 1 \ldots n\,,$$

  is introduced to reduce the impact of discrete events and measurements noise on the closed-loop.

The desired closed-loop response is obtained thanks to an appropriate tuning of ω^*_{Bi}, ω_u, and ω^*_{Ti}. The parameters are set as

$$\omega^*_{Bi} = \alpha_p \frac{\text{mean}_i\{\rho_{\text{air}} V_i C_v\}}{\rho_{\text{air}} V_i C_v}, \quad \omega_u = \alpha_u \text{mean}_i\{\omega^*_{Bi}\}, \quad \omega^*_{Ti} = \alpha_t \omega^*_{Bi},$$

to take into account the fact that faster control can be achieved in rooms with faster time constants (smaller volume). The design problem is reduced to the choice of three scalar parameters α_p, α_u, and α_t.

Simulation results for the mixed-sensitivity H_∞ synthesis applied to our UFAD model are discussed in Section 5.5.

5.4.3 Controller Synthesis with Communication Constraints

In this section, we consider two approaches in which the delay introduced by the IEEE 802.15.4 network is included in the controller synthesis.

We consider the simplified model of the system

$$\dot{x} = Ax(t) + Bu(t) + Ew(t)\,, \tag{5.5}$$

corresponding to Equation (5.4) in Section 5.4.1.

Two filters $W_u(s)$ and $W_p(s)$ are added to the system, such that the system dynamics is extended to

$$\begin{aligned}
\begin{bmatrix} \dot{x} \\ \dot{x}_e \\ \dot{x}_u \end{bmatrix} &= \underbrace{\begin{bmatrix} A & 0 & 0 \\ -B_p & A_p & 0 \\ 0 & 0 & A_u \end{bmatrix}}_{A_g} \begin{bmatrix} x \\ x_e \\ x_u \end{bmatrix} + \underbrace{\begin{bmatrix} B \\ B_u \end{bmatrix}}_{B_g} u + \underbrace{\begin{bmatrix} E\delta & 0 \\ 0 & B_p \\ 0 & 0 \end{bmatrix}}_{E_g} \begin{bmatrix} w \\ x_{ref} \end{bmatrix} \\
\begin{bmatrix} e_f(t) \\ u_f(t) \end{bmatrix} &= \underbrace{\begin{bmatrix} -D_p & C_p & 0 \\ 0 & 0 & C_u \end{bmatrix}}_{C_g} \begin{bmatrix} x \\ x_e \\ x_u \end{bmatrix} + \underbrace{\begin{bmatrix} 0 \\ D_u \end{bmatrix}}_{D_g} u + \underbrace{\begin{bmatrix} 0 & D_p \\ 0 & 0 \end{bmatrix}}_{F_g} \begin{bmatrix} w \\ x_{ref} \end{bmatrix}
\end{aligned}, \tag{5.6}$$

where $\delta > 1$ is a weight on the disturbances and

$$\begin{bmatrix} A_p & B_p \\ C_p & D_p \end{bmatrix} = W_p(s) \qquad \begin{bmatrix} A_u & B_u \\ C_u & D_u \end{bmatrix} = W_u(s)$$

are weights on the tracking error $e = x_{ref} - x$ and controlled input u.

The aim is to compute a controller that:

1. asymptotically stabilizes the system for any transmission delay smaller than some constraint D;

2. minimizes the H_∞ norm of the transfer function $\begin{bmatrix} w \\ x_{ref} \end{bmatrix} \rightarrow \begin{bmatrix} e_f \\ u_f \end{bmatrix}$;

where e_f and u_f are filtered version of the tracking error e and the control input u, defined by $E_f(s) = W_p(s)E(s)$ and $U_f(s) = W_u(s)U(s)$ in the Laplace domain.

The considered controller is a state-feedback controller of the form:

$$u(t) = K_1 x(t) + K_2 x_e(t) + K_3 x_u(t)\,, \tag{5.7}$$

where the gains K_i have to be determined.

A first approach for the controller gain synthesis is based on the following result [81].

Lemma 5.4.1. There exists a control law (5.7) that asymptotically stabilizes the system (5.6) with an H_∞ bound on the transfer $(w, x_{ref}) \rightarrow (e_f, u_f)$ lower than $\gamma > 0$ if and only if there exist matrices $P = P^T \succ 0$ and Y of appropriate dimensions such that the linear matrix inequality

$$\begin{bmatrix} A_g P + P A_g^T + B_g Y + Y^T B_g^T & E_g & P C_g^T + Y^T D_g^T \\ \star & -\gamma I & F_g^T \\ \star & \star & -\gamma I \end{bmatrix} \prec 0$$

is fulfilled. Moreover, suitable controller gains are given by

$$\begin{bmatrix} K_1 & K_2 & K_3 \end{bmatrix} = Y P^{-1}\,.$$

In order to characterize the stability of the closed-loop system with delays, we assume that the controller maintains the last measurement on its inputs until a new measurement is available. We also suppose that the same delay acts simultaneously on all the measurement. This is equivalent to a system output sampled at a time-varying sampling period. Hence, it is possible to use stability analysis of systems with time-varying sampling period to analyze the system stability under communication constraints. Most of the works on such systems assume that the delay acts on the control input. In the current problem, the delay acts on the output of the model. However, since a state-feedback controller is considered, the problem is symmetric and available results are directly applicable.

An alternative approach is to consider the delay constraint directly during the controller synthesis, as proposed in [71]. The controller is then obtained from the following lemma.

Lemma 5.4.2. The closed-loop system given by the interconnection of Equations (5.6) and (5.7) is asymptotically stable for all delay belonging to $[0, D]$ if there exist matrices $P = P^T \succ 0$, $S = S^T \succ 0$, $R = R^T \succ 0$ and N of appropriate dimensions such that the following linear matrix inequalities hold:

$$\Pi_1 + D\Pi_2 \prec 0, \quad \begin{bmatrix} \Pi_1 & DN \\ \star & -DR \end{bmatrix} \prec 0,$$

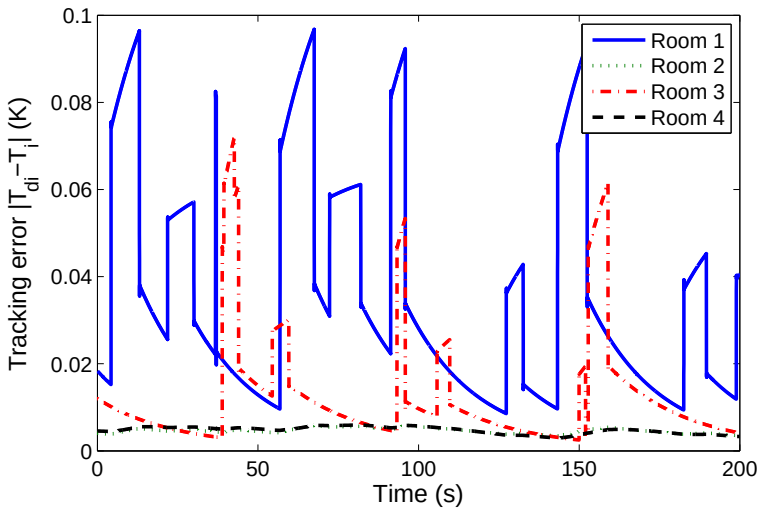

Figure 5.7: Mixed-sensitivity H_∞ controller: temperature tracking error without communication over IEEE 802.15.4.

with

$$\begin{aligned}\Pi_1 &= M_1^T P M_3 + M_3^T P M_1 - M_2^T S M_2 - N M_2 - M_2^T N^T\,,\\ \Pi_2 &= M_2^T S M_3 + M_3^T S M_2 + M_3^T S M_3\,,\end{aligned}$$

and $M_1 = \begin{bmatrix} I & 0 \end{bmatrix}$, $M_2 = \begin{bmatrix} I & -I \end{bmatrix}$, and $M_3 = \begin{bmatrix} A_g & B_g K \end{bmatrix}$.

In the following section, we show simulation results and performance comparisons for the proposed synthesis approaches.

5.5 Simulation Results

We consider the room flat test case in Figure 5.6 and we set the desired room temperature as $T_d = 273.15 \cdot [1 \quad 1 \quad 1 \quad 1]^T + [18 \quad 21 \quad 19 \quad 23]^T$ K. Figure 5.7 shows the temperature tracking error $|T_{d,i} - T_i|$ for the control system based on the mixed-sensitivity H_∞ synthesis described in Section 5.4.2 when there is no delay from the communication network. The controller parameters are set as $\alpha_p = 1000$, $\alpha_u = 10$, and $\alpha_t = 1$. The high value of the parameters implies that all the desired bandwidth is available for control purposes, as the aim of this first test case is to get the best achievable performances without communication constraints. The higher sensitivity to door actuation observed in rooms 1 and 3 is due to the fact

that these rooms have a lower temperature than the adjacent ones, combined with the limitation to single-direction flows induced by the 0-D model (see Section 4.2).

The communication constraints are introduced thanks to the IEEE 802.15.4 network model described in Section 5.1.2. Sampling, delay, and packet losses are introduced between the measurements and the controller. In order to ensure the closed-loop stability and give satisfying performances, the control parameters are set as $\alpha_p = 0.1$, $\alpha_u = 1$, and $\alpha_t = 10$. The resulting temperature tracking errors are presented in Figure 5.8, for both synchronous and asynchronous modes. Note that the maximum errors in both cases are very similar ($\approx 2.5°$ C), which illustrates the robustness and performance limitation of the closed-loop to the network setup, and the weak influence of the mode choice in the WSN operation (synchronous or not).

The controllers obtained from the Lemmas 5.4.1 and 5.4.2 are tested as follows. We choose $W_u(s) = s/(s+\omega_1)$, $W_p(s) = (s/M + \omega_b)/(s + A\omega_b)$, $\delta = 10$, $M_s = 2$, $\omega_b = 0.5$, $A = 10^{-4}$, $\omega_1 = 10$. By using Lemma 5.4.1, we obtain $\gamma = 0.93294$. However, such a small performance criterion is related to large values for eigenvalues and thus is responsible for a high sensitivity to delays. Thus in order to reduce this sensitivity, we impose $\gamma = 10$ and get the following gains:

$$K_1 = \begin{bmatrix} 2.1921 & 0.0093 & 0.0009 & 0.0029 \\ 0.0065 & 2.5798 & 0.0060 & 0.0003 \\ 0.0010 & 0.0092 & 2.1173 & 0.0029 \\ 0.0072 & 0.0013 & 0.0067 & 1.3593 \end{bmatrix},$$

$$K_2 = \begin{bmatrix} -1.1461 & -0.0009 & -0.0004 & 0.0002 \\ -0.0011 & -1.1673 & -0.0008 & -0.0002 \\ -0.0004 & -0.0011 & -1.1516 & 0.0001 \\ -0.0016 & -0.0005 & -0.0014 & -1.1115 \end{bmatrix},$$

$$K_3 = \begin{bmatrix} 7.3908 & -0.0042 & -0.0011 & -0.0056 \\ -0.0054 & 7.6000 & -0.0054 & -0.0011 \\ -0.0010 & -0.0040 & 7.2683 & -0.0054 \\ -0.0029 & -0.0008 & -0.0029 & 5.4823 \end{bmatrix}.$$

A bisection approach on the value of D allows us to find the maximal admissible value as $D_{\max} = 0.2426\,s$, which is sufficient for our application as the mean peak value for the delay is $0.2\,s$. The temperature tracking error for such controller is shown in Figure 5.9. A significant improvement is obtained with respect to the mixed-sensitivity approach.

On the other hand, when Lemma 5.4.2 is used for synthesis with the simplifications $S = \varepsilon_s P$, $\varepsilon_s = 67$, $R = \varepsilon_r P$, $\varepsilon_r = 34$, and $D = 0.2\,s$, we get errors evolving as depicted in Figure 5.10. We can clearly see that the maximal error values and the time needed to compensate a perturbation are significantly larger when the delay is included in the controller synthesis by using Lemma 5.4.2. This is related to the inherent conservatism associated with such method.

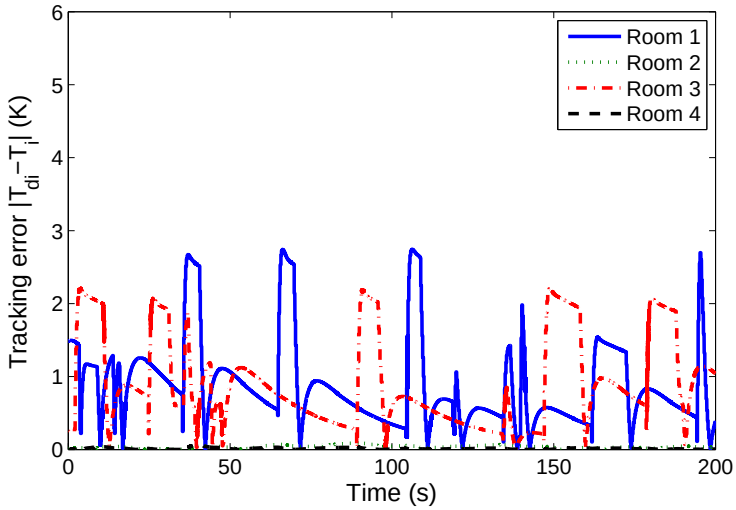

(a) Synchronous mode

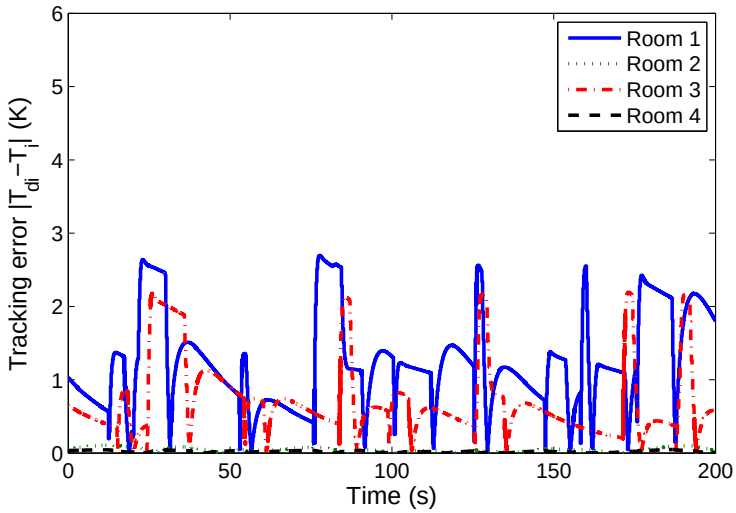

(b) Asynchronous mode

Figure 5.8: Mixed-sensitivity H_∞ controller: temperature tracking error with communication over IEEE 802.15.4.

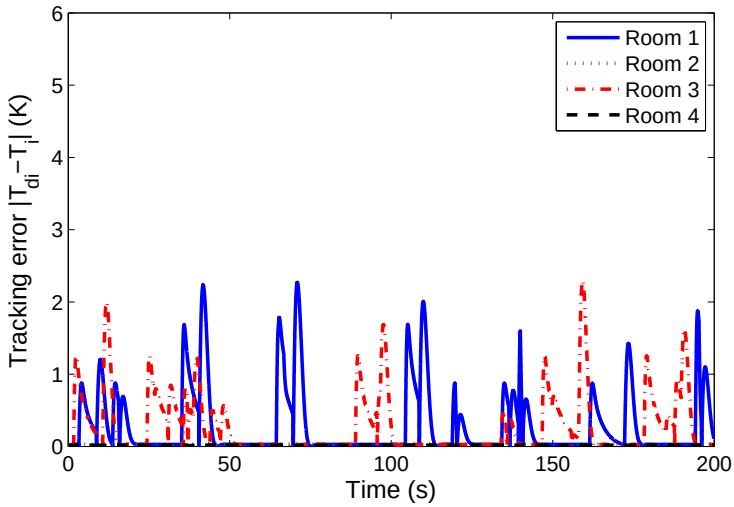

Figure 5.9: Controller from Lemma 5.4.1: temperature tracking error with communication over IEEE 802.15.4.

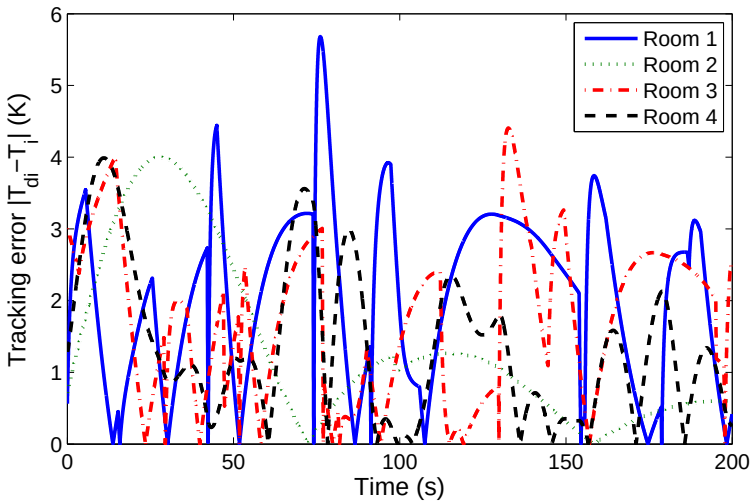

Figure 5.10: Controller from Lemma 5.4.2: temperature tracking error with communication over IEEE 802.15.4.

5.6 Summary

In this chapter, we considered the problem of temperature regulation in intelligent buildings as the real-time control of an actuated UFAD process based on WSN measurements. A flexible model of the airflows was studied based on the thermodynamics properties of the room control volume. Discrete events such as doors openings, people presence, and the use of computers or printers were introduced as Markovian processes, which resulted in a hybrid nonlinear state-space description of the complete interconnected system. Reliability and delay of a IEEE 802.15.4 WSN were considered. Synchronous and asynchronous communications were both studied.

Various MIMO H_∞ controllers were synthesized based on linearized model dynamics and compared in terms of temperature regulation performance. It was shown that the WSN has a strong impact on the closed-loop stability. It was also noted that synchronous or asynchronous transmissions do not have a strong impact on the closed-loop system.

A second controller obtained using the bounded-real lemma was then proposed. An appropriate choice of the norm allowed us to tune the sensitivity to delays and the maximum admissible delay was computed a posteriori. This controller appeared to be the most efficient, in terms of temperature regulation (maximum peaks and response time).

Finally, a third controller was designed with consideration of the maximum allowable delay in the gain synthesis. The resulting closed-loop performances appeared to be worse than the other two design strategies, with a larger error and longer response time. This is probably related to the conservatism induced by the method.

Table 5.11: Main symbols used in Chapter 5.

α_p	performance control parameter
α_t	disturbance control parameter
α_u	input control parameter
ρ_i	density in room i
h_{tot}	total hentalpy
$\dot{m}$	mass flow rate
C_p	constant pressure specific heat
C_v	constant volume specific heat
D	delay
E_i	energy in room i
K	control gain
N	number of nodes in the network
N_d	number of doors in each room
N_{pl}	number of diffusers in each room
N_q	number of power sources in each room
$\dot{Q}$	heat exchange
S	sensitivity function
T	complementary sensitivity function
$T_{d,i}$	desired temperature in room i
T_i	temperature in room i
T_s	sampling time
V_i	volume of room i
W_p	performance weight
W_t	disturbance weight
W_u	input weight

Chapter 6

Conclusions and Future Work

In this thesis, we proposed an analytical framework to model and design MAC, routing, and control application layers for energy efficient networks with application in industrial and building automation. We proceeded by analyzing the problem in three steps.

First, we studied the mutual influence between routing decisions and MAC performance in terms of reliability, delay, and load balancing, by considering the ROLL routing specifications over unslotted IEEE 802.15.4 MAC. To do so, we introduced an analytical model that includes the important features of multi-hop networks, such as heterogeneous distribution of the traffic and hidden terminal nodes. We showed that the distribution of traffic load in the network influences the performance in terms of reliability, delay, and energy consumption of the links. This effect depends strongly on the carrier sensing range of nodes in the network. Furthermore, we derived conditions in which routing decisions based on packet loss probability or delay may lead to an unbalanced distribution of the traffic load across paths with potential dangerous effects on the energy consumption.

We extended then our perspective by including the effect of the requirements from the application in the design of a communication protocol stack compliant with ROLL and IEEE 802.15.4, as we developed TREnD, a novel cross-layer solution for control applications over wireless networks, which satisfies application requirements on reliability and delay while minimizing energy consumption. We posed and solved an optimization problem to select the protocol parameters. We presented a test-bed implementation of the protocol that we designed with TinyOS and Tmote sensors. An experimental campaign was conducted to validate the protocol in an indoor environment. Experimental results showed that the protocol achieves the reliability and delay requirements also in practice, while minimizing the energy consumption. In addition, the protocol showed good load balancing performance and scalability.

As final step, we considered the influence of communication performance indicators in the design and synthesis of a robust controller for an actuated under floor air distribution process based on wireless sensor network measurements. A hybrid

nonlinear state-space description of the complete interconnected system was proposed based on the thermodynamic properties of the room control volume. Three MIMO H_∞ controllers were synthesized based on a linearized model and compared in temperature regulation performance.

6.1 Future Work

A design methodology that integrates communication and control layer aspects for energy efficient applications requires a thorough understanding of the protocol stack interactions. A suitable control synthesis is often strongly dependent on the characteristics of the underlying communication network. Moreover, a multitude of applications may share the same network infrastructure and thereby need to be able to adapt their load demands. New routing and MAC protocols with proper interfaces to the these applications should be developed. A challenge is in how to generalize the problem discussed in the thesis in this direction without increasing the complexity of the design framework.

Besides the contribution presented in this thesis, there are various aspects of this problem that are under development and ideas for future studies. Here, we describe three lines of research, as continuation, completion, and extension of the study of the block diagram framework presented in Figure 1.4.

6.1.1 Analytical Modeling of MAC Protocols

The model of the hybrid TDMA/CSMA solution of TREnD, can be extended to heterogeneous traffic in the nodes. The problem is formulated as follows: each node V_i has a buffer of λ_i packets that have been generated during the sleeping time (inactive TDMA-slots). N nodes contend the medium by using p-persistent MAC or CSMA/CA mechanism, and need to deliver their packets within a deadline given by the TDMA-slot duration S. When the buffer is empty, the node goes to sleep. The Markov chain in Figure B.1 can be extended to a two-dimensional chain, in which the two states represent the number of packets to deliver and the number of contending nodes. A tradeoff between accuracy and tractability of the equations is important for a practical implementation of the protocol.

An interesting evolution of the current standards is proposed by the IEEE 802.15.4e working group, which is extending the MAC layers specification of the IEEE 802.15.4 standard, by including functionalities for factory and home automation. TDMA with frequency hopping is included in the MAC of the IEEE 802.15.4e. An analytical model of the full MAC architecture of the IEEE 802.15.4e standard would be a relevant contribution.

6.1.2 Routing Protocols for Energy Efficient Wireless Networks

The ROLL standardization process is ongoing. An interesting problem is the choice of a suitable metric for the RPL protocol. The proposal of a routing metric that

takes into account performance of random access MAC layers explicitly is a potential contribution. In particular, the path selection process might retrieve information about the average number of channel contentions that each node in a certain path may experience, to guarantee QoS requirements and distribute the traffic fairly.

As described in Chapter 2, nodes perform global and local maintenance through DIO messages. A slow update of the routing information reduces the energy consumption, but it might make the routing sensitive to channel variabilities and thereby degrade performance. Conversely, a fast update might cause continuous routing topology changes and generate instability in the network. A tradeoff might be exploited to offer energy efficiency and stable routing.

Eventually, a complete implementation of the RPL protocol in the TREnD protocol stack would be useful to validate our proposed ideas.

6.1.3 Control Applications in Building Automation

The application of a robust controller over a IEEE 802.15.4 network showed how critically performance indicators as the delay or packet losses influence the design strategy for under floor air distribution control. Less conservative approaches for controller synthesis can be exploited and implemented.

Finally, the design and synthesis of a building automation application can be integrated with a full description of the communication stack, including MAC and routing over multi-hop networks, to complete the block diagram framework in Figure 1.4. An implementation of the proposed communication protocol and controller strategies in a real building automation system would be useful to validate our design methodology.

Appendix A

Proof for Chapter 3

Transition Probabilities of the Markov Chain in Figure 3.3

The transition probabilities of the Markov chain in Figure 3.3 are

$$\Pr[i,k,j|i,k+1,j] = 1, \text{ for } k \geq 0\,, \tag{A.1}$$

$$\Pr[i,k,j|i-1,0,j] = \frac{\alpha_l}{W_i}, \text{ for } i \leq m\,, \tag{A.2}$$

$$\Pr[0,k,j|i,0,j-1] = \frac{(1-\alpha_l)P_{coll,l}}{W_0}, \text{ for } j \leq n\,, \tag{A.3}$$

$$\Pr[\text{idle}|m,0,j] = (1-q_l)\,\alpha_l, \text{ for } j < n\,, \tag{A.4}$$

$$\Pr[\text{idle}|i,0,n] = (1-q_l)(1-\alpha_l), \text{ for } i < m\,, \tag{A.5}$$

$$\Pr[\text{idle}|m,0,n] = 1-q_l, \tag{A.6}$$

$$\Pr[0,k,0|\text{idle}] = \frac{q_l}{W_0}, \text{ for } k \leq W_0 - 1\,. \tag{A.7}$$

Equation (A.1) gives the decrement of backoff counter, which happens with probability 1. Equation (A.2) represents the probability of finding busy channel in the CCA and of choosing a state uniformly in the next backoff stage. Equation (A.3) gives the unsuccessful transmission probability after finding a clear channel, and a node selects uniformly a state in the next retransmission stage. Equations (A.4) and (A.5) represent the probability of going back to the idle stage due to the channel access failure and retry limits, respectively. Equation (A.6) is the probability of going back to the idle stage at backoff counter m and retransmission stage n, as function of the traffic q_l. Equation (A.7) models the probability of going back to the first backoff stage from the idle stage.

Proof of Proposition 3.3.1

We need to compute the stationary distribution of the Markov chain in Figure 3.3, i.e., $b_{i,k,j} = \lim_{t\to\infty} \Pr(s(t) = i, c(t) = k, r(t) = j), i \in (-2, m), k \in (-1, \max(W_i -$

$1, L_s-1, L_c-1)), j \in (0,n)$. Owing to the chain regularities and Equations (A.1) – (A.7), we have

$$b^{(l)}_{i,k,j} = \frac{W_i - k}{W_i} b^{(l)}_{i,0,j}\,, \tag{A.8}$$

where $W_i = \begin{cases} 2^i W_0 & i \le m_b - m_0 \\ 2^{m_b - m_0} W_0 & i > m_b - m_0\,. \end{cases}$

From Equation (A.2), for $i \le m$ we obtain

$$b^{(l)}_{i,0,j} = \alpha_l^i b^{(l)}_{0,0,j}. \tag{A.9}$$

From Equation (A.3), $b^{(l)}_{0,0,j}$ is rewritten as follows,

$$b^{(l)}_{0,0,j} = (1-\alpha_l) P_{coll,l} \sum_{i=0}^{m} b^{(l)}_{i,0,j-1} = \left((1-\alpha_l) P_{coll,l} \sum_{i=0}^{m} \alpha_l^i \right)^j b^{(l)}_{0,0,0}\,. \tag{A.10}$$

By the normalization condition, we know that

$$\sum_{i=0}^{m} \sum_{k=0}^{W_i-1} \sum_{j=0}^{n} b^{(l)}_{i,k,j} + \sum_{j=0}^{n} \left(\sum_{k=0}^{L_s-1} b^{(l)}_{-1,k,j} + \sum_{k=0}^{L_c-1} b^{(l)}_{-2,k,j} \right) + b^{(l)}_{idle} = 1\,. \tag{A.11}$$

We next derive the expressions of each term in Equation (A.11). From Equations (A.8), (A.9), and (A.10) we have

$$\sum_{i=0}^{m} \sum_{k=0}^{W_i-1} \sum_{j=0}^{n} b^{(l)}_{i,k,j} = \sum_{i=0}^{m} \sum_{j=0}^{n} \frac{W_i+1}{2} \alpha_l^i\, b^{(l)}_{0,0,j} \tag{A.12}$$

$$= \begin{cases} \frac{b^{(l)}_{0,0,0}}{2} \left(\frac{1-(2\alpha_l)^{m+1}}{1-2\alpha_l} W_0 + \frac{1-\alpha_l^{m+1}}{1-\alpha_l} \right) \frac{1-y_l^{n+1}}{1-y_l} \\ \quad \text{if } m \le \bar{m} = m_b - m_0 \\ \frac{b^{(l)}_{0,0,0}}{2} \left(\frac{1-(2\alpha_l)^{\bar{m}+1}}{1-2\alpha_l} W_0 + \frac{1-\alpha_l^{\bar{m}+1}}{1-\alpha_l} + (2^{m_b}+1)\alpha_l^{\bar{m}+1} \frac{1-\alpha_l^{m-\bar{m}}}{1-\alpha_l} \right) \frac{1-y_l^{n+1}}{1-y_l} \\ \quad \text{otherwise,} \end{cases}$$

where $y_l = P_{coll,l}(1-\alpha_l^{m+1})$.
Similarly,

$$\sum_{j=0}^{n} \left(\sum_{k=0}^{L_s-1} b^{(l)}_{-1,k,j} + \sum_{k=0}^{L_c-1} b^{(l)}_{-2,k,j} \right)$$

$$= (L_s(1-P_{coll,l}) + L_c P_{coll,l})(1-\alpha_l^{m+1}) \frac{1-y_l^{n+1}}{1-y_l}\, b^{(l)}_{0,0,0}\,. \tag{A.13}$$

By considering that the successful transmission and the failure events are due to the limited number of backoff stages m and the retry limits n, the idle state probability

is

$$
\begin{aligned}
b_{idle}^{(l)} =& (1-q_l)\, b_{idle}^{(l)} + (1-q_l) \left[\sum_{j=0}^{n} \alpha_l\, b_{m,0,j}^{(l)} \right. \\
& \left. + \sum_{i=0}^{m} P_{coll,l}\, b_{i,0,n}^{(l)} + \sum_{i=0}^{m} \sum_{j=0}^{n} (1-P_{coll,l})\, b_{i,0,j}^{(l)} \right] \\
=& \frac{1-q_l}{q_l} \left[\frac{\alpha_l^{m+1}(1-y_l^{n+1})}{1-y_l} + P_{coll,l}(1-\alpha_l^{m+1}) y_l^n \right. \\
& \left. + (1-P_{coll,l}) \frac{(1-\alpha_l^{m+1})(1-y_l^{n+1})}{1-y_l} \right] b_{0,0,0}^{(l)} \,. \qquad \text{(A.14)}
\end{aligned}
$$

Note that Equations (A.12)–(A.14) give the state values $b_{i,k,j}^{(l)}$ as a function of $b_{0,0,0}^{(l)}$. By replacing Equations (A.12)–(A.14) in the normalization condition given by Equation (A.11), we obtain the expression of $b_{0,0,0}^{(l)}$, given in Equation (3.3).

As last step, we can derive τ_l by summing up the probability of being in the generic sensing stage $b_{i,0,j}^{(l)}$,

$$
\tau_l = \sum_{i=0}^{m} \sum_{j=0}^{n} b_{i,0,j}^{(l)} = \left(\frac{1-\alpha_l^{m+1}}{1-\alpha_l} \right) \left(\frac{1-y_l^{n+1}}{1-y_l} \right) b_{0,0,0}^{(l)}.
$$

Appendix B

Proofs for Chapter 4

Proof of Claim 4.4.1

Let k be the generic number of packets that a cluster has to evacuate at the beginning of a transmitting TDMA-slot. In the analytical derivations, we consider the worst case scenario for packet collisions, which occurs when k packets are distributed over k different nodes. The cluster behavior is modeled by a discrete time Markov chain (DTMC), where the state is associated to the number of nodes that have to forward packets (Figure B.1). The state 0 corresponds to the situation where no packets are stored in the cluster. Then, p_k is the probability to go from state k to $k-1$ in the chain. In an ideal CSMA, all nodes are able to sense ongoing transmissions avoiding collisions. By this hypothesis, p_k is the probability to have at least one node attempting to transmit the packet (i.e., $(1-(1-\tau)^k)$), given the probability that a beacon is received p_{bc}. Since all N nodes in the receiving cluster are candidate to send the beacon, $p_{\mathrm{bc}} = \gamma N \omega (1-\omega)^{N-1}$. Packet collisions occur when a simultaneous sensing attempt is done by more than one node (i.e., $p_{\mathrm{cl}}^{\tau(k-1)}$ where $\tau(k-1)$ is the expected number of additional accesses to the channel in the same CSMA-slot by the $k-1$ nodes in the same cluster). By considering all these factor, the successful transmission probability is given in Equation (4.4).

Proof of Claim 4.4.2

Let $P(n,S,k)$ be the probability to be in the state n after a number S of steps in the DTMC when there are k packets in the cluster. In other words, $P(n,S,k)$ is the probability of losing n out of k packets in a cluster after a time of S CSMA-slots. In fact, if there are still n packets left after S CSMA-slots, these packets are discarded. Let $p_n^* = 1 - p_n$ where p_n is the successful transmission probability given in Equation (4.4). We derive $P(n,S,k)$ recursively, by noting that:

$$P(n,S,k) = P(n+1,S-1,k)\, p_{n+1} + P(n,S-1,k)\, p_n^* \,,$$

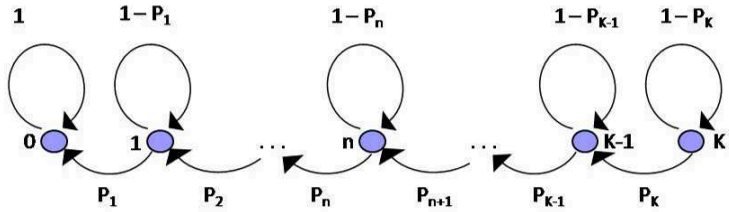

Figure B.1: Markov chain model. The state k represents the number of packets in a cluster.

where

$$P(k, S-k+n, k) = (p_n^*)^{S-k+n}\,,$$
$$P(n, k-n, k) = \prod_{l=n+1}^{k} p_l\,.$$

By defining a set $V(n) = \{p_n^*, p_{n+1}^*, ..., p_k^*\}$ and a matrix that contains all the M_c combinations with repetition of the elements in $V(n)$, taken in groups of $S-k+n$: $A(n) = [a_{i,j}]_{M_c}^{S-k+n}$, a closed form expression of $P(n,S,k)$ is

$$P(n,S,k) = \prod_{l=n+1}^{k} p_l \left(\sum_{i=1}^{M_c} \prod_{j=1}^{S-k+n} a_{i,j} \right)\,,$$

for all n, k, S, where $n \leq k \leq S$.

Let us consider a numerical example. Let $k = 3$ and $S = 4$, we determine $P(1,4,3)$, which is given by the sum of the probabilities of all possible paths in the DTMC that start from the state 3 and end in 1 within exactly four steps. It follows that

$$P(1,4,3) = p_2 p_3 [p_1^* p_1^* + p_2^* p_2^* + p_3^* p_3^* + p_1^* p_2^* + p_1^* p_3^* + p_2^* p_3^*]\,.$$

The product $p_2 p_3$ is present in all paths, whereas, within brackets, there are all the combinations with repetition of the elements p_1^*, p_2^*, p_3^*, taken two per time. Then,

$$V(1) = \{p_1^*, p_2^*, p_3^*\}\,,$$
$$A(1) = \begin{bmatrix} p_1^* & p_2^* & p_3^* & p_1^* & p_1^* & p_2^* \\ p_1^* & p_2^* & p_3^* & p_2^* & p_3^* & p_3^* \end{bmatrix}^T\,.$$

The reliability R over $h_{\max}$ hops is:

$$R = \left(\sum_{n=0}^{k} \frac{k-n}{k} P(n,S,k) \right)^{h_{\max}}\,,$$

where Equation (4.5) follows after substitutions.

Proof of Claim 4.4.3

R_j^{ag} is computed iteratively by considering the dependance on the number of aggregated packets that the hop j has to forward from the hop $j+1$, and R_{j-1}^{ag}. Suppose $h_i = 4$, then

$$\begin{aligned} R_4^{\mathrm{ag}} &= R_3^{\mathrm{ag}} r_1 = R_3^{\mathrm{ag}} R_1 \,, \\ R_3^{\mathrm{ag}} &= R_2^{\mathrm{ag}}[(1-r_1)r_1 + r_1 r_2] = R_2^{\mathrm{ag}} R_2 \,, \\ R_2^{\mathrm{ag}} &= R_1^{\mathrm{ag}}[(1-R_2)r_1 + (1-r_1)r_1 r_2 + r_1 r_2 r_3] = R_1^{\mathrm{ag}} R_3 \,, \\ R_1^{\mathrm{ag}} &= [(1-R_3)r_1 + (1-r_2)r_1 r_2 + (1-r_1)r_1 r_2 r_3 + r_1 r_2 r_3 r_4] = R_0^{\mathrm{ag}} R_4 \,. \end{aligned}$$

By defining $r_j = \sum_{i=1}^{j}(1-r_{i-1}) \prod_{z=1}^{j-i+1} R_z$, with $r_0 = 0$, it follows that Equation (4.6) holds for a generic h_i.

Explanation of Claim 4.4.4

According to the DTMC in Figure B.1, the required number of CSMA-slots to advance in the chain from state j to $j-1$ follows a Geometric distribution of parameter p_j. By the Central Limit Theorem, the cluster evacuation time T_e is approximated by a normal random variable having mean μ and variance σ^2. These moments are given by the sum of the expected times and variances, respectively, to advance a step in the chain. Consequently, we have that $T_e \sim \mathcal{N}(\mu, \sigma^2)$, where $\mu = \sum_{j=1}^{k} 1/p_j$, and $\sigma^2 = \sum_{j=1}^{k}(1-p_j)/p_j^2$.

By considering the properties of the CDF (cumulative distribution function) of T_e, we derive Equation (4.8).

Proof of Claim 4.4.5

Let us consider a single TDMA-slot. According to the p-persistent MAC mechanism described in Section 4.3, the number of CCAs performed in a TDMA-slot depends on the average number of packets to be forwarded λT_{cyc} according to the relation:

$$W_{\mathrm{cca}} = \sum_{j=1}^{\lambda T_{\mathrm{cyc}}} j \frac{\tau\omega}{\gamma} \,,$$

where τ, ω, and γ respectively account for wake up probability in transmission, wake up probability in reception and good channel probability. Given a successful CCA, the number of transmitted packets is approximated by $W_{\mathrm{pkt}} \approx \lambda T_{\mathrm{cyc}}$. Similarly, the number of acknowledgements is $W_{\mathrm{ack}} \approx \lambda T_{\mathrm{cyc}}$.

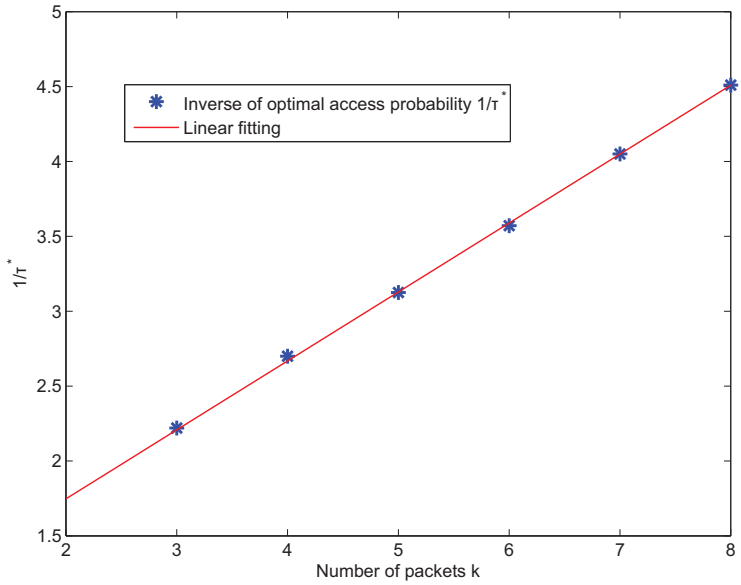

Figure B.2: Empirical evaluation of optimal wake up probability in transmission τ^*.

The costs for beacon transmission, wake up, and listening in a TDMA-slot depend on the sleeping discipline in reception by introducing the factor:

$$W_{\mathrm{rx}} = \omega \frac{NW}{M_s},$$

which accounts for the average number of times there is an awake node.

Hence, considering a total time T_{tot}:

$$E_{\mathrm{tot}} = \frac{T_{\mathrm{tot}}}{S}\left(W_{\mathrm{cca}}E_{\mathrm{cca}} + W_{\mathrm{pkt}}E_{\mathrm{pkt}} + E_{\mathrm{ack}} + W_{\mathrm{rx}}\left(E_{\mathrm{bc}}\frac{S}{\delta} + E_w + E_l S\right)\right).$$

where Equation (4.9) follows after substitutions.

Proof of Claim 4.4.6

For a p-persistent CSMA, it is shown that the access probability optimizing in terms of reliability is $\tau^* = 1/j$, given that there are j packets to be sent during a CSMA-slot [16]. Such a probability, however, depends on the entire cluster state, namely the current number of packets to be forwarded in a cluster, which can be hardly used. In fact, a node does not have knowledge of the number of packets in a cluster at a given CSMA time slot. Therefore, the choice of a constant access

probability for the whole duration of the TDMA-slot is reasonable. We derive the optimal empirical constant access probability by evaluating numerically the access probability τ^* that optimize the reliability in Equation (4.5) as function of $k = \lambda M_s S$. By a linear fitting of the results (see Figure B.2), we derive the coefficients: $c_1 = 2.17$, $c_2 = 1.81$.

The wake up probability in reception ω is determined by similar arguments. In reception, the number of contending nodes is constant during a slot and upper bounded by the number of nodes in the cluster N, which is known at the controller. Hence, the sub-optimal wake up probability is $\omega^* = 1/N$.

Bibliography

[1] G. Scheible, D. Dzung, J. Endresen, and J.-E. Frey. Unplugged but connected, design and implementation of a truly wireless real-time sensor/actuator interface. *IEEE Industrial Electronics Magazine*, 1(2):25–34, 2007.

[2] *WirelessHART Specitications*, 2007. `http://www.hartcomm2.org`.

[3] ISA. *SP-100*, 2008. `http://www.isa.org/isasp100/`.

[4] *IEEE 802.15.4 Wireless Medium Access Control (MAC) and Physical Layer (PHY) Specifications for Low-Rate Wireless Personal Area Networks (WPANs)*, 2006. `http://www.ieee802.org/15/pub/TG4.html`.

[5] A. Willig. Recent and emerging topics in wireless industrial communication. *IEEE Transactions on Industrial Informatics*, 4(2):102–124, 2008.

[6] Frost & Sullivan. *Wireless Devices in the Factory Automation - An Overview of Adoption Trends*, 2008. `http://www.frost.com/prod/servlet/frost-home`.

[7] D. Snoonian. Smart buildings. *IEEE Spectrum*, 40(8):18–23, 2003.

[8] *Stockholm Royal Seaport*, 2010. `http://www.stockholmroyalseaport.com/`.

[9] L. Schenato, B. Sinopoli, M. Franceschetti, K. Poolla, and S. S. Sastry. Foundations of control and estimation over lossy networks. *Proceedings of the IEEE*, 95(1):163–187, 2007.

[10] W. Zhang, M. S. Braniky, and S. M. Phillips. Stability of networked control systems. *IEEE Control Systems Magazine*, 21(1):84–99, 2001.

[11] M. Rabi and K. H. Johansson. Event-triggered strategies for industrial control over wireless networks. In *Proceedings of the 5th Annual International Wireless Internet Conference (WICON)*, 2008.

[12] U. Tiberi, C. Fischione, K. H. Johansson, and M. D. Di Benedetto. Adaptive self-triggered control over IEEE 802.15.4 networks. In *Proceedings of the IEEE Conference on Decision and Control*, 2010.

[13] *Routing over low power and lossy networks (ROLL)*, 2010. `http://www.ietf.org/dyn/wg/charter/roll-charter.html`.

[14] T. Abdelzaher, T. He, and J. Stankovic. Feedback control of data aggregation in sensor networks. In *Proceedings of the IEEE Conference on Decision and Control*, 2004.

[15] J. P. Hespanha, P. Naghshtabrizi, and Y. Xu. A survey of recent results in networked control systems. *Proceedings of the IEEE*, 95(1):138–162, 2007.

[16] A. Bonivento, C. Fischione, L. Necchi, F. Pianegiani, and A. Sangiovanni-Vincentelli. System level design for clustered wireless sensor networks. *IEEE Transactions on Industrial Informatics*, 3(3):202–214, 2007.

[17] C. Gomez, J. Paradells, and J. Caballero. *Sensors Everywhere (Wireless Network Technologies and solutions)*. i2CAT Fundation and Fundacion Vodafone, 2010.

[18] J. Polastre, J. Hill, and D. Culler. Versatile low power media access for wireless sensor networks. In *Proceedings of the ACM Conference on Embedded Networked Sensor Systems (SenSys)*, New York, NY, USA, 2004.

[19] M. Buettner, G. Yee, E. Anderson, and R. Han. X-MAC: A short preamble MAC protocol for duty-cycled wireless sensor networks. In *Proceedings of the ACM Conference on Embedded Networked Sensor Systems (SenSys)*, 2006.

[20] K. Jamieson, H. Balakrishnan, and Y. C. Tay. Sift: A mac protocol for event-driven wireless sensor networks. Technical report, MIT Laboratory for Computer Science, 2003.

[21] V. Rajendran, K. Obraczka, and J.J. Garcia-Luna-Aceves. Energy efficient, collision free medium access control for wireless sensor networks. In *Proceedings of the ACM Conference on Embedded Networked Sensor Systems (SenSys)*, 2003.

[22] K. Pister and L. Doherty. TSMP: Time synchronized mesh protocol. In *Proceedings of the IASTED International Symposium on Distributed Sensor Networks (DSN)*, 2008.

[23] J. Heidemann W. Ye and D. Estrin. Medium access control with coordinated adaptive sleeping for wireless sensor networks. *IEEE/ACM Transactions on Networking*, 12(3):493–506, 2004.

[24] T. van Dam and K. Langendoen. An adaptive energy-efficient MAC protocol for wireless sensor networks. In *Proceedings of the ACM Conference on Embedded Networked Sensor Systems (SenSys)*, 2003.

[25] R. Injong, A. Warrier, M. Aia, M. Jeongki, and M. L. Sichitiu. ZMAC: A hybrid MAC for wireless sensor networks. *IEEE/ACM Transactions on Networking*, 16(3):511–524, 2008.

[26] J. Gutiérrez. On the use of IEEE std. 802.15.4 to enable wireless sensor networks in building automation. *International Journal of Wireless Information Networks*, 14(4):295–301, 2007.

[27] IETF. *The internet engineering task force*, 2010. `http://www.ietf.org`.

[28] ZigBee Alliance. *ZigBee Specification*, 2005. `http://www.caba.org/standard/zigbee.html`.

[29] W. Heinzelman, A. Chandrakasan, and H. Balakrishnan. An application-specific protocol architecture for wireless microsensor networks. *IEEE Transactions on Wireless Communications*, 1(4):660–670, 2002.

[30] P. R. Kumar. New technological vistas for systems and control: the example of wireless networks. *Control Systems Magazine, IEEE*, 21(1):24–37, 2001.

[31] Q. Liu and P. Linden. An extended model for under floor air distribution. In *SimBuild: Building Sustainability and Performance Through Simulation*, 2004.

[32] V. Kawadia and P. R. Kumar. A cautionary perspective on cross-layer design. *IEEE Wireless Communications*, 12(1):3–11, 2005.

[33] G.C. Walsh, Hong Ye, and L.G. Bushnell. Stability analysis of networked control systems. *IEEE Transactions on Control Systems Technology*, 10(3):438–446, May 2002.

[34] G.N. Nair, F. Fagnani, S. Zampieri, and R.J. Evans. Feedback control under data rate constraints: An overview. *Proceedings of the IEEE*, 95(1):108–137, 2007.

[35] W. S. Wong and R.W. Brockett. Systems with finite communication bandwidth constraints. ii. stabilization with limited information feedback. *IEEE Transactions on Automatic Control*, 44(5):1049 –1053, 1999.

[36] Jean-Pierre Richard. Time-delay systems: an overview of some recent advances and open problems. *Automatica*, 39(10):1667 – 1694, 2003.

[37] S. Pollin, M. Ergen, S. Coleri Ergen, B. Bougard, L. Van der Perre, I. Moerman, A. Bahai, P. Varaiya, and F. Catthoor. Performance analysis of slotted carrier sense IEEE 802.15.4 medium access layer. *IEEE Transactions on Wireless Communications*, 7(9):3359–3371, 2008.

[38] J. Mišić, S. Shaf, and V.B. Mišić. Performance of a beacon enabled IEEE 802.15.4 cluster with downlink and uplink traffic. *IEEE Transactions Parallel and Distributed Systems*, 17(4):361–376, 2006.

[39] P. Park, P. Di Marco, P. Soldati, C. Fischione, and K. H. Johansson. A generalized Markov chain model for effective analysis of slotted IEEE 802.15.4. In *Proceedings of the 6th IEEE International Conference on Mobile Ad-hoc and Sensor Systems (MASS)*, 2009.

[40] C. Buratti and R. Verdone. Performance analysis of IEEE 802.15.4 non beacon-enabled mode. *IEEE Transactions on Vehicular Technology*, 58(7):3480 –3493, 2009.

[41] J. He, Z. Tang, H.-H. Chen, and Q. Zhang. An accurate and scalable analytical model for IEEE 802.15.4 slotted CSMA/CA networks. *IEEE Transactions on Wireless Communications*, 8(1):440–448, 2009.

[42] P. Park, P. Di Marco, C. Fischione, and K. H. Johansson. Adaptive IEEE 802.15.4 protocol for reliable and timely communications. *IEEE/ACM Transactions on Networking*, 2010. Provisionally accepted.

[43] G. Bianchi. Performance analysis of the IEEE 802.11 distributed coordination function. *IEEE Journal on Selected Areas in Communications*, 18(3):535–547, 2000.

[44] I. Ramachandran, A. K. Das, and S. Roy. Analysis of the contention access period of IEEE 802.15.4 MAC. *ACM Transactions on Sensor Networks*, 3(1):4–20, 2007.

[45] D. Malone, K. Duffy, and D. Leith. Modeling the 802.11 distributed coordination function in nonsaturated heterogeneous conditions. *IEEE/ACM Transactions on Networking*, 15(1):159–172, 2007.

[46] M. Chen, G. Liu, D. Wu, and G. Zhu. A unified model for performance analysis of 802.11 in heterogeneous traffic and saturation condition. In *Proceedings of the IEEE International Communications Conference (ICC)*, 2008.

[47] E. Ndih, N. Khaled, and G. De Micheli. An analytical model for the contention access period of the slotted IEEE 802.15.4 with service differentiation. In *Proccedings of the IEEE International Communications Conference (ICC)*, 2009.

[48] T. Kim and J.T. Lim. Throughput analysis considering coupling effect in IEEE 802.11 networks with hidden stations. *IEEE Communication Letters*, 13(3):175–177, 2009.

[49] H. Wu, F. Zhu, Q. Zhang, and Z. Niu. Analysis of IEEE 802.11 DCF with hidden terminals. In *Proceedings of the IEEE Global Communications Conference (GLOBECOM)*, 2006.

[50] M. Hira, F. Tobagi, and K. Medepalli. Throughput analysis of a path in an IEEE 802.11 multihop wireless network. In *Proceedings of the IEEE Wireless Communications and Networking Conference (WCNC)*, 2007.

[51] J. Baras, V. Tabatabaee, P. Papageorgiou, and N. Rentz. Modelling and optimization for multi-hop wireless networks using fixed point and automatic differentiation. In *Proceedings of the 6th Intl. Symposium on Modeling and Optimization in Mobile, Ad Hoc, and Wireless Networks (WiOpt)*, 2008.

[52] M. Martalò, S. Busanelli, and G. Ferrari. Markov chain-based performance analysis of multihop IEEE 802.15.4 wireless networks. *Elsevier Performance Evaluation*, 66(12):722–741, 2009.

[53] S. Coleri Ergen, P. Di Marco, and C. Fischione. MAC protocol engine for sensor networks. In *Proceedings of the IEEE Global Communications Conference (GLOBECOM)*, 2009.

[54] Y. Xu, J. Heidemann, and D. Estrin. Geography-informed energy conservation for ad hoc routing. In *Proceedings of the Annual International Conference on Mobile Computing and Networking (MobiCom)*, 2001.

[55] B. Chen, K. Jamieson, H. Balakrishnan, and R. Morris. SPAN: An energy-efficient coordination algorithm for topology maintenance in ad hoc wireless networks. In *Proceedings of the Annual International Conference on Mobile Computing and Networking (MobiCom)*, 2001.

[56] M. Zorzi and R. R. Rao. Energy and latency performance of geographic random forwarding for ad hoc and sensor networks. In *Proceedings of the IEEE Wireless Communications and Networking Conference (WCNC)*, 2003.

[57] N. Burri, P. von Rickenbach, and R. Wattenhofer. Dozer: ultra-low power data gathering in sensor networks. In *Proceedings of the IEEE/ACM International Conference on Information Processing in Sensor Networks (IPSN)*, 2007.

[58] Ö. B. Akan and F. Akyildiz. Event-to-Sink Reliable Transport in Wireless Sensor Networks. *IEEE Transactions on Networking*, 13:1003–1016, 2005.

[59] F. Stann and J. Heidemann. RMST: Reliable Data Transport in Sensor Networks. In *Proceedings of the IEEE Workshop on Sensor Network Protocols and Applications*, 2003.

[60] S. Kim, R. Fonseca, P. Dutta, A. Tavakoli, D. Culler, P. Levis, S. Shenker, and I. Stoica. Flush: a reliable bulk transport protocol for multihop wireless networks. In *Proceedings of the ACM Conference on Embedded Networked Sensor Systems (SenSys)*, 2007.

[61] E. Felemban, C.-G. Lee, and E. Eylem. MMSPEED: Multipath multi-speed protocol for QoS guarantee of reliability and timeliness in wireless sensor networks. *IEEE Transactions on Mobile Computing*, 5(6):738–754, 2006.

[62] P. Park, C. Fischione, A. Bonivento, K. H. Johansson, and A. Sangiovanni-Vincentelli. Breath: a self-adapting protocol for wireless sensor networks in control and automation. In *Proceedings of the 5th Annual IEEE Communications Society Conference on Sensor, Mesh and Ad Hoc Communications and Networks (SECON)*, 2008.

[63] Moteiv, San Francisco, CA. *Tmote Sky Data Sheet*, 2006. `http://www.moteiv.com/products/docs/tmote-sky-datasheet.pdf`.

[64] D. Gay, P. Levis, and D. Culler. Software Design Patterns for TinyOS. *Proceedings of the ACM Conference on Languages, Compilers and Tools for Embedded Systems*, 2005.

[65] C. Oliveira and P. Pardalos. A survey of combinatorial optimization problems in multicast routing. *Computers and Operations Research*, August 2005.

[66] M. Zuniga, B. Krishnamachari. Analyzing the transitional region in low power wireless links. In *Proceedings of the 1st IEEE International Conference on Sensor and Ad hoc Communications and Networks (SECON)*, 2004.

[67] Center for the Built Environment (CBE). Design guide on underfloor air distribution systems. Technical report, ASHRAE, 2002.

[68] O. Sename and A. Fattouh. Robust H_∞ control of bilateral teleoperation systems under communication time-delay. In *LNCIS Applications of Time Delay Systems*. Springer, 2007.

[69] E. Fridman, A. Seuret, and J. P. Richard. Robust sampled-data stabilization of linear systems: An input delay approach. *Automatica*, 40:1441–1446, 2004.

[70] P. Naghshtabrizi, J.P. Hespanha, and A.R. Teel. Exponential stability of impulsive systems with application to uncertain sampled-data systems. *Systems & Control Letters*, 57:378–385, 2008.

[71] A. Seuret. Stability analysis for sampled-data systems with a time-varying period. In *Proceedings of the IEEE Conference on Decision and Control*, 2009.

[72] E. Witrant, P. Park, and M. Johansson. Time-delay estimation and finite-spectrum assignment for control over multi-hop WSN. In *Wireless Network Based Control*. Springer, 2010.

[73] R.E. Sonntag, C. Borgnakke, and G.J. Van Wylen. *Fundamentals of Thermodynamics*. John Wiley & Sons, 5^{th} edition, 1998.

[74] B.R. Morton. Forced plumes. *Journal of Fluid Mechanics*, 5(1):151–163, 1959.

[75] C-S Yih. Stratified flows. *Annual Review of Fluid Mechanics*, 1:73–110, 1969.

[76] C. Gladstone and A. Woods. On buoyancy-driven natural ventilation of a room with a heated floor. *Journal of Fluid Mechanics*, 441:293–314, 2001.

[77] E. Witrant, A. D'Innocenzo, G. Sandou, F. Santucci, M.D. Di Benedetto, A.J. Isaksson, K.H. Johansson, S.-I. Niculescu, S. Olaru, E. Serra, S. Tennina, and U. Tiberi. Wireless ventilation control for large-scale systems: the mining industrial case. *International Journal of Robust and Nonlinear Control*, 20(2):226–251, 2010.

[78] E. Witrant, S. Mocanu, and O. Sename. A hybrid model and MIMO control for intelligent buildings temperature regulation over WSN. In *Proceedings of the IFAC Workshop on Time Delay Systems*, Sinaia, Romania, 2009.

[79] S. Skogestad and I. Postlethwaite. *Multivariable Feedback Control: analysis and design*. John Wiley & Sons, 2^{nd} edition, 2005.

[80] K. Zhou and J.C. Doyle. *Essentials Of Robust Control*. Prentice Hall, 1997.

[81] R.E. Skelton, T. Iwasaki, and K.M. Grigoriadis. *A Unified Algebraic Approach to Linear Control Design*. Taylor & Francis, 1997.